Novel trends in homogenous and superwettable functional surfaces with a focus on siloxane and silane chemistry

Zur Erlangung des akademischen Grades einer

DOKTORIN DER NATURWISSENSCHAFTEN

von der KIT-Fakultät für Chemieingenieurwesen und Verfahrenstechnik des Karlsruher Instituts für Technologie (KIT)
genehmigte

DISSERTATION

von

(M.Sc.) Dorothea Paulssen
aus Frankfurt am Main

Tag der mündlichen Prüfung: 15. November 2023

Erstgutachter: Prof. Dr. Jürgen Hubbuch

Zweitgutachter: Prof. Dr. Pavel Levkin

Abstract

Functional surfaces refer to surfaces that have been modified to have specific properties or functionalities that are different from their original state. Examples are surfaces with super-wettable properties, such as surfaces with a high repellency or adhesiveness for different liquid classes. Albeit a surface's topography – the physical contour of a surface – can highly influence a surface's wettability, to achieve super-wettable properties, the surface's chemistry needs to be optimized as well. For this, a surface can be coated either chemically or through physical adsorption with a protective layer. This thesis is primarily focused on this well-established reagent class for surface coatings: siloxanes and silanes. Owing to their commercial availability and simple application, silanization is the most applied strategy for the functionalization of hydroxylated surfaces in Academia.[1, 2] Siloxanes, on the other hand, are the most commonly used lubricant type when coating surfaces with unbound protective lubricant molecules.[3]

Despite the wealth of knowledge about surface design, this research field witnesses constant novel innovations regarding advanced protocols and many questions about surfaces' functionality remain open. Likewise, constantly novel use cases for siloxanes and silanes as surface modifiers and binders are proposed, such as controllable topography[4] or binders in 3D printing efforts.[5] In the present thesis, selected novel use cases for siloxanes and silanes in the broader context of surface modification and their utility are examined.

In the first part, siloxane as unbound surface modifiers is studied. Here, strategies are examined on how to structure surfaces with unbound siloxanes. That is how to structure surfaces with unbound siloxanes, i.e., through patterning other liquids with siloxane liquids. It is then investigated how siloxane regions on a surface can influence droplet flow along the surface and how much of it is explicable through known liquid-liquid-solid interactions. This is necessary to understand whether simple siloxanes can play a role in flow control applications of these surface types. Here, siloxanes showed surprising and promising capabilities of confining liquids with even lower surface tension than themselves. Nevertheless, the particular spreading coefficients of siloxanes led to cloaking effects that affected drop migration on patterned surfaces. Therefore, it was found that siloxanes acting as a controllable surface lubricant to guide drop mobility on permanently lubricated surfaces are of limited utility when compared to other lubricant types.

In the second part, simple under-characterized covalent surface modification protocols with silanes were studied theoretically, and the possibility of controlling the topography of resulting surfaces is investigated. In the first project, the robustness of oligomeric siloxanes in various solvents to reliably modify surfaces for subsequent surface patterning was investigated. Here, oligomeric siloxanes exhibited the property to lead to highly regularly modified surfaces under a wide variety of conditions. In the second project, an example of self-condensation, the

molecular basis for amino acid catalyzed condensation of silanols is characterized under different solvent conditions. This basic work is meant to help understand the influence of solvent systems on surface modification rates. Here, silane self-condensation activation energies and, therefore, reaction rates proved to be highly modulable by distinct amino acid types as well as solvents. Theoretical results promised that green routes for protocol optimization of silane condensation will prove highly flexible and optimizable in practice.

Zusammenfassung

Funktionale Oberflächen beziehen sich auf Oberflächen, die modifiziert wurden, um bestimmte Eigenschaften oder Funktionalitäten aufzuweisen, die sich von ihrem ursprünglichen Zustand unterscheiden. Beispiele sind Oberflächen mit superbenetzbaren Eigenschaften wie Oberflächen mit hoher Abstoßung oder Haftfähigkeit für unterschiedliche Flüssigkeitsklassen. Obwohl die Topographie einer Oberfläche – die physikalische Kontur einer Oberfläche – die Benetzbarkeit einer Oberfläche stark beeinflussen kann, muss die Chemie der Oberfläche ebenfalls optimiert werden, um superbenetzbare Eigenschaften zu erreichen. Dazu kann eine Oberfläche entweder chemisch oder durch physikalische Adsorption mit einer Schutzschicht überzogen werden. Diese Arbeit konzentriert sich hauptsächlich auf eine etablierte Reagenzienklasse für Oberflächenbeschichtungen: Silikone. Diese sind eine Klasse von synthetischen Polymeren, wie z.B. Siloxane und Monomeren, wie z.B. Silane. Aufgrund ihrer kommerziellen Verfügbarkeit und einfachen Anwendung ist die Silanisierung die am häufigsten angewandte Strategie zur Funktionalisierung von hydroxylierten Oberflächen im akademischen Bereich. [1, 2] Siloxane sind andererseits die am häufigsten verwendete Gleitmittelart, wenn Oberflächen mit ungebundenen schützenden Gleitmittelmolekülen beschichtet werden. [3]

Trotz des reichen Wissens über das Oberflächendesign hat dieses Forschungsfeld ständig neue Innovationen in Bezug auf fortschrittliche Protokolle erlebt, und viele Fragen zur Funktionalität von Oberflächen bleiben offen. Hier ist leicht absehbar, dass etablierte Oberflächenreagenzienklassen, wie z.B. Silikone weiterhin zu neuen Themen in den Oberflächenwissenschaften beitragen werden, wie z. kontrollierbare Topographie oder Bindemittel in 3D-Druckbemühungen. In der vorliegenden Arbeit wird daher auf einfache Strategien zur Oberflächenmodifikation mit Silikonen näher eingegangen und zukünftige Forschungsrichtungen zur verbesserten Kontrolle von Reaktionen und Oberflächenmodifikationen versucht aufzuzeigen.

In einem ersten Teil werden Siloxane als ungebundene Oberflächenmodifizierer untersucht. Hier wird nach Strategien gesucht, wie man Oberflächen mit ungebundenen Siloxanen strukturieren kann, z. B. durch Strukturieren anderer Flüssigkeiten mit Siloxanflüssigkeiten. Anschließend wird untersucht, wie Siloxanregionen auf einer Oberfläche den Tropfenfluss entlang der Oberfläche beeinflussen können und wie viel davon durch bekannte Flüssig-Flüssig-Feststoff-Wechselwirkungen erklärbar ist. Dies ist notwendig, um zu verstehen, ob einfache Siloxane in Fließkontrollanwendungen dieser Oberflächentypen eine Rolle spielen können. Hier zeigten Siloxane überraschende und vielversprechende Fähigkeiten, Flüssigkeiten mit einer noch niedrigeren Oberflächenspannung als sie selbst einzuschließen. Dennoch führte die extrem niedrige Oberflächenspannung von Siloxanen zu Cloacking-Effekten, die die Tropfenmigration

auf strukturierten Oberflächen beeinträchtigten. Es wurde daher festgestellt, dass Siloxane als kontrollierbares Oberflächenschmiermittel zur Steuerung der Tropfenmobilität auf dauerhaft geschmierten Oberflächen im Vergleich zu anderen Schmiermitteltypen von begrenztem Nutzen sind.

In einem zweiten Teil werden einfache, untercharakterisierte kovalente Oberflächenmodifikationsprotokolle mit Silanen theoretisch untersucht und die Möglichkeit untersucht, die Topographie der resultierenden Oberflächen zu kontrollieren. In einem ersten Projekt wurde die Robustheit von oligomeren Siloxanen in verschiedenen Lösungsmitteln untersucht, um Oberflächen für die anschließende Oberflächenstrukturierung zuverlässig zu modifizieren. Dabei zeigten oligomere Siloxane die Eigenschaft, unter verschiedensten Bedingungen zu hochgradig regelmäßig modifizierten Oberflächen zu führen. In einem zweiten Projekt werden am Beispiel der Selbstkondensation die molekularen Grundlagen für die aminosäurekatalysierte Kondensation von Silanolen unter verschiedenen Lösungsmittelbedingungen charakterisiert. Diese Grundlagenarbeit soll dazu beitragen, den Einfluss von Lösungsmittelsystemen auf die Oberflächenmodifikationsraten zu verstehen. Hier erwiesen sich die Aktivierungsenergien der Silan-Selbstkondensation und damit auch die Reaktionsgeschwindigkeiten als hochgradig modulierbar durch unterschiedliche Aminosäuretypen sowie Lösungsmittel. Theoretische Ergebnisse versprachen, dass grüne Wege zur Protokolloptimierung der Silankondensation sich in der Praxis als äußerst flexibel und optimierbar erweisen werden.

Acknowledgments

Supervision

Prof. Pavel A. Levkin is thanked for his supervision and support and for granting me scientific freedom.

Prof. Jürgen Hubbuch is thanked for his supervision and support.

Funding bodies

The research was supported by the ERC Starting Grant (DropCellArray 337077), ERC Proof-of-Concept grant (CellPrintArray 768929) and the HGF-ERC-0016 grant from the Helmholtz Associations' Initiative and Networking Fund.

Collaborators

Prof. Steffen Hardt is thanked for his huge support within the project on drop sorting on patterned lists.

Udo Geckle (IAM/KIT) is thanked for taking the SEM image displayed in supplementary Figure S4.

Students and Trainees

William Jefferson is thanked for his ambitious and motivated contributions.

Miscellaneous

Thanks to all the wonderful people and friends I've met and who accompanied me during this journey.

Special thanks to my family, who supported me throughout this time.

Table of Contents

List of Figures

1. Introduction

1.1 Basic concepts

The outermost layer of a bulk solid, its surface, determines how a solid interacts with the world, that is, its ability to either repel or attract liquids (wettability).[6] Wettability is a surface property that is determined by the energy of the surface, which is influenced by its chemical composition and physical structure.[6] A surface with low surface energy will tend to repel liquids, while a high surface energy surface will tend to attract them.

Silicone surfaces are particularly well-known for their repellent properties.[7] This is due to their unique surface structure, which consists of a highly cross-linked network of silicon and oxygen atoms. The surface energy of silicone is very low, which means that it repels most liquids. In addition, the surface of silicone is very smooth and uniform, which minimizes the contact area between the surface and the liquid, further enhancing its repellent properties.

The repellent properties of silicone surfaces have made them popular in many applications, including coatings for medical devices, protective coatings for electronic components, and non-stick coatings for cooking utensils. However, the properties of silicone surfaces can also be modified through the use of surface treatments and functionalization, allowing for greater control over their wettability and expanding their potential applications.[8]

Silicones are a group of synthetic materials that are made up of repeating units of silicon-oxygen (Si-O) chains, with organic groups attached to the silicon atoms (Figure 1.1).[9] The organic groups can be methyl, phenyl, vinyl, or other groups. These materials are also known as polysiloxanes or silicone polymers.

(A)

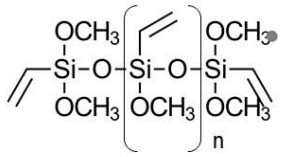

(B)

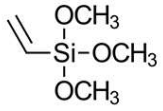

Figure 1.1: Structure of (A) an oligomeric siloxane (with potential n repeats) and (B) a monomeric alkoxy silane, each with vinyl side chains.

The chemical structure of siloxanes can be represented as (-Si-O-)n, where n represents the number of repeating units in the polymer chain. The organic groups attached to the silicon atoms can vary in type and position along the chain, giving rise to a wide range of silicone materials with different properties.[10]

The discovery of silicone can be traced back to the early 1900s when a French chemist named Frederic Kipping began investigating the reactions between silicon and organic compounds. He found that when silicon reacted with organic compounds such as ethyl alcohol and acetic acid, it produced compounds that had unusual physical properties, such as high heat resistance and water repellency.[11]

In 1904, Kipping coined the term "silicone" to describe these new compounds, and he continued to study and develop them for several decades. In the 1940s and 1950s, advances in silicone chemistry led to the commercial production of a wide range of silicone materials with various properties, such as high-temperature resistance, electrical insulation, and water repellency.

Silanes are monomeric molecules that consist of a central silicon atom bonded to four other atoms or groups.[7] These groups can be hydrogen, alkyl, aryl, or other functional groups. Silanes are typically used as coupling agents or adhesion promoters in the production of coatings, sealants, and adhesives. In the case of alkoxy silanes, the central silicon atom is linked to oxygen atoms, just like the single unit of siloxanes. Therefore, despite their differences in chemical structure and properties, silanes and siloxanes are related because silanes are often used in the production of silicone materials. If two or more alkoxy silane molecules condense, the resulting molecule will be a siloxane compound.

1.1.1 Monolayers through the Example of Silanization

Coating a bulk solid with a thin layer of another substance does not erase the bulk physical properties of the uncoated solid, yet it can modify them. Many of the resulting material’s properties cannot be explained solely by the properties of the starting solid and substances, as the morphology and dynamic behavior of the thin coating layer on the solid influences the composite’s properties at least just as much as the chemical composition of the coating substance. Much research efforts are therefore directed at creating controllably assembled surface coatings. The simplest case of a surface coating imaginable is a single layer of coating molecules – down to nm thin - regularly deposited onto a surface.[12] Typically, for such a coating, molecules that consist of dedicated binding moieties (interacting with the bulk solid) and exposed moieties (interacting with the physical surroundings) are used. Surface

properties can be straightforwardly controlled by choosing adequate exposed moieties.[13, 14] Several dedicated techniques have been developed and studied in-depth to optimize the regular deposition of such coating molecules on surfaces.

In the case of silanization, a covalent linkage between the oxygen on the surface and the silicon atom of the silane is formed through condensation.[15] A typical silane is composed of three side chains that are capable of binding to the surface or cross-condense with other silane molecules to form oligomeric/polymeric structures and one further side chain that will be exposed to the surface exterior. Spatially controllable secondary derivatization of silanized surfaces can be greatly enhanced through the presence of special reactive groups in this interfacial side chain. Silanes can condense with each other, freeing one water molecule. The resulting structures are called siloxanes and are characterized by a backbone where two silane atoms are connected through an oxygen atom. While, in general, the siloxane backbone is considered rather unreactive and siloxanes with non-reactive side chains are typically used as lubricants, single molecules can still interact and even covalently bind to hydroxylated surfaces.[16]

Silane can be physically or chemically adsorbed to a surface – the two processes are characterized by distinct rates.[5] The interplay of physisorption and chemisorption is highly relevant as it dictates both the kinetics of the overarching process and the properties of the resulting film. For example, lateral condensation of physisorbed silanes can lead to growth by island films of silanes on a surface, as well as uneven strain within the film and detachment of films upon removal. Typically, silanes are deposited onto a surface through the aid of a continuous phase – be it a solvent system or a vapor. Yet, direct stamping of pure silane or oligomeric siloxane liquid onto a surface has also been widely exploited to create patterned silane films.[17, 18] The density of silane monomers can vary and is influenced by many factors, e.g. surface hydroxyl group density but also interference by silane tail groups.[19, 20] Currently, the degree and shape of silane oligomerization are accepted to be highly sensitive to variations in reaction conditions.[21-28] For some tasks, such as creating liquid-repellent surfaces or creating shear-resistant surfaces, batch-to-batch variability in layer outcome is functionally ignorable.[29, 30] However, for other tasks, it is not. Examples where variations in surface modification easily compromise function include, among others, high packing density of a protective layer to prevent corrosion of implants,[31, 32] flexible substrates that need a flexible protectant layer,[33] reactive group density introduced in micro-arrays,[34, 35] homogeneity of chemical and physical make-up of tissue and cell culture scaffolds, [36, 37] as well as 3D-printing silicone/solid (e.g. in the form of powder) composites.[5, 38-41]

1.1.2 Definition Thin Solid Films

“Thin” and “thick” film coatings are terminologies invented in the micro-electronics industry. In this context, thick film coatings do not only refer to coatings above a certain minimum thickness but also refer to specific coating manufacturing routes. In this thesis, however, thick coatings simply refer to coatings above 0.1 µm height independent of manufacturing strategies. Thicker coatings have obvious advantages over thin coatings, such as potentially greater mechanical stability, greater insensitivity to damage, higher shielding against vapor, vertical space that can be varied for optimal repellency while maintaining functionality,[42] and coating properties that are closer to a bulk than a nanoscopic material, among others.[43] In principle, for example, it is possible to derive above 0.1 µm thick coatings from silane monomers through sol-gel processes.[44] During this research work, no such coatings were investigated. To create amorphously thick coatings, previously established protocols for either a thick coating based on deposition, stabilization, and modification of fumed silica nanoparticles[45-47] or a thick coating based on the *in-situ* preparation of a µm-high monolithic porous polymer coating that could be patterned[48, 49] were used.

Monolayer coatings on surfaces can be arbitrarily “thick” depending on the dimensions of the monomeric species. However, typically, they will not exceed the nm range. Such films are not visible to the human eye and possess distinct properties from thicker coatings.[50, 51] In fact, coatings consisting of multiple layers of molecules rather than a monolayer may also be referred to as thin films, depending on the definition, films with a thickness below either 0.1 µm or 1 µm. Besides a difference in optical properties, thin films can vary from visible films in several properties that scale with coating thickness. That is not to say that even for the thickness dimensions of thin films, size-dependent variations in properties can be observed.[51] Besides monolayer assemblies, monomeric silanes can be grafted from surfaces into network-like structures.[52] These allow higher grafting densities to be reached than silane monolayers and, subsequently, greater insensitivity to grafting defects. Control of the formed siloxane network is not trivial. Still, through varying grafting conditions, films with distinct thicknesses and morphology can be created.[53, 54] Variations in these two properties can influence, for example, tensile strength and wettability of thin film coatings.

1.1.3 Definition of Composite Films

Composite films, in the context of this thesis, are surfaces that are characterized by an overlying film that is stable and locked in place by a surface and can repel intruding immiscible liquids. The concept is introduced further in its historical context in the Methods section.

1.2 Historical Context of Liquid Behavior on Surfaces

Strategies for characterizing the ability of a surface to be wet or repel liquids will be presented in detail in this chapter. Accordingly, some examples of how the physical properties of surfaces lead to their function are presented. There are also some original research articles and reviews;[55-57] this section is mainly based on books on the topic of wettability[58-63] or open-access PhD-thesis.[64-67] Note: much of the methods presented here in this section are mainly technically non-challenging.

1.2.1 A Local Quality to classify them all: the Contact Angle of the Triple Contact Line.

1.2.1.1 Young's Contact Angle and Static Contact Angle

The shape of a sufficiently small liquid entity, i.e., a drop, on a rigid solid surface is governed by the interfacial tensions of the three-phase system: solid, liquid, and vapor.[58] For an ideal, i.e., perfectly smooth, solid surface, Thomas Young had already concluded in the early 19th century that trigonometrically, the contact angle, cos (θ), at the three-phase interface of the liquid drop on the surface relates to the interfacial tensions, γ, as:

$$\gamma_{sv} = \gamma_{sl} + \gamma_{lv} * \cos(\theta). \quad (1.1)$$

Young's equation considers a system in complete equilibrium – in terms of mechanical equilibrium - and is therefore said to express the relation of the ***static*** contact angle to the three interfacial tensions.[55] It reflects a local property - cos (θ) - that can be measured simply and macroscopically instead of on the scale of the intermolecular forces being the physical cause of the single interfacial surface tensions. However, for Young's relationship to be fulfilled, an ideal surface is considered – both perfectly smooth and chemically homogenous. Many functional and real surfaces diverge from this ideal, as will be discussed later. Measuring static contact angles bears pitfalls – when placed on the surface, the drop's initial contact angle may deviate from it - and will hardly be used in this thesis; for the interested reader, I would like to recommend the following references for a deeper look into static contact angles.[57, 68-70] Moreover, two of the three involved interfacial tensions –

between solid and vapor, γ_{sv}, and between solid and liquid, γ_{sl} - cannot be measured reliably. [60]

1.2.1.2 Molecular Origin of Surface Tensions and Miscibility

If the liquid were in contact with only one other entity belonging to another physical phase, it would vary its shape accordingly. In a rigid solid - with atoms and molecules tightly bound to each other assuming a static shape - the liquids can be easily reshaped and readily adapt to the shape of their surrounding container.[58] In an open, immiscible gaseous environment or void, a liquid will adopt the smallest possible surface area – a sphere - to minimize its surface energy. From a molecular perspective, minimization of the liquid's surface area is explained as follows: while in the liquid's bulk, its molecules are surrounded by other liquid molecules, on the liquid interface with another substance, molecules experience only half of the cohesive energy, *E*. Indeed, it is possible to approximately relate the macroscopically measurable surface tension to the forces acting on the molecular level of the liquid, i.e., their cohesive energy, *E*. When expressing surface tension in terms of the cohesive energy experienced by the molecules of the liquid on the liquid-vapor interface, it is in the order of:

$$\gamma_{lv} \sim E / (2 * a_m^2), \quad (1.2)$$

where a_m corresponds to the area of a single liquid molecule.

The reason for the dominant cohesive energy between atoms, however, can vary; immiscible liquids tend to be dominated by different molecular cohesive forces, such as organic oils through van-de-Waal type interactions and aqueous fluids through hydrogen bonding.[71] These liquid classes can accordingly vary considerably in surface tension. While many organic solvents possess low surface tension, such as Hexane with ~ 18 mJ/m², water, which is shaped through hydrogen bonding, has a distinctively high surface tension, which is commonly determined as ~ 72 mJ/m².[58, 71] A particularly notable class of chemical compounds are chemicals with a high number of fluorine atoms. As fluorine has a very low polarizability, its interactions are dominated by weak London dispersion forces.[72] This renders them both hydrophobic and lipophobic, albeit being non-polar and immiscible with almost all common solvents. Likewise, other chemical categories exist that show peculiar miscibility with common aqueous and organic solvents. For example, siloxanes – which are characterized by siloxane bonds with methyl groups attached to each silicone atom, are

neither purely hydrophilic nor purely hydrophobic, albeit they overall display a hydrophobic character and are poorly miscible with many organic oils.[7] The miscibility of siloxane compounds can be greatly tuned by the side-chains bound to siloxane atoms in their repetitive unit.[73, 74] In any case, many aspects of the molecular causes for surface tension and macroscopic behavior of surface tension are poorly understood – even for standard liquids such as water[75] – albeit their study dates back to the 19th century.[58]

It has been attempted multiple times in the literature to interpret macroscopic measurable contact angles through the nanoscopic molecular interactions within involved fluids and solids and resulting surface energies. This has led, for example, to well-established techniques for relating contact angles to surface-free energies, such as methods presented by Girifalco and Good or the Zismann plot.[60, 76] None of these methods are universally applicable, and each comes with its own pitfalls. Nevertheless, as pointed out by Derjaguin in 1936,[77] intermolecular forces are indispensable in quantitatively explaining the difference in pressure between a bulk liquid phase and a thin liquid film adsorbed on a solid. The pressure difference has been termed disjoining pressure and later tried to be quantitatively expressed by Hamaker[78] as well as in a modulated form by Lifshitz and Ninham.[79] Disjoining pressure and the Hamaker constant find frequent application for the prediction and interpretation of nano- and micro-scale phenomena, for example, as encountered in MEMS fabrication.[80, 81]

1.2.2 Wetting on Real Surfaces: Advancing, Receding and Sliding Contact Angles

The ***static*** contact angle is assumed to be the shape in mechanical equilibrium of a liquid drop on a surface.[60] Yet, on most – even smooth – surfaces, a drop can assume different shapes that cover a given range of contact angles called ***hysteresis***. Many other metastable contact angle states exist within the hysteresis range. Furthermore, when a drop is positioned on a surface that is then slowly tilted, the drop will start moving at a characteristic angle called the ***sliding*** angle (or roll-off angle). It can be observed that when placing a drop on a horizontal surface and then tilting the surface below the sliding angle of the drop on the surface – the angle when the drop starts sliding down the surface – the liquid will assume different angles on its leading and trail edge – with the former always being larger than the latter for homogenous surfaces. Likewise, when slowly dispensing a drop onto a surface, it will assume a larger angle (***advancing*** angle) than when slowly sucking the drop up from the surface (***receding*** angle) (Figure 1.2). The hysteresis is defined as the difference between advancing and receding contact angles (θ_a - θ_r). For certain hysteresis ranges, the advancing

and receding angles correspond to leading and trailing angles. The origins of contact angle hysteresis are still under active discussion, and several lines of explanation exist which have been covered elsewhere.[60]

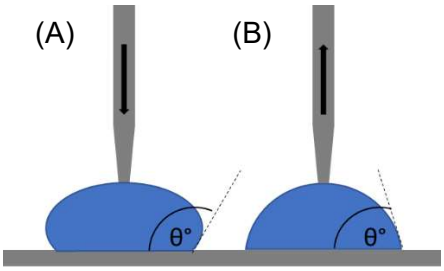

Figure 1.2: representative contour of a potentially (A) advancing drop and (B) receding drop of the same liquid.

Contact angle measurements are very simple yet indispensable measurements of a surface's physical functionality. For water drops, a distinction is made between surfaces, such that if a water drop forms a static contact angle cos (θ) < 90° on a given surface, the surface is said to be hydrophilic; if cos (θ) > 90° the surface is said to be hydrophobic. If the cut-off value of 90° is physically meaningful, it has been discussed elsewhere.[60] In short, for water, evidence exists that both supports and refutes a 90° cut-off value. In general - because of the reduced contact area with the surface – droplets exhibit smaller roll-off angles on composite surfaces (solid-air interfaces) than on smooth surfaces.[58, 60]

1.2.3 A Closer Look on Topography: Wenzel and Cassies-Baxter

Most surfaces in real life are not perfectly smooth but exhibit a certain degree of roughness. [58, 61] This is important as it was theoretically recognized and has been experimentally proven that the interaction between a liquid drop and a solid surface is fundamentally influenced by the surface's roughness. At least two regimes can be imagined in how the drop rests on a rough surface (Figure 1.3): (A) the drop homogenously wets the surface with the interface strictly following the shape of the rough protrusions (Figure 1.3) – a condition known as the Wenzel model. Here, the apparent contact angle, cos* (θ), on the rough surface diverges from the contact angle the drop would assume if the surface would be perfectly smooth by the roughness factor, *r*:

$$\cos^*(\theta) = r * \cos(\theta) \quad (1.3)$$

The roughness factor is a simple ratio between the actual surface area and the projected surface area ($r = A/A_0$). If $r = 1$, the surface is perfectly smooth and $\theta^* = \theta$. However, if $r \neq 1$, the equation proposed by Wenzel predicts that the roughness reinforces the liquid-solid interaction, as $\theta^* < \theta < 90°$ and $\theta^* > \theta > 90°$. Indeed, super-wetting states – such as superhydrophilicity and superhydrophobicity – can be reached on rough surfaces. Superwettable states are formally classified by static contact angles of liquids on solids. On a superhydrophilic surface, water forms a contact angle of <5°-10°, while on a superhydrophobic surface, water forms a contact angle of $\theta > 150°$.

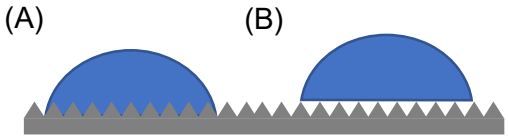

Figure 1.3: Contours of a (A) Wenzel-state and (B) Cassie-Baxter model drop.

The drop can rest on the surface in at least one alternative regime (B) where it is only in contact with the protrusions' tips and otherwise rests on air trapped in the pockets of the rough surface (Figure 1.3) – a condition known as the Cassie-Baxter model. For the sake of simplicity, here, it is just summarized that at equilibrium, the apparent contact angle of the drop on the surface relates to the fraction, *f*, of the liquid interface in contact with either solid or air, as:

$$\cos^*(\theta) = f_1 * \cos((\theta)_{sl} + 1) - 1 \quad (1.4)$$

This relationship predicts remarkable drop shapes on rough surfaces as the apparent contact angle is raised to values equal or less to ($f_1 - 1$) – ultimately approaching -1 (contact angles of 180°) if the solid fraction is reduced.

The question arises as to which of the two states – Wenzel or Cassie-Baxter – is more stable. This has been the subject of both theoretical and experimental analysis.[82] In short, for certain surface chemistries, it is indeed favorable that air remains trapped in the surface's pockets, i.e., the surface energy of the dry solid is less than for a wet surface;[83] chemical

repellence of the surface material against the liquid strongly favors this condition. However, in such a scenario the Cassie-Baxter state has been proposed to only present a local energy minimum: even on surfaces optimized for liquid repellence, the Wenzel state is assumed to represent the optimal energy minimum. The stability of the Cassie-Baxter state is reached when transitions to the Wenzel state are not spontaneous, i.e., an energy barrier separating the two states exists. As the stability of the Cassie-Baxter state depends on the stability of the trapped air cushion in the surface's roughness, many factors that can destabilize the air cushion, such as pressure, temperature, airflow, strong vibrational forces, and humidity, can lead to a wetting state transition.[59]

A critical parameter for the stability of the Cassie-Baxter state of any liquid on rough protrusions is the angle formed between the side-walls of the protrusions and an imaginary horizontal line.[84] Here, the overhang angle, $\theta_{overhang}$, can be either greater or smaller relative to the angle the liquid would form on a flat surface of equal chemistry, θ_{flat}. For $\theta_{flat} < 90°$ but $\theta_{overhang} < \theta_{flat}$, the liquid-vapor interface is concave, causing the liquid to enter the pocket. If $\theta_{overhang} \geq \theta_{flat}$, the liquid drop is stable in the Cassie-Baxter state, assuming that gravity can be ignored. Low surface tension liquids are not only characterized by a lower contact angle on flat surfaces than water but also among them, many, such as oils and organic solvents, possess a contact angle $\theta_{flat} < 90°$.[85, 86] Indeed, low surface tension liquids require, in addition to surface chemistry and general surface roughness, precise surface topography, such as re-entrant structure or double re-entrant structure, in order for them to achieve super-repellence on a surface in air. Albeit this perception has been challenged,[87, 88] micro-fabrication of such precise topographical features to produce amphiphobic structures on industrially relevant surfaces remains an active area of research.[89, 90]

1.2.4 A Drop's Contour

1.2.4.1 What is the Capillary Length?

Static contact angles conform to roundish contours atop rigid solid surfaces, which meet the solid at the triple phase interface by a contact angle cos θ. This can be explained by the general tendency of droplets to adopt the lowest energy shape as well as the internal pressure of the drop. However, this assumption only holds true if gravity can be ignored; if a drop of large enough volume is applied onto a surface, it will exhibit a flattened contour (see Figure 1.4). The force preventing the drop from completely collapsing into a flat shape is the surface tension. The maximum radius of the drop, for which there is still no observed

flattening of the drop's contour due to gravity, corresponds to the ***capillary length***. The capillary length, λ_c, can be seen as the length scale below which surface tension forces balance out gravitational forces in a small drop:

$$\lambda_c = \sqrt{(\gamma/\Delta\rho g)} \quad (1.5)$$

where $\Delta\rho$ is the mass density difference between a drop of surface tension γ and the surrounding phase, while g corresponds to the gravitational acceleration. Higher surface tension liquids, such as water (λ_c = 2.7 mm), have higher capillary length values than lower surface tension liquids, such as methanol (λ_c = 1.7 mm) under constant conditions.

Figure 1.4: Drop with a volume larger than its capillary length and thus flattened contour on a surface.

If the drop's dimensions are larger than its capillary length, the drop's weight will cause pressure on liquid molecules inside the drop. This is known as the ***hydrostatic pressure,*** which increases proportionally with the depth measured from the surface due to a build-up in weight from fluid from the surface. Thus, for drops with dimensions larger than the capillary length, besides surface tension forces, hydrostatic pressure needs to be accounted for in order to determine its sessile profile on a horizontal rigid solid surface. In short, the thickness, *h*, of the drop's flat part can be calculated in terms of the capillary length by:[58]

$$h = 2 * \lambda_c^{-1} \sin(\theta_{static} / 2) \quad (1.6)$$

Thus, the capillary length in relation to the characteristic length, Λ, of the drop (e.g., its radii of curvature) can be used to derive a drop's surface tension based on its shape profile. The relationship between characteristic length and capillary length is formally expressed by the Bond number: $Bo = \Lambda / \lambda_c$. In other words, when $Bo < 1$, the shape of the drop is almost

spherical due to the dominance of surface tensions; for Bo > 1, the shape is dominated by gravity and deviates notably from a spherical shape.

1.2.5. From Drop Shape to Internal Flow Dynamics: Young-Laplace

If cohesive energy alone existed between the molecules of a liquid entity, the liquid would collapse into an infinitely small object. However, if single molecules within a liquid approach too closely to each other, repulsive forces hinder their complete collision. In the absence of rigid ordering, as in a solid, liquid molecules are subjected to a greater extent to thermal agitation. Thus, a liquid entity held together by its surface tension, γ, harbors a fair amount of internal pressure. In other words, increasing the surface area, δA, and volume, δV, - as measurable by a change of the radius (δr) – of the liquid sphere requires work (δW) as a function of the change in pressure, Δp:

$$\delta W = \gamma * - \delta A – \Delta p * \delta V \quad (1.7)$$

$$<=> \delta W = (\gamma * 8\pi r - \Delta p * 4\pi r) * \delta r \quad (1.8)$$

At equilibrium, contraction forces should balance pressure forces, and δW = 0. Therefore:

$$\Delta p = 2\gamma / r \quad (1.9)$$

The last relationship is known as the Young-Laplace equation for spherical phases. Besides Young's work, it is based on the work of another scientist, Pierre-Simon Laplace, who conducted research at the beginning of the 19th century. It, for example, notes that the pressure within a smaller bubble or drop is higher than in a larger entity of the same fluid (i.e., a liquid possessing the same surface tension). It basically states that for any given liquid shape, the change in pressure of a liquid upon traversing its interface is proportional to the liquid's surface tension relative to its curvature, C. The general form of the Young-Laplace equation therefore states:

$$\Delta p = \gamma * (1/R_1 + 1/R_2) = \gamma * C \quad (1.10)$$

If the liquid entity becomes large enough, e.g., for drops with a diameter of 10 cm, the Laplace pressure becomes effectively insignificant. For smaller entities, Laplace pressure and pressure differences dictate liquid behavior as well as internal flow patterns. This has been used several times in the literature to propose designer drop shapes that enable analytics on open and miniaturized microfluidic platforms, such as for simple determination of fluid viscosities.[91] Despite Laplace-pressure-induced flows, other forces exist that can induce spontaneous and stable flows within small open liquid entities. Famous examples include evaporation-induced flows[59] and the highly related field of (solutal or thermal) Marangoni flows.[92, 93] Interestingly, forced flows – such as through pumping a fluid over an open, wettable surface can overcome spontaneous fluid flows[94, 95] yet only within certain size ranges for a given fluid shape. It remains to be seen how this can be exploited in applications, albeit research efforts exist, for example, in the area of suspended microfluidics.[96-98]

1.2.6. Spreading - the Movement of Small Liquid Entities along Open Surfaces

As stated before, a liquid will adopt a shape that minimizes the liquid's surface energy. This means that a small liquid entity will optimize its shape towards a sphere on a surface that is chemically repellent to it while it will maximize its spread on a surface that is chemically attractive to it.[55, 58] A measure of whether a liquid droplet is able to spread on a surface can be defined as the spreading coefficient, S,[99] in terms of the work of adhesion, W_a, and cohesion, W_c, such that $S = W_a - W_c$. The onset of spreading and the equilibrium conditions of spreading are ongoing research subjects that have been discussed in detail elsewhere.[56] Here, it just should be noted that an arbitrary liquid drop on a given solid surface can assume different wetting regimes; thus, a drop equilibrium state on a surface can be categorized as non-wetting, partial wetting, or complete wetting depending on which spreading coefficient the solid-liquid interaction possesses.[60]

Previously, it was pointed out that when tilting a surface on which a drop rests, the ***leading*** and ***trailing*** edges caused by the tilting may not correspond to the advancing and receding angle. Indeed, the drop stays pinned to the surface for as long as $\theta_{adv} > \theta_{lead}$ and $\theta_{rec} < \theta_{trail}$. Here, the Laplace pressure difference between the leading edge and trail creates a force strong enough to oppose gravity. Thus, the sliding angle, α_s, at which the drop starts moving down the surface can be calculated by looking at the forces acting on the contact line alone – the capillary forces – and the counteracting gravitational forces along the surface. Likewise,

the work associated with de-wetting an area while wetting another area of the same surface can be determined; for this, the actual shape of the drop can have an influence. In general, however, sliding is caused by the action of three forces: (1) the capillary force, (2) gravity normal to the plane, and (3) viscous drag of the surface. The existence of a threshold energy before a drop starts moving and correlating with the drop's sliding angle relative to its weight is independent of the actuation method chosen.

By combining regions of controlled shape, which differ in their wettability, an energy barrier is created which a drop needs to overcome when trying to cross from a more wettable into a less wettable region.[100] Many scenarios of combining more wettable with less wettable regions are possible, e.g., when more wettable regions are chosen that still sustain droplet mobility; depending on the relative wettability contrast to the less wettable regions, several drop manipulations are possible. Intriguing outcomes include drops adapting shapes that greatly vary from the shapes they would adapt on a homogenous surface;[101, 102] robustly guiding droplet transport along a pre-determined path and independent of actuation method; [103, 104] drop motion characteristic in terms of shape deformation to patterned but not homogenous surfaces;[105] deflection of moving drops due to the presence of chemical patterns drop sorting.[100, 106] Moreover, removal of fluids from patterned surfaces, i.e., possessing highly wettable and repellent regions, can result in liquid pinning on wettable regions and thus incomplete removal of fluid from the solid surface (i.e., discontinuous dewetting).[107, 108]

1.2.7. Composite Surfaces

So far, liquid interacting with solids has been discussed. However, liquids permanently wetted by a liquid can also repel intruding non-miscible objects and liquids. Here, the principle of stable lubricant-impregnated surfaces (SLIPSs) will be discussed in relation to "classical," i.e., "dry" repellent surfaces. Note that since 2011 SLIPSs have received much attention as they may offer solutions to many real-world problems encountered in Surface Sciences.[3] It has to be stressed here that so far, it seems realistic that SLIPSs can become tools for an extraordinarily wide range of application areas. Noteworthy examples include high-throughput bacteria research – where SLIPSs can, for example, enable droplet array formats; bio-analytics where SLIPSs can help to prevent bio-fouling of applied surfaces; *in-situ* surface modifications to enhance industrial processes such as tank improvements, airplane travels, and condensate capture; as well as through related concepts helping to increase sustainable chemical synthesis.

1.2.7.1. What is a SLIPS?

In principle, SLIPSs are easy to manufacture, and the strategies introduced in section 2.1 can be used directly for them. SLIPSs require the fabrication of a suitable scaffold, which is then impregnated with a chemically matching lubricant. The scaffold can be rough – e.g., in the case of porous polymer coatings – or just swellable – e.g., in the case of polymer brushes or gel structures. Silanization of naturally rough or roughened substrates, for example, has allowed the turning of metals, ceramics, glass, wood, and paper[109] into a SLIPS scaffold. The resulting composite surface exhibits properties, such as ultra-slipperiness, which may not be reached when separating a SLIPS into its single components (e.g., dry rough surface and non-stabilized lubricant film on a perfectly smooth surface).

It was suggested that SLIPSs should be classified on strict cut-off values, such as possessing an extremely low sliding angle (<5°) and apparent contact angle hysteresis (<2.5°) for all kinds of intruding liquids that are non-miscible with the lubricant.[110] Yet, long-term stability and, thus usability of SLIPSs may not be guaranteed when focusing on these simple parameters. For example, lubricant can be lost from the surface while being dragged away from it when intruding liquids slide down it.[111] This effect is intensified if the intruding liquid is cloaked by the lubricant. Ways to prevent this include, for example, more careful choice of lubricant, re-impregnation of SLIPS, or covalently bounding the lubricant to the surface so that it cannot be washed away (slippery-like). A universal solution to this problem has not been suggested so far. Potential ways around it include surfaces where the lubricant has been stably grafted onto a surface comparable to dense polymer-brush surfaces. Note that some of the composite surfaces used in this thesis do not match these exact cut-off values but still showed enhanced repellence compared to dry surfaces of the same scaffold type.

1.2.7.2. Liquid Drops on SLIPSs (Meniscus, Speed, and Friction)

A drop deposited on a SLIPS lubricated with an immiscible liquid overlay will form a hemispherical shape on this composite surface type. Instead of a visible solid-drop interface – and independent of whether the lubricant spreads over the drop or not – an intersect point between the drop and the bulk of the lubricant meniscus spreading around the drop will be formed. Thus, the definition of an apparent contact angle of a drop sitting on a SLIPS is distinctively defined from the one for a dry classical repellent surface; the apparent contact angle on a SLIPS refers to the drop's contact angle at the intersect with the meniscus. However, fluorescence microscopy showed that within the lubricant phase, the drop's

curvature notably diverges from this contact angle measured on top of the lubricant phase.[112] Care of the determination of the meniscus tip has to be taken as the oil film thickness, oil type, and viscosity can influence the thickness of the meniscus. Apparent contact angles on SLIPSs are still proportional to and can still be used to determine the actual contact angle of the intruding drop on the surface.[113]

Drop mobility – even of small drops – is high on SLIPS, which exhibit ultra-low sliding angles for liquids of varying surface tensions and high interfacial slip length. As on dry repellent surfaces, drop motion is influenced by the size of the drop, yet also by the lubricant's viscosity.

2. Research Proposal

Siloxanes and silanes are ideal surface coaters as they possess a very low surface energy easing their homogenous distribution on a surface as well as consequentially rendering surfaces highly repellent. As outlined in the previous chapters, forming regular surfaces – even with silicones and silanes – is not trivial. Nevertheless, a surface's homogeneity has a large effect on the surface's functionality.

One recent strategy to create smooth and seemingly defect-free surfaces is stably lubricant-infused surfaces (SLIPSs). By utilizing a two-phase system with a liquid lubricant and a textured solid surface, such surfaces have been shown to significantly reduce friction and enhance intruding objects' mobility on the surface.[3] Siloxanes are common lubricants for this surface type. Many questions remain open about this surface type – also with regards to the drop dynamics on them. One open research area is the control – either active or passive – of drop motion on these surfaces. Several active strategies for drop movement control have been proposed on these surfaces, ranging from magnetism to heat. Passive strategies proposed so far have ranged from adjusting the viscosity of lubricants to patterning underlying surfaces. Interestingly, it has been shown that SLIPSs can also be patterned by locking immiscible lubricants next to each other. This strategy has been proposed only in one research article so far.[114] This is unfortunate as it has been shown for dry surfaces that patterning surfaces can highly benefit the control of drop actuation on surfaces.[103, 104, 115] This is needed in the context of surface applications in fields such as biotechnology but also highly non-related areas such as fog harvesting.[116, 117]

Here, the ability to pattern lubricants on SLIPSs matrices shall be further characterized. The variety of lubricants that can be patterned next to each other shall be further detailed. Also, the ease of manufacturing such surfaces shall be tested relative to the original paper and related articles.[118] Finally, it is tested whether these surfaces, if patterned, can act as flow modifiers for drop mobility on them – an aspect so far largely unexplored. Understanding the influence of patterned slippery surfaces on flow dynamics is of critical importance for the development of more efficient and effective fluidic systems.

Therefore, the main objective of this first part of the thesis is to investigate the effect of patterned SLIPSs on drop flow dynamics. Specifically, the following research questions will be addressed:

1. How does the patterning of SLIPSs affect the flow behavior of fluids?
2. How can the drop behavior on patterned SLIPSs be explained analytically?
3. How can we optimize the design of patterned SLIPSs to achieve desired flow behaviors?

This research will contribute to the development of a fundamental understanding of the mechanisms by which surface patterning modifies flow behavior. The research will also provide guidelines for the design and optimization of patterned SLIPSs for specific flow control applications. The outcomes of this research will have potential applications in many fields, including microfluidics, biomedical devices, and self-cleaning surfaces.

In the second part of this thesis, underexplored simple but robust strategies, such as how to create dry homogenous surfaces using monomeric or oligomeric alkoxy silanes, will be characterized. Again, a focus is placed on patterned surfaces. The proposed research involves surface modifications of various substrates and subsequent secondary derivatization of substrates in highly wettable and repellent regions using click-chemistry. Substrates are modified using various deposition conditions and solvents to map out condition ranges with an optimal outcome. This initial exploratory work would allow us to assess both literature reports and non-characterized functionalities and compare them with future theoretical molecular dynamics studies.

Alkoxy silanes and silicones have the disadvantage that their uncatalyzed reaction with certain surface types is too slow to be competitive with the environmentally less friendly halogenated silanes. To overcome the reaction barriers, environmentally friendly catalysts, such as amino acids, have been proposed. To gain insights for future protocol optimizations, the condensation of silanes in the presence of an amino-acid catalyst was studied theoretically. The mechanism of amino acid catalysis of silane condensation has not been studied previously, and the influence of amino acid main chains is not well understood. Likewise, the influence of green solvents on the reaction is underexplored. These are nevertheless important factors to understand if we want to create homogenous surface coatings with silanes through amino acid catalysis.

3 Outline of Thesis

- ***Chapter 4***: A phenomenological account of the formation of surfaces on which three different phases were stably patterned next to each other. Patterned SLIPSs with two phases had been proposed before in literature),[116] and were here extended to several phases. Additionally, it was recorded that patterned SLIPS formation can be easily created by infusing a surface with the lubricant first and then introducing an intruding liquid to be patterned – as similarly studied before on smooth surfaces by Carlson et al.[120] Within the porous polymer, liquid-liquid displacement seemed to agree well with the extensive body of literature focusing on these phenomena – with the exception of hexane. Lastly, the wettability of hydrophobic surfaces that have been infused with a highly matching lubricant and lubricants belonging to a different chemical phase were compared.
- ***Chapter 5***: Drop dynamics on patterned SLIPSs. The ability to modify the path of drops sliding down inclined SLIPSs possessing various surface patterns of immiscible but hydrophobic lubricants was qualitatively assessed. Experimentally, lubricant patterns were tested to deflect aqueous drops according to magnetism and drop size. For this, the ability to rapidly create new chemical pattern designs through UV modification, even when using self-printed photomasks on commercially available polypropylene foil, was exploited. Through cooperation, it was shown that the passage of drops from one lubricant pattern into an underlying lubricant pattern fairly agrees with quantitative predictions, as long as only one or none of the lubricant cloaks the drop. Different combinations of lubricants – even those that do not entirely engulf drops (such as mineral oil and ionic liquid) were tested.
- ***Chapter 6:*** The robustness and simplicity of modifying glass and silicone surfaces with oligomeric methoxy siloxanes (VMS) for secondary derivatization of surfaces is assessed. Secondary modification of the thus formed surfaces is demonstrated.
- ***Chapter 7***: Computational characterization of amino acid-catalyzed condensation of silanols to elucidate potential bottlenecks. Different implicit solvent environments were compared.

3.1 Overview collaborators and helpers for single projects

Contributors are either cited or contributed as in the list below:

Contributor:	Contributed To:
Dorothea Paulssen	**4**: Planned and conducted experiments, wrote outline, wrote and revised the manuscript; **5**: Suggested topic, planned and conducted experiments, wrote and revised the manuscript; **6**: Suggested topic, planned and conducted experiments, wrote the outline for the manuscript; 7: Suggested topic, planned and conducted experiments, wrote the outline for the manuscript
Pavel Levkin	**4**: Suggested topic, suggested several experiments, revised the manuscript; **5**: Revised the manuscript; **6:** suggested an experiment with solvent removal
Steffen Hardt	**5**: wrote the theoretical part of the paper and suggested experiments according to the suggested literature, revised the manuscript
Wenqian Feng	**4**: helped with technical questions, revised the manuscript
Ivana Pini	**4**: Carried out a parallel project evaluating patterned SLIPSs and supervised a control student's project
Jasmin Sandoval	**4**: Carried out a control student's project for the manuscript
Timotius William Jefferson	**4:** Took photos of Droplet Arrays integrated into a Figure for the final manuscript; **Outlook**: Carried out exploratory experiments for Outlook project 3
Aquarray	**5**: Provided alternative porous coatings

4. Formation of liquid-liquid micropatterns through guided liquid displacement on liquid-infused surfaces.

Dorothea Paulssen[1], Wenqian Feng[1], Ivana Pini[1], Pavel A. Levkin[1]*
1 Institute of Toxicology and Genetics (ITG), Karlsruhe Institute of Technology (KIT), 76344 Eggenstein-Leopoldshafen, Germany
*Corresponding author: levkin@kit.edu

Abstract: Here, we demonstrate a method to pattern liquids of varying surface tension and composition into droplets by utilizing slippery liquid-infused surfaces prepared on chemically-patterned substrates. We study the capability of different liquids to displace the lubricant from higher surface energy regions and show that both high and low-surface tension liquids can imbibe the polymer, thereby forming droplets sharply following underlying surface energy patterns. For all liquids tested, droplet arrays of arbitrary shapes of each liquid were formed with precision down to 50 µm. By changing the chemical patterning from fluorinated to aliphatic groups, patterns of mineral and silicone oils were created. Finally, we demonstrate the formation of two-dimensional micropatterns of three-phase liquid systems – fluorinated, organic, and aqueous phases.

Keywords: slippery surfaces, imbibition, liquid displacement, surface patterning, droplet microarrays

---

Published in *Adv. Mater. Interfaces*, DOI: 10.1002/admi.201800852

4.1 Introduction

Liquid patterning on solid surfaces is an essential process in micro- and nano-fabrication. It has been used for microelectromechanical systems (MEMS)-fabrication,[119-121] microfluidic-device design[122, 123] bio-scaffold creation,[124] or high-throughput screening efforts.[102, 125-129] It is usually accomplished by applying liquids via a highly controlled method such as contact or non-contact printing,[130-134] pre-structured surfaces,[135-137] micropatterning through thin liquid film instabilities[138, 139] or wettability patterning such as superhydrophobic-hydrophilic patterns.[102, 140] The latter example enables the formation of patterns of aqueous solutions using the effect of a discontinuous de-wetting process.[135, 141-143]

How liquids spread on a surface is determined by their surface tension relative to the surface tension of the solid at the contact line of the three-phase system.[55, 144] Thus, low surface tension liquids, such as perfluorinated oils (e.g., perfluoropolyether), silicone oils, and many organic solvents can easily wet different materials,[145] while liquids with higher surface tension often form confined droplets. Several methods were recently developed that enable patterns of low surface tension liquids using the effect of discontinuous de-wetting.[141, 146] Tuteja et al. introduced a method requiring superoleophobic-superoleophilic patterns,[141, 146, 147] while the approach of Feng et al. relies on the formation of defect-free surfaces to create patterns of regions with strong de-wettability towards organic solvents.[129] However, neither of those methods enables the patterning of liquids with extremely low surface tensions below 18 mN/m. To pattern such liquids, including fluorinated or silicone oils, “double-re-entrant” topographies[145, 147] are required. However, these do not prevent liquids from spreading laterally once in contact with these features.[148-152]

Another problem is that aqueous solutions containing proteins, lipids, sugars or other biological components derived from cells, cell lysates or growth medium and may not only possess lower surface tensions but can also hydrophilize surfaces by adsorbing biomolecules, thereby degrading the liquid-repellent character of such surfaces.[149, 153] For this reason, the formation of complex surface patterns of organic solvents or biofluids remains difficult.

Liquid-infused interfaces or slippery surfaces possessing excellent liquid repellence were recently introduced by impregnating a nano/micro-structured or porous surface with a lubricant, thereby creating a stable lubricant layer on top of this surface.[16, 110, 112, 114, 154, 155] A favorable disjoining pressure maintains a stable lubricant film on the surface.[156-158] In contrast to air-filled repellent surfaces, such liquid-locked surfaces reveal

greater robustness against pressure and hydrodynamic shear.[159] There is evidence that slippery surfaces are superior in anti-fog, anti-icing, and anti-biofouling applications[102, 140, 152, 155, 160] to traditional hydro- and omniphobic or polyethylene glycol-functionalized (PEGylated) surfaces.

Here, we demonstrate that the displacement of one lubricant liquid by another liquid depends on the underlying substrate's surface chemistry. We show that by patterning the substrate with superhydrophobic/hydrophilic features, we can control the liquid-liquid displacement process spatially. This process can be used to spontaneously form micropatterns of liquid droplets with surface tensions ranging from 72 mN/m (water) down to <18 mN/m (n-hexane). In addition, by forming surface patterns of fluorinated, alkylated and hydroxylated regions, it was possible to create three-phase patterns using fluorinated, organic and aqueous fluids.

4.2 Results and Discussion

The fabrication of superhydrophobic-hydrophilic patterned surfaces was performed using the following approach (Figure 1A).[49] First, a 15 µm thin porous poly(2-hydroxyethyl methacrylate-co-ethylene dimethacrylate) (HEMA-EDMA) layer with pore sizes ranging from 80 nm to 250 nm[50] was polymerized on a glass slide. The polymer layer can be rendered superhydrophobic (SH) (advancing water contact angles θadv = 170°±2 receding water contact angles θrec = 157°±0.5) or hydrophilic (θadv = 46°± 5 and θrec = 0°) through the esterification with 4-pentynoic acid (alkylated surface) and the UV-induced thiol-yne reaction with 1H,1H,2H,2H-perfluorodecane-1-thiol (PFDT) or ß-mercaptoethanol, respectively. The polymer film can be patterned via sequential UV-induced thiol-yne reactions with the aid of quartz photomasks.[48] Previously, this method has reported yield patterns with sizes as small as 10 µm and below.[48]

The wetting abilities of both fluorinated PFDT-modified and hydrophilic HEMA-EDMA surfaces were investigated with a set of liquids with different surface tensions ranging from 16 mN/m to 72 mN/m (Table 1). The PFDT-modified polymer was non-wettable for liquids with surface tensions higher than ~ 40 mN/m (Figure 2), and the liquid droplets remained in the Cassie state.[161, 162] However, it was wetted by liquids with surface tension below 40 mN/m, such as ethanol, DMF as well as by low-surface tension lubricants Krytox GPL 103 (PFPE) (20 mN/m), silicone oil (20.1 mN/m) or mineral oil (32 mN/m). On the other hand, high-surface energy hydrophilic porous HEMA-EDMA could be infused by all the liquids studied (Table 1).

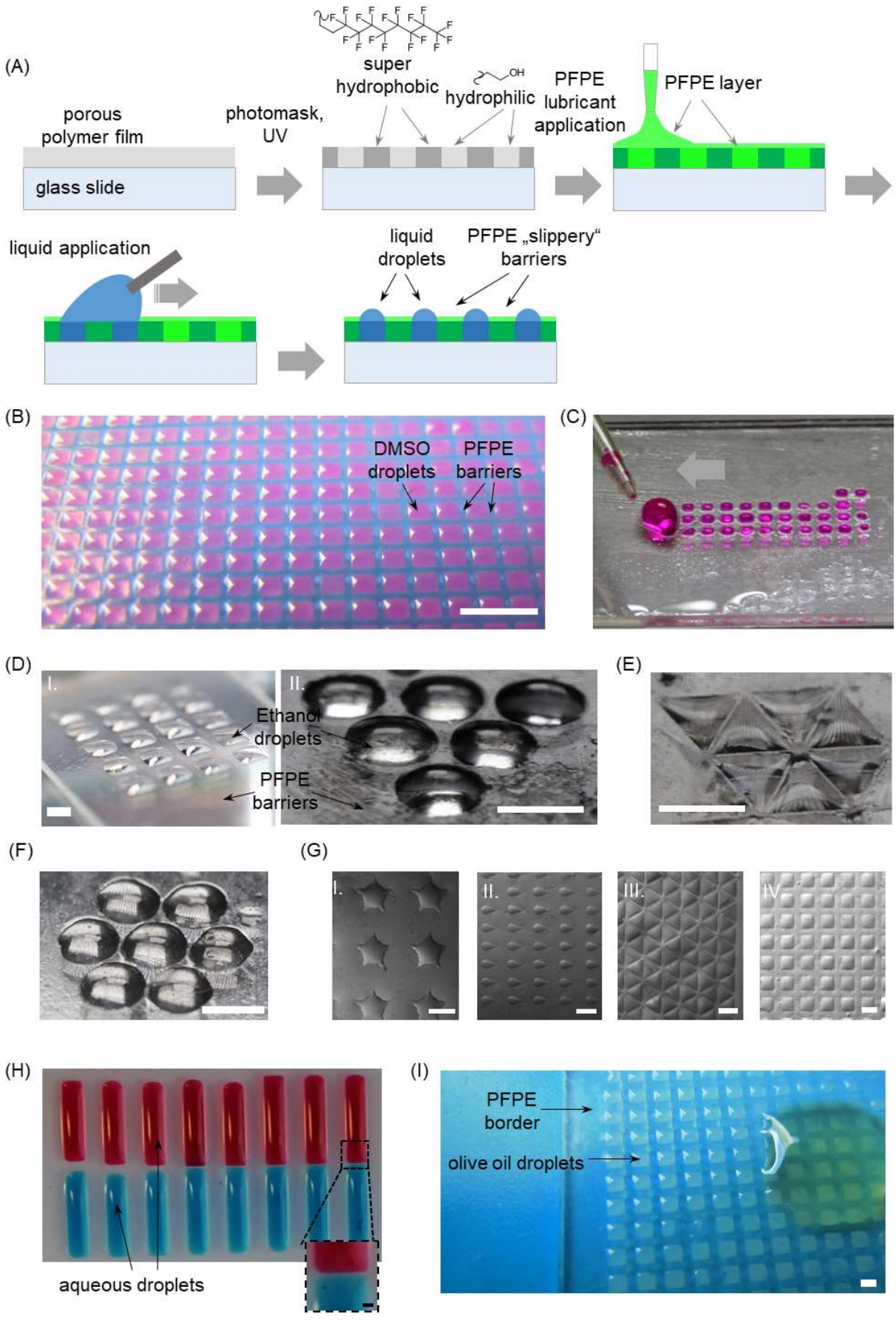
(A)
super hydrophobic
hydrophilic
PFPE lubricant application
PFPE layer
porous polymer film
glass slide
photomask, UV
liquid application
liquid droplets
PFPE „slippery“ barriers
(B)
DMSO droplets
PFPE barriers
(C)
(D)
I.
II.
Ethanol droplets
PFPE barriers
(E)
(F)
(G)
I.
II.
III.
IV
(H)
aqueous droplets
(I)
PFPE border
olive oil droplets

Figure 4.1. Strategy for liquid patterning on porous poly(2-hydroxyethyl methacrylate-co-ethylene dimethacrylate) (HEMA-EDMA) polymer. A) Schematic representation of the manufacturing process of surface patterned HEMA-EDMA and subsequent infusion with liquids into defined compartments. B) Photographs of an array where hydrophilic patterns are differentially wetted with rhodamine-containing DMSO while superhydrophobic borders are wetted with a perfluorinated oil (PFPE). (C) Photograph of the production of such an array by discontinuous de-wetting. Images of ethanol droplets (D) (scale bar corresponds to 3 and 2 mm respectively), silicone oil droplets (E) (scale bar corresponds to 1 mm), mineral oil (F) (scale bar corresponds to 2 mm), and N-hexane (G) droplets (scale bars correspond to 350 μm, 350 μm, 350 μm and 1 mm) formed on hydrophilic patterns of different shapes. (H) Photograph of water droplets stained with food dyes separated by small borders – the smallest being just 50 μm. The water droplets were formed on a surface lubricated with surfactant-spiked PFPE (see Materials and Methods). (I) Photograph of mineral oil drops formed on hydrophilic spots within a PFPE background – the scale bar corresponds to 1 mm.

Surprisingly, there is a difference in contact angle values for PFDT and CH3 substrates infused with the same PFPE lubricant (Table 1). A possible explanation is the presence of defects on the lubricant-infused surfaces that lead to an exposed substrate and the differences in contact angles. In addition, the number of defects should depend on the type of surface functionality, thereby making such liquid-infused surfaces even more different.

Table 4.1 List of tested liquids

Liquid Name	*Surface tension [mN/m] @ 20°C*	*Density [g/cm³] @ 20°C*
Water	72[163]	0.998
Glycerol	64[163]	1.261
Diiodomethane (DIM)	50.8[163]	3.325
DMSO	43.54[163]	1.1004
Dimethylformamide (DMF)	37.10[163]	0.948
Cyclohexanol	34.4 (at 25°C)[163]	0.9624
Mineral oil light – bioreagent	32[164]	0.8
Toluene	28.40[163]	0.87
n-Hexadecane	27.5[163]	0.77
Dichloromethane	26.5[163]60	1.3266
Ethanol	22.10[163]	0.810
Silicone oil 10 cSt	20.1 (at 25°C)[165]	0.95
Krytox GPL 103 (PFPE)	20[166]	1.88
n-Hexane	18.43[163]	0.6606
FC40	16[167]	1.855

The roughness of the porous HEMA-EDMA layer and its capillary network are key to forming stable liquid-infused surfaces and liquid-liquid patterns. On a smooth surface, exposing perfluorodecanethiol (PFDT) functional groups (see Feng et al.),[168] PFPE cannot be stabilized and does not form a stable liquid layer. On the rough PFDT-modified HEMA-EDMA surface, however, stable PFPE liquid layers can be formed. The ‘slipperiness’ of a surface is characterized by low contact angle hysteresis or low sliding angles.[114, 152] The sliding

angles of different liquids on PFPE-lubricated PFDT-modified HEMA-EDMA are small enough to classify this lubricant-infused surface as slippery, and the contact angle hysteresis (CAH) was also significantly reduced. Organic solvents (e.g., hexane, ethanol, toluene, dichloromethane, dimethyl formamide, DMSO) exhibited sliding angles of around 5° (Table 3) and CAH values were reduced to around 10° (Figure 2A).

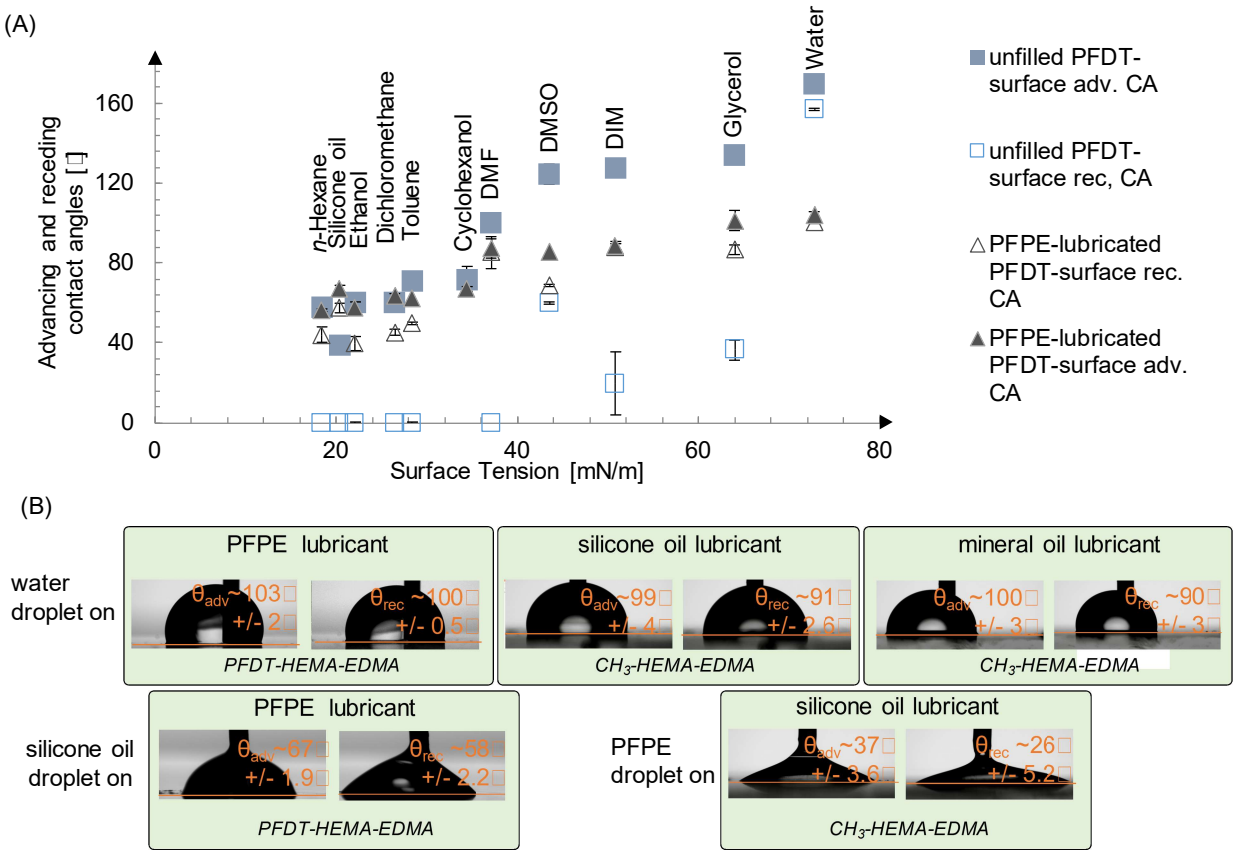

Figure 4.2. Change in material properties through lubrication with oil. A) Change in advancing and receding angles of surfaces between dry state and upon lubrication with PFPE for standard liquids. B) Advancing and receding angles of water (upper row) as well as silicone oil/ PFPE (lower row) on alkylated poly(2-hydroxyethyl methacrylate-co-ethylene dimethacrylate) polymer lubricated by either mineral oil (right) or silicone oil (middle) or perfluorinated and lubricated by PFPE (left).

Table 4.3. Sliding angles of solvents on PFDT-functionalized, PFPE-infused HEMA EDMA

Liquid Name	*Sliding angle [°]*
Water	4.85 ± 0.35
Glycerol	6.34 ± 0.5
Diiodomethane (DIM)	4.36 ± 0.25
DMSO	4.49 ± 0.52
Dimethylformamide (DMF)	4.85 ± 0.17
Cyclohexanol	5.38 ± 0.0.53
Mineral oil light - bioreagent	4.9 ± 0.14
Toluene	3.81 ± 0.35
Dichloromethane	4.42 ± 0.2660
Ethanol	5.25 ± 0.61
Silicone oil 10 cSt	4.37 ± 0.4
n-Hexane	5.44 ± 0.5

We then investigated the ability of different liquids to spontaneously replace PFPE-impregnating hydrophilic porous HEMA-EDMA lubricant. We found that all studied liquids could replace PFPE from the pores of the hydrophilic polymer (Table 2). Lower surface tension liquids, such as ethanol and DMSO, pinch more readily to the underlying surface (Video S1). It took around 15 to 20 seconds for water to pinch on a PFPE-lubricated surface (Video S3), while it took only around 1 second for ethanol to replace the lubricant on this surface (Video S1 and S1). The replacement took place even with liquids less dense than that of PFPE.

Table 4.2. Overview of tested combinations between lubricant, surface patterning and intruding liquid.

Infusing liquid	Water	Mineral Oil			Silicone Oil			PFPE		
Substrate´s chemistry	OH	PFDT	CH3	OH	PFDT	CH3	OH	PFDT	CH3	OH
Intruding liquid										
PFPE	θadv 0 θrec 0	d	θadv 0 θrec 0	θadv 0 θrec 0	d	θadv 37 θrec 26	θadv 34 θrec 31	-	-	-
Silicone oil	θadv 0 θrec 0	D	d	d	-	-	-	θadv 67 θrec 58	d	d
Mineral oil	θadv 0 θrec 0	-	-	-	θadv 40 θrec 0	θadv 29 θrec 0	θadv 30 θrec 0	θadv 74 θrec 50	d	d
Cyclohexanol	θadv 0 θrec 0	Miscible	Miscible	Miscible	θadv 26 θrec 13	θadv 50 θrec 42	D	θadv 67 θrec 48.5	d	d
Water	-	θadv 101 θrec 60	θadv 100 θrec 90	d	θadv 113 θrec 81	θadv 99 θrec 91	D	θadv 103 θrec 100	θadv 121 θrec 83	d

d = displacement of the infused liquid by the intruding liquid;

θadv = advancing contact angle of the intruding liquid on a corresponding liquid-infused surface;

θrec = receding contact angle of the intruding liquid on a corresponding liquid-infused surface;

Hydroxylated: OH; Perfluorinated: PFDT; Alkylated: CH3; Standard deviations can be found in the supplementary information.

Krummel et al.[169] and Datta et al.[170] demonstrated that the complete displacement of oil in a porous substrate through the wetting fluid is achievable, provided the capillary number (the relative effect of viscous forces versus surface tension) rises above a certain threshold value. We observed that when a solvent was applied on a patterned SLIPS, the lubricant was displaced from the hydrophilic pattern (see Figures S1 and S2). Thus, cells could be grown in the hydrophilic patterns from which the lubricant had been replaced (see Figure S3). Interestingly, after the evaporation of the solvent, PFPE did not flow into the dried hydrophilic features again (but in a reverse pattern, PFPE features would flow out into the dried background – see Video S5) if the access PFPE had been removed with an air gun prior to the experiment. On the other hand, the PFPE lubricant could not be replaced by any of the used liquids from the PFDT-modified regions. The exception was hexane. Even though it did not wet PFPE-infused PFDT-borders when wetting dried features with hexane, small PFPE droplets were pulled from the borders into the hexane phase (see Figure S2 and Video S4). However, n-hexane would stay confined to the hydrophilic features (see Figure 1 and S4).

By combining superhydrophobic PFDT-modified with hydrophilic porous polymer regions on the same surface, it becomes possible to achieve spatially controlled selective de-wetting of the PFPE lubricating liquid with different solvents (Figure 1). Such patterned surfaces can serve as a template for an array of high and low surface tension liquids.[54] As shown in Figure 1, porous HEMA-EDMA patterned with either hydrophilic (HL) or fluorinated (PFDT-modified) regions is completely wetted with PFPE lubricant. However, the PFPE oil is displaced from the HL parts (and not from the PFDT areas) after introducing a secondary liquid, such as n-hexane, silicone oil, ethanol, water, DMSO, etc. (Figure 1B-D). This leads to a binary liquid-liquid pattern of the higher surface tension liquid in HL parts and lower surface tension liquid in the PFDT-regions. Thus, by a simple, two-step process, non-miscible liquids can be spatially arranged into precise two-dimensional compartments (Figures 1, S1). The homogeneity of the heights of droplets was measured by sliding a 100 µL droplet down a 30°-inclined pattern of hydrophilic 3 mm circles in a PFDT-background and measuring the heights of 10 droplets. The heights of glycerol, DMSO, and n-hexadecane droplets varied by 0.1%, 4.8%, and 3.5%, respectively (Figure S3). Droplets could be formed both on features of several millimeters in diameter as well as on small features down to 40 µm in width (see Figure S5).

Modifying HEMA-EDMA with dodecanethiol[49] instead of PFDT by a thiol-yne click reaction created a hydrophobic but non-fluorinated surface with advancing and receding WCAs being 154±2 and 82±4, respectively, as well as 85±3 and 0 CAs for DMSO. However, the alkylated porous surface allowed the formation of slippery surfaces with oil types other than the perfluoro lubricants (Figures 3B, 4). When infused with either silicone or mineral oils, dodecanethiol-modified HEMA-EDMA exhibited a stable lubricant film that could not be washed off with water or even perfluoro oils. On both oil-infused surfaces, non-miscible liquids (such as water and silicone oil DMSO) exhibited roll-off and hysteresis angles close to 0 (Table 2). However, while silicone oil-infused surfaces were slippery for perfluorocarbon solvents such as PFPE and FC40, as reported elsewhere,[43] mineral oil-infused surfaces were not. Perfluorinated oils would readily wet and spread on mineral oil-infused dodecanethiol-modified HEMA-EDMA (Table 2). Thus, spatially controlled droplets of PFPE and FC40 could be created using silicone oil-infused borders (Figures 3 and S6). In contrast to higher surface tension liquids, PFPE droplets varied in height by 25% when formed on PFDT-modified 3 mm diameter circles in a dodecanethiol-modified background (Figure S5).

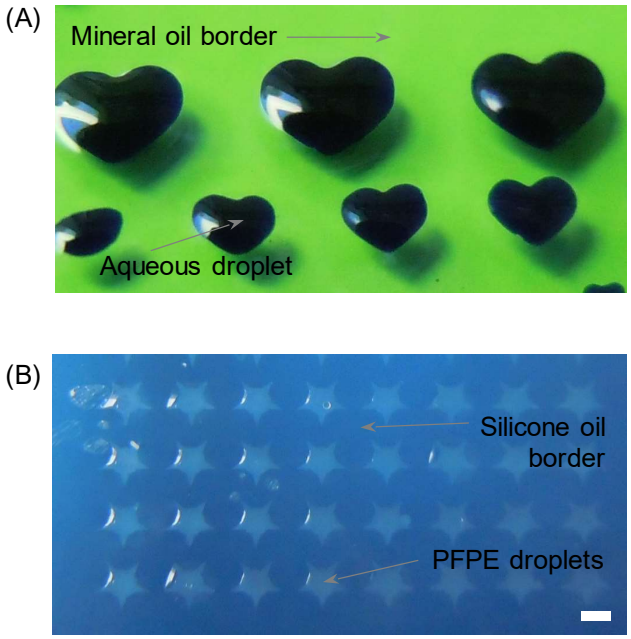

Figure 4.3. Droplet formation on alkylated surfaces. (A) aqueous droplets formed on mineral oil-lubricated alkylated polymer. (B) PFPE droplets formed on silicone oil-lubricated alkylated polymer. Scale bars represent 1 mm.

The ability to pattern any two liquids on the same substrate next to each other has various applications, e.g., in liquid-liquid extractions,[55] chemical process design,[171, 172] and microfabrication research, such as tuneable micro-lenses[173, 174] to list a few. One of the applications is to use such liquid patterning to stably position an oil shield around an aqueous compartment to avoid evaporation of small aqueous reservoirs. Aqueous droplets evaporate fast on an open surface if not protected from the environment. To circumvent this problem, droplets can be covered with a layer of oil. However, shielding droplets via a continuous oil layer can lead to cross-contamination between aqueous compartments.[175] Instead, it is advisable to shield each droplet via an individual oil layer not connected to neighboring aqueous compartments. To realize this, HL circles (1.5 mm in diameter) were surrounded by alkylated SH 4 mm wide rings, which were again surrounded by PFDT-modified borders (Figure 4). The surface was then covered with a PFPE layer, followed by a sequential replacement of the fluorinated oil from the hydrophilic spots by water and then from the alkylated rings by a mineral oil to form aqueous compartments in the hydrophilic spots covered by individual mineral oil droplets kept fixed on the surface with the alkylated rings. Thus, a three-phase array of water-in-oil-droplets separated by a slippery PFPE-infused surface was created (Figure 4). Such arrays of shielded aqueous compartments can have applications, for example, in DNA sequencing, related nucleotide operations,[176] enzymatic assays and protein crystallization,[137, 177, 178] as well as in cellular assays requiring long term stability of water droplets. The water-oil structures were kept stable by the surrounding slippery PFPE border for at least 4 weeks. Figure 4 demonstrates the ability of such a system to significantly reduce the evaporation of aqueous droplets even after heating the sample at 100°C for 5 minutes.

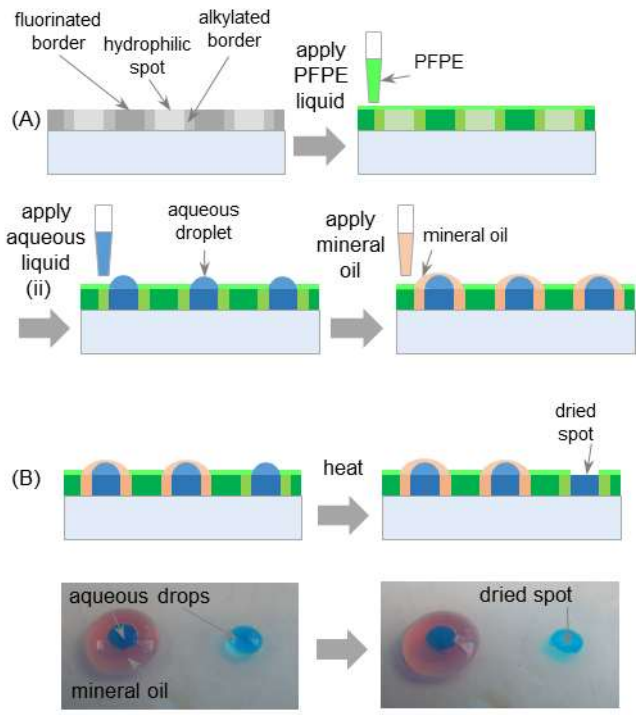

Figure 4.4. Formation of evaporation-resistant compartments. A) Schematic representing the three-phase system enabled through surface patterning of perfluorinated, alkylated and hydrophilic patches next to each other. B) Photographs of a mineral oil protected droplet next to an unprotected droplet before (left) and after (right) heating.

4.3 Conclusion

In conclusion, we demonstrate that by choosing the appropriate chemical surface patterning, liquid-liquid displacement can be spatially controlled for a wide range of lubricant-intruding liquid pairs. Arrays of both high and low surface tension liquids can thus be formed on a single surface. Spontaneous formation of droplet microarrays on slippery lubricant-infused surfaces pre-patterned with matching surface chemistry was shown. The resulting arrays of an intruding liquid follow precisely the underlying surface patterning with, for example, circular, square or other geometries. By modifying the same porous polymer surface with patterns of aliphatic alkyl groups, hydroxy and perfluoro groups, three-phase liquid micropatterns – fluoro, organic, aqueous – could be formed. This approach demonstrates the potential of three immiscible liquids being patterned adjacently in arbitrary droplet shapes as long as the matching lubricant-intruding liquid pair and corresponding surface chemistries have been carefully chosen. This flexibility carries enormous potential for the miniaturization of various processes where liquids of varying surface tensions need to be patterned, confined or manipulated on surfaces or in channels.

4.4 Materials and Methods

4.4.1 Chemicals

2-Hydroxyethyl methacrylate, ethylene dimethacrylate, 2,2,3,3,3-pentafluoropropyl methacrylate (PFPMA), trichloro(1H, 1H, 2H, 2H-perfluorooctyl)silane, 2,2-dimethoxy-2-phenylacetophenol, benzophenone, cyclohexanol, 1-decanol, rhodamine B, mineral oil, were purchased from Sigma-Aldrich (Taufkirchen, Germany) at purity >97%.

Krytox GPL 103 was purchased from DuPont (Hamm, Germany). FC40, as well as PicoSurf2TM, were supplied by Dolomite Microfluidics (Royston, UK). The quartz photomask was developed with Autodesk Inventor 2011 software and manufactured by Rose Fotomasken (Bergisch Gladbach, Germany). Glass plates were obtained from Schott Nexterion (Mainz, Germany). All other chemicals were purchased from Carl Roth (Karlsruhe, Germany).

4.4.2 Hydrophobic/hydrophilic Patterned Surface Fabrication

Glass slides were activated by submerging in 1M NaOH for 30 minutes, followed by thorough rinsing with mQ H2O. Then, the slides were left in 1M HCl for one hour and rinsed with water again. After drying, slides were modified by a 20% (v/v) 3-(trimethoxy silyl)propyl methacrylate (Sigma-Aldrich) in ethanol. To avoid the formation of air bubbles, a 70 µL modification solution was evenly applied twice between the active sites of two glass slides for 30 minutes. Glass slides were washed with acetone. Fluorinated glass slides were prepared for the manufacturing of polymer surfaces. For this, activated glass slides were incubated overnight in a vacuumed desiccator in the presence of trichloro(1H, 1H, 2H, 2H-perfluorooctyl) silane.

Polymerization solution consisted of polymers (24% wt. 2-hydroxyethyl methacrylate as monomer and 16% wt. ethylene dimethacrylate as a cross-linker) as well as an initiator (1% wt. 2,2-dimethoxy-2-phenylacetophenone) dissolved in 1-decanol (12% wt.) and cyclohexanol (48% wt.). The 60 µL polymerization mixture was pipetted onto modified glass slides. These were then covered by fluorinated glass slides separated through 15 µm silica bead spacers from modified glass slides. Slides were irradiated for 15 minutes with 5.0 to 4.0 $mW \cdot cm^{-2}$, 260 nm UV-light. The mould was then carefully opened using a scalpel and polymer washed for at least 2h in ethanol.

Hydrophilic polymer surfaces were esterified by immersion of 2 slides in 50 mL dichloromethane containing 4-pentynoic acid (111.6 mg, 1.14 mmol) and catalyst 4-(dimethylamino)pyridine (DMAP) (56 mg, 0.46 mmol) at -20°C. After 20 min, 180 µL coupling reagent N,N′-diisopropylcarbodiimide (DIC) was added, and the solution stirred at room temperature for at least 4h or overnight. Esterified slides were washed in ethanol for 2h.

The patterning of esterified slides was based on photomask lithography. Slides were irradiated either with “superhydrophobic” or “hydrophilic” click-chemistry solution first under the pattern of choice, followed by washing with acetone and drying. In a second step, slides were wetted with the complementary solution, covered with a quartz slide and irradiated with UV.

Superhydrophobic click-chemistry solution 1 was always prepared fresh by dissolving 10% vol./vol. 1H,1H,2H,2H-perfluorodecanethiol in ethyl acetate. Hydrophilic solution 2 consisted of 2-mercaptoethanol (10% vol./vol.) dissolved in a 50:50 vol./vol. ethanol/water mix.

In the first patterning step, slides were wetted with 200 µL solution 1 in the dark. Slides were covered by the desired photomask pattern and irradiated for 2 minutes (5.0 mW•cm-2, 260 nm). After irradiation, the slides were rinsed twice with acetone in the dark. They were wetted with solution 2 and covered by a quartz slide. Immediately after, slides were irradiated for 2 minutes by UV again (5.0 mW•cm-2, 260 nm) and subsequently washed for at least 2h in ethanol before use.

4.4.3 SEM Images

Patterned HEMA-EDMA slides were coated with gold particles, and images were taken using a thermal field emission SEM using an FE-REM (type Merlin, Zeiss).

4.4.4 Contact and Sliding Angle Measurements

60 µL of PFPE were applied and allowed to spread evenly for all contact and sliding angle measurements. If any other lubricant was used, 60 µL of the lubricant was spread on the surface. To obtain surfactant-spiked PFPE, a 2% wt./wt. stock solution of PicoSurf2TM (Dolomite, Royston, UK) dissolved in FC40 was mixed 1:3 with pure PFPE solution, and the FC40 was allowed to evaporate.

Advancing and receding contact angles (for Figure 2) were determined by an inhouse-build system encompassing a UK1117 camera (EHD imaging GmbH, Damme, Germany), a stage

and 5 µL syringe (Hamilton, Bonaduz, Switzerland) connected to a pump operating at stable flow speed (15 µl/min). Images were taken at 100 ms per frame. Contact angles were measured using the ImageJ plug-in DropSnake.[64], [65] For each condition measured, 3 slides were used, and advancing/receding angles were measured on 5 different positions on each chip. Sliding angles were determined manually on an adjustable angle stage. For Table 2, advancing and receding contact angles were measured 3 times on 2 different surfaces using a Krüss contact angle goniometer (Hamburg, Germany). For this, the liquid was either flushed from or sucked into the syringe at a rate of 2.67 µL/min and videos were recorded.

4.4.5 Cell Culture

Human Cervical tumor cell line HeLa expressing GFP was purchased from BioCat (Heidelberg, Germany). Cell lines were cultured in DMEM (Gibco, Life Technologies GmbH, Darmstadt, Germany), supplemented with 10% (vol./vol.) FBS (Sigma), and 1% of Penicillin/Streptomycin (Gibco, Life Technologies GmbH, Darmstadt, Germany). Additionally, the HeLa growth medium was supplemented with 0.2% G418 (Gibco, Life Technologies GmbH, Darmstadt, Germany). Cells were cultured at 37°C in a humidified atmosphere of CO2 and 95% air. The cultured cells were observed with an inverted light microscope (CKX 31 Olympus, Japan). Once cells covered ~75-80% of the culture dish, they were trypsinized using 0.25% trypsin/EDTA (Gibco, Life Technologies GmbH, Darmstadt, Germany) and diluted in fresh medium – using a blood cell counting chamber (Neubauer, celeromics, Cambridge, UK) – to a density of 15–20×103 cells/cm2.

For seeding onto superhydrophobically/hydrophilically patterned HEMA-EDMA lubricated with surfactant-spiked PFPE, a drop of a cell containing medium was slid over the patterns; small parts of the medium attached to hydrophilic spots, thus forming micro-droplets of cell-containing growth medium. Alternatively, a large drop of 500 µL was laid over several hydrophilic spots and allowed to rest in order that cells could sediment down. After 30 seconds, the array slide was tilted, allowing excess liquid to flow off. Fluorescent images were taken with a Keyence BZ-9000 fluorescent microscope (Osaka, Japan).

4.4.6 Microscopic Imaging

All microscopic bright field images and videos were taken with a Keyence BZ-9000 fluorescent microscope (Osaka, Japan).

4.5 Supporting Information

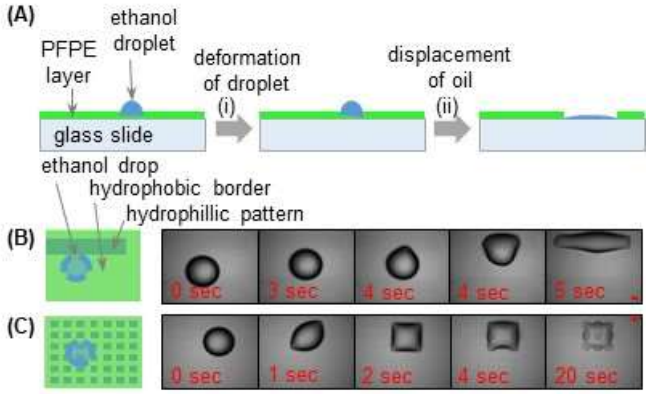

Figure S4.1. Mechanism of droplet formation. A) Schematic representing oil film thinning and subsequent deformation of an (i) intruding liquid droplet until (ii) it pinches on the surface. Snapshots of pinching of intruding ethanol drop on stripe (B) or square patterns (C). Scale bars correspond to 1 mm.

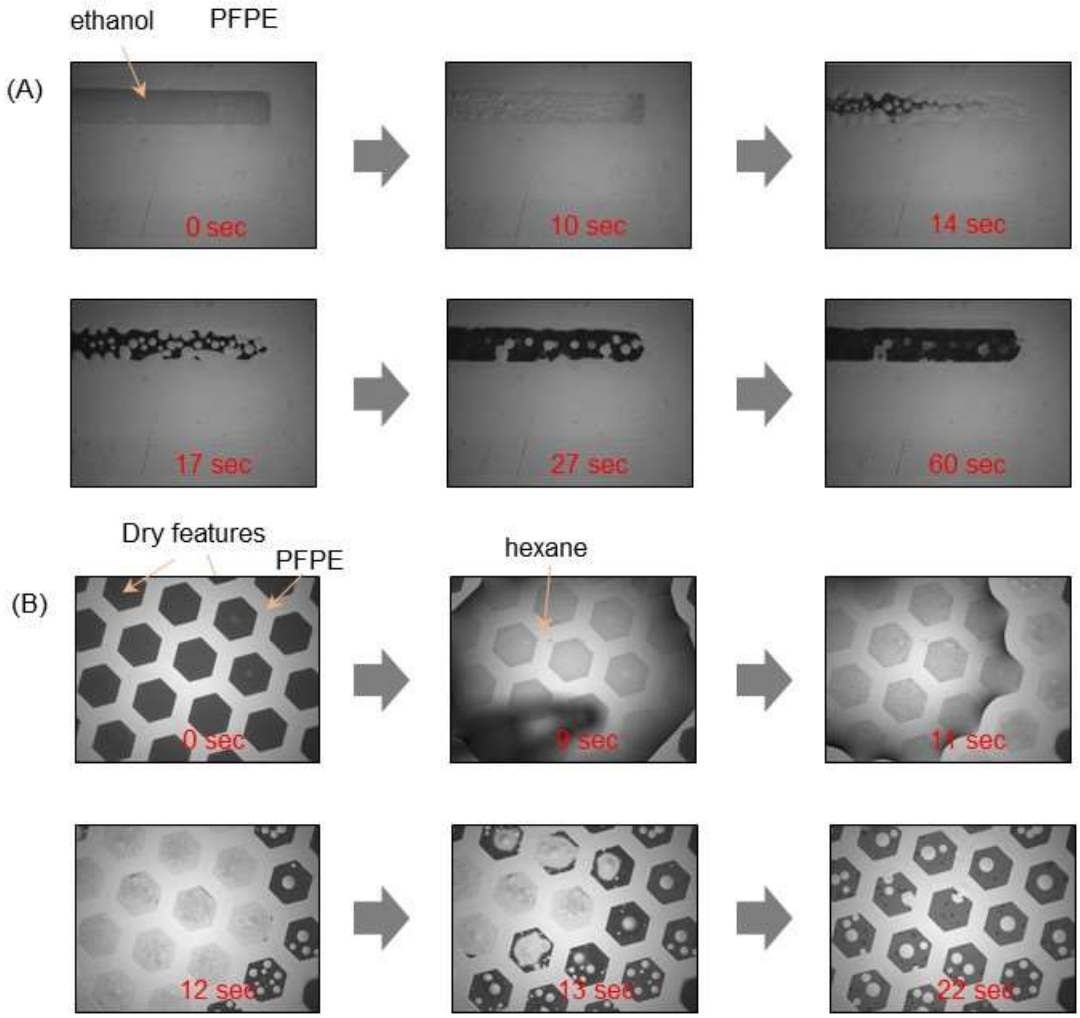

Figure S4.2. Drying of hydrophilic parts after organic solvent exposure. (A) Ethanol evaporating from a rectangle, hydrophilic features surrounded by perfluoropolyether-lubricated borders. (B) A hexane drop is placed on empty, dry hydrophilic features surrounded by perfluoropolyether-lubricated borders. It evaporates from these features pulling small perfluoropolyether droplets into the features.

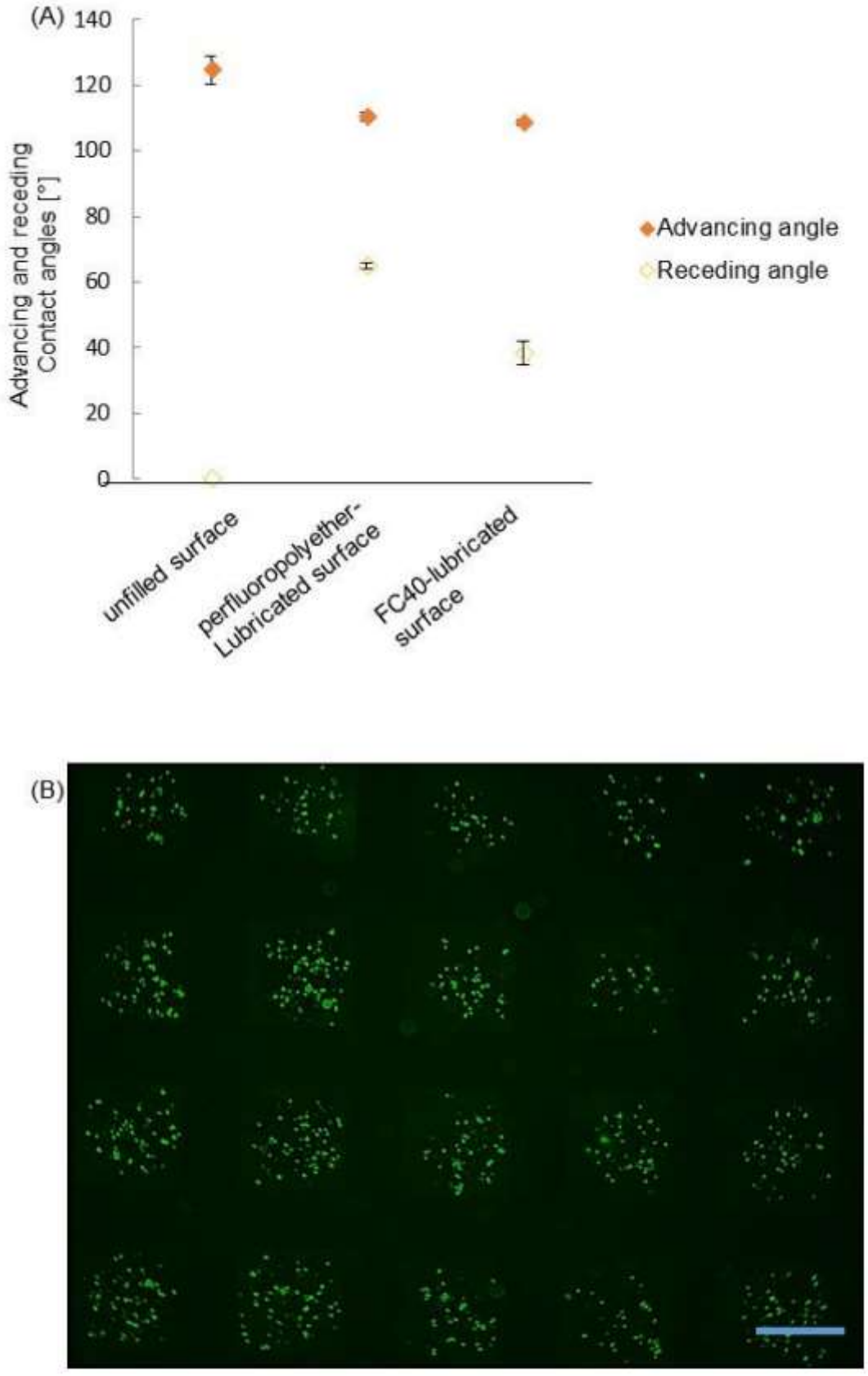

Figure S4.3. Suitability of patterned slips for the handling of complex biological liquids. (A)

Advancing and receding contact angles of cell growth medium on an unfilled surface, perfluoropolyether-lubricated or FC40-lubricated surfaces. (B) GFP-expressing HeLa Cells growing on hydrophilic patterns surrounded by perfluoropolyether-lubricated borders.

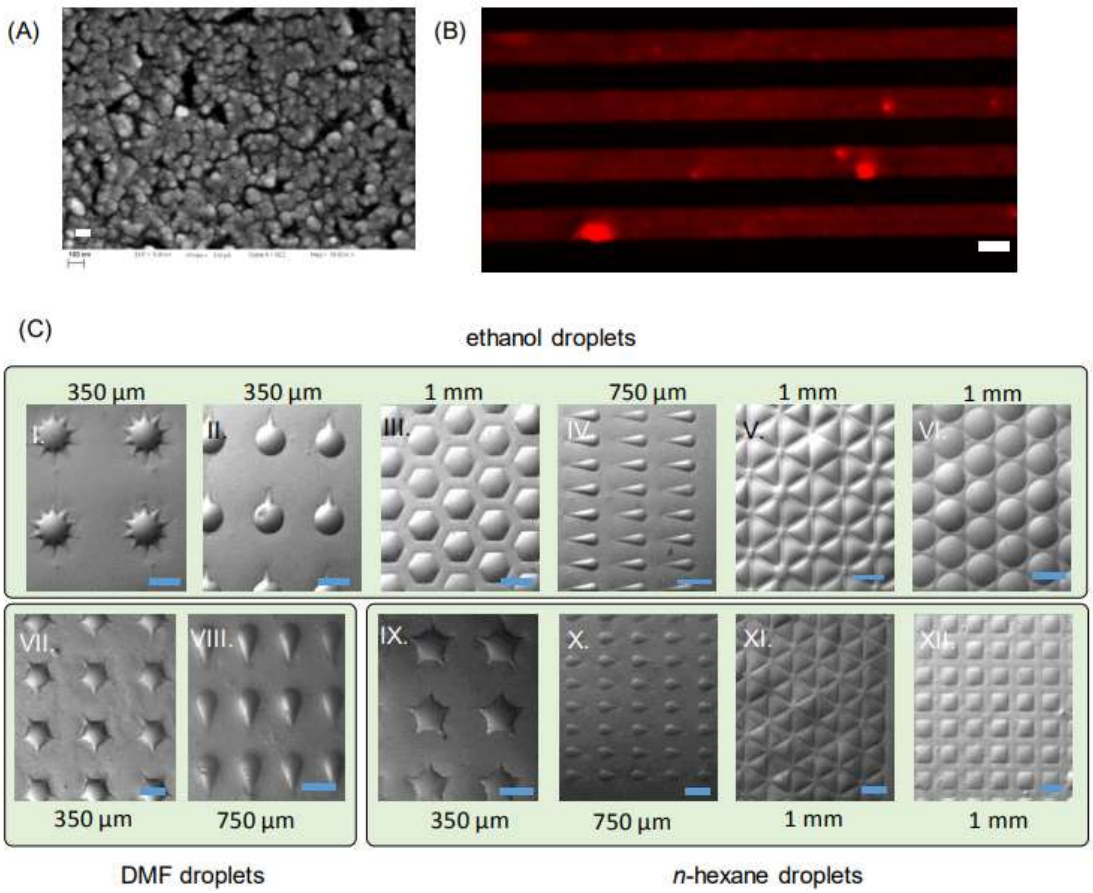

Figure S4.4. Low-surface tension droplet arrays on PFPE-lubricated PFDT-surfaces. A) SEM image of the surface of HEMA-EDMA (Scale bar represents 100 nm). B) 40 µm wide *n*-Heptane stripes stained with red-fluorescent Nile Red on PFPE-lubricated polymer (black) with a 40 µm wide scale bar. C) Low-surface tension droplet arrays: Images I. to VI. correspond to ethanol droplets, VII. To VIII. To DMF droplets, and IX. to XII. to n-hexane droplets. The length of the scale bar is written above (upper row) or below (lower row) the corresponding image.


PFPE
N-Hexadecane
DMSO
Glycerol

Figure S4.5. Height profiles of Droplets. Droplets were formed by allowing 100 µL droplets of intruding liquid to slide down a 30°-inclined pattern of 3 mm wide circles. Surfaces were either infused with PFPE (for glycerol, DMSO, and n-hexadecane droplets) or 20 cSt silicone oil (for PFPE droplets). Blue lines correspond to the measured height profile of droplets and their reflections.

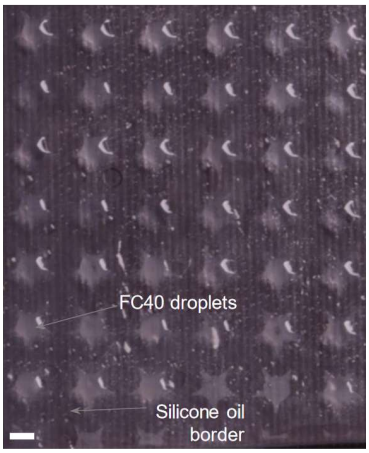

Figure S4.6. FC40 droplets formed on PFDT-modified star patterns in a silicone oil-lubricated alkylated polymer background. Scale bars represent 1 mm.

Table S1. Overview of tested combinations between lubricant, surface patterning and intruding liquid.

Infusing		Water	Mineral Oil			Silicone Oil			PFPE		
Intruding		OH	F	CH3	OH	F	CH3	OH	F	CH3	OH
PFPE		θadv 0 θrec 0	d	θadv 0 θrec 0	θadv 0 θrec 0	D	θadv 37 ±4 θrec 26+/-5	θadv 34+/-0.5 θrec 31+/-1	-	-	-
Silicone oil		θadv 0 θrec 0	d	D	d	-	-	-	θadv 67+/-2 θrec 58+/-2	d	d
Mineral oil		θadv 0 θrec 0	-	-	-	θadv 40+/-2.7 θrec 0	θadv 29+/-2 θrec 0	θadv 30+/-4 θrec 0	θadv 74+/-3.25 θrec 50+/-3.5	d	d
Cyclohexanol		θadv 0 θrec 0	miscible	Miscible	miscible	θadv 26+/-3 θrec 13+/-2	θadv 50+/-1 θrec 42+/-2.5	d	θadv 67+/-1 θrec 48.5+/-1.45	d	d
Water		-	θadv 101+/-0.5 θrec 60+/-7	θadv 100+/-3 θrec 90+/-3	d	θadv 113+/-0.5 θrec 81+/-2	θadv 99+/-4 θrec 91+/-3	d	θadv 103+/-2 θrec 100+/-0.5	θadv 121+/-5 θrec 83+/-0.5	d

d = displacement of the infused liquid by the intruding liquid;

θadv = advancing contact angle of the intruding liquid on a corresponding liquid-infused surface;

θrec = receding contact angle of the intruding liquid on a corresponding liquid-infused surface;

Hydroxylated: OH; Perfluorynated: F; Alkylated: CH3;

Overview of Videos:

S4.1 Ethanol droplet on hydrophilic square pattern with PFPE-lubrication

A 2 µL ethanol droplet is placed on an all PFPE-lubricated surface. The underlying surface is patterned with PFDT-borders and hydrophilic 500*500 µm square patterns. In the video, the droplet pinches first on one square and starts displacing the lubricant from the hydrophilic features. Then, it pinches on neighboring squares and displaces the lubricant from them. When the droplets dry they leave dried, non-transparent polymer behind them. Since the PFPE lubricant was applied in excess on the surface (100 µL onto a single microscopic glass slide with a 15 µm high polymer layer), it starts flowing into the patterns again. However, this does not happen through fingering but by homogenous shifting of the PFPE-void interface into the pattern.

S4.2 Ethanol droplet on hydrophilic stripe pattern with PFPE-lubrication

A 2 µL ethanol droplet is placed on an all PFPE-lubricated surface. The underlying surface is patterned with PFDT-borders and hydrophilic stripe patterns. In the video, once the droplet pinches first on one stripe, it instantaneously extends into the whole stripe pattern, displacing the lubricant from it. When it starts drying, PFPE droplets that had been trapped in the pattern are mobilized and fuse into the PFPE-lubricated border. Since excess PFPE had been blown away from the surface prior to the video, the PFPE lubricant will not flow into the dried hydrophilic stripe pattern again, but stays confined to the PFDT-modified borders.

S4.3 Water droplet on hydrophilic square pattern with PFPE-lubrication

A 2 µL water droplet is placed on an all PFPE-lubricated surface. The underlying surface is patterned with PFDT-borders and hydrophilic 500*500 µm square patterns. In the video, the droplet pinches first on one square and starts displacing the lubricant from the hydrophilic features. However, in contrast to ethanol, it does not displace the lubricant from the entire feature but only a subset of the feature. Also, the water droplet does not undergo as profound a shape transformation as the ethanol droplet. In contrast to ethanol, the water droplet is easily detached with a pipette from the features again, leaving small water droplets attached to the hydrophilic features. These do not fill out complete hydrophilic features.

S4.4 n-Hexane droplet on dried hydrophilic pattern with PFPE-lubricated borders

On a microscopic glass slide with a 15 µm high polymer layer that is patterned with octagonal hydrophilic features with PFDT-patterned borders, 70 µL PFPE lubricant is applied, and excess lubricant is blown off with an air gun. Ethanol droplets are formed by dipping the slide into ethanol and then dried off again with an air gun. This results in a slide with transparent, lubricated PFDT-borders and dried, non-transparent hydrophilic features. In the video, 20 µL of n-hexane is applied onto this slide and sucked up by the pipette again. It can be observed how, during solvent application and drying, PFPE droplets enter the previously PFPE-free features. The features remain slightly transparent, i.e., wetted by lubricant, with pronounced PFPE droplets inside them, after n-hexane has dried completely.

S4.5 PFDT-features (circles) in a hydrophilic background onto which ethanol is applied

40 µL of ethanol is applied onto a PFPE-lubricated slide with alkylated borders and PFDT-patterned circle features. The ethanol displaces the PFPE lubricant from the alkylated borders. When it dries, it leaves dried, non-transparent alkylated borders in which some PFPE droplets are trapped beside the formed PFPE circle features. Once the ethanol has dried completely, the PFPE starts flowing out of the PFDT features into the alkylated borders. In this process, the interface between PFPE and void is diffusive and not as sharply defined as in video S5.

S4.6 DMSO droplet applied to all hydrophilic, patterned and all SH-surface lubricated with PFPE

A 5 µL DMSO droplet stained with rhodamine is applied to different all PFPE-lubricated surfaces. The first one is all PFDT-modified, and when the DMSO droplet is applied to it, the DMSO droplet forms a perfect sphere. When placed on a surface with a hydrophilic stripe pattern, the droplet will extend along the hydrophilic stripe until it perfectly follows the underlying shape. Once placed on an all hydrophilically modified HEMA-EDMA surface lubricated with PFPE, the droplet will immediately displace the PFPE from all regions it touches and can extend into.

S4.7 Water and ethanol droplet on PFPE lubricated, alkylated surface with PFDT-features

A surface is patterned with PFDT star features in an alkylated background and lubricated with PFPE. A 2 µL droplet of water is placed on the lubricated surface. In the video, the droplet of water, which remained a perfect sphere on the surface, is dragged over the

surface using a pipette tip. When placing a 2 µL ethanol droplet onto the surface next to the water droplet, the ethanol drop immediately pinches on the surface and extends into the alkylated parts, displacing the lubricant from it. Once the droplet dries, it leaves behind an empty void into which excess PFPE slowly flows.

5. Droplet sorting and manipulation on a patterned two-phase slippery lubricant-infused surface.

D Paulssen[1], S Hardt[2], PA Levkin[1]*

1 Institute of Toxicology and Genetics (ITG), Karlsruhe Institute of Technology (KIT), 76344 Eggenstein-Leopoldshafen, Germany

2 Institute for Nano- and Microfluidics, Technische Universität (TU) Darmstadt, 64287 Darmstadt, Germany

*Corresponding author: levkin@kit.edu

ABSTRACT Slippery lubricant-infused surfaces are composite materials consisting of a solid matrix permanently infused with a lubricant. Such surfaces proved to be highly repellent to various liquids immiscible with the lubricant. Depending on the underlying surface chemistry, different lubricants can be used, including perfluorinated or alkylated oils. Here, we construct patterned slippery surfaces that consist of virtual channels permanently impregnated with an organic oil and surrounded by areas permanently impregnated with a perfluorinated oil. We demonstrate that water droplets preferentially occupy the organic-oil lubricated virtual channels. Based on a simple model, we evaluate the forces acting on droplets crossing over to the regions impregnated with perfluorinated oil and show that the cloaking of the droplets plays an important role. We study the actuation of droplets in virtual oil-in-oil channels based on gravity and magnetic fields. Finally, we construct a variety of organic oil-lubricated channel architectures permitting droplet sorting according to size. We believe that the novel approach to the formation of virtual all-liquid surface tension-confined channels based on lubricant-infused surfaces, channel networks or patterns will advance the field of droplet-based microfluidics. The presented approach can be useful for applications in biotechnology, diagnostics or analytical chemistry.

KEYWORDS: Droplet Microfluidics, Patterned Slippery Surfaces, Open Microfluidics, Liquid-Liquid Interfaces

Published in *ACS Appl. Mater. Interfaces* https://doi.org/10.1021/acsami.8b21879

5.1 Introduction

Controlled manipulation of droplets on open planar substrates is a key capability in numerous research areas ranging from energy and water harvesting[179] systems to diagnostics and point-of-care systems, as well as digital microfluidics.[180, 181] Droplet sorting, that is, discrimination between droplets with different cargo, is of importance[182] for applications in diagnostics and bio-sensing,[183] in micro-reactors,[184] as well as in drug discovery.[185] A powerful sorting approach should be adaptable to the specific application and capable of separating droplets with different properties. There are two different approaches to sorting: active and passive.[183] While the former requires the active stimulation of the microfluidic environment to guide droplets into new paths, the latter term describes a microfluidic environment that is, by design, biased towards differing droplet types, i.e., deflects them into different paths. Passive sorting has advantages over active sorting, such as higher robustness and higher throughput.[183] So far, only active sorting has been realized in digital microfluidics.[186] However, four passive sorting mechanisms have been proposed on open planar surfaces based on either mass or interfacial tensions of the droplets.[106, 187-189] In this context, droplets are either deflected at different angles when moving along a surface or become immobilized in different zones of a surface. While the former bears the disadvantage that differences in deflection may be minute and droplets must travel long distances to be truly separated, the latter suffers from permanent immobilization of droplets on surfaces. Thus, further separation strategies for droplets are needed.

Recently, lubricant-infused surfaces (LIS) have been proposed for droplet manipulation due to very low sliding angles (<5°) that allow for droplet actuation by low energy methods, such as weak electric[190] or magnetic fields[191] and that even viscous fluids can be easily actuated on slippery LIS.[191] So far, droplets have been manipulated on LIS by gravitational,[123] magnetic,[192, 193] surface-acoustic wave,[194] thermocapillary[16] or electric actuation.[195] LIS are created through the entrapment of a lubricant in a porous or textured surface.[110, 154] Various liquid types immiscible with the lubricant are repelled from such surfaces, given that the lubricant possesses a higher affinity to the surface than the intruding liquid.[118] The surface of the composite material is exceptionally smooth and chemically homogenous, leading to extremely low contact angle hysteresis.

To define pathways for droplets, You et al.[123] introduced repellent hydrophilic patches in a slippery LIS to deflect, slow down and stop droplets actuated by gravity. Such surface patterns and pathways have been studied previously as a design principle for open microfluidic systems based on classical, “dry” superhydrophobic surfaces. Thus, Elsharkawy et al.[196] who altered a hydrophobic path’s width on a superhydrophobic paper background demonstrated control over droplet sliding angles in this manner - slowing down or halting actuated droplets. However, in contrast to slippery LIS, dry-repellent and patterned surfaces have been shown to be capable of sorting droplets according to size. Thus, Kusumaatmaja and Yeomans proposed that droplets on superhydrophobic surfaces patterned with hydrophilic stripes can be sorted according to size or wetting properties.[100] Their simulations were later confirmed by Suzuki et al.,[106] who experimentally sorted droplets according to size on superhydrophobic surfaces that consisted of a strip pattern of alternating alkylated and fluorinated regions.

In the present work, we explore the potential of two-phased patterned slippery LIS to manipulate the paths of droplets and sort them, thereby introducing novel planar geometries to sort droplets according to size. Alkylated channels in a perfluorinated background were fabricated, and both regions were impregnated with matching liquids: perfluoropolyether (Krytox) and either mineral oil or silicone oil (20 cSt), respectively. We demonstrate that water droplets below a certain size glide along the alkylated channels and are unable to penetrate the surrounding perfluoro phase (Figure 1, 2). Instead, the droplets undergo significant deformations to precisely follow the alkylated channels as if trapped by solid walls (Figure 2 and Supplementary Information Videos S1 and S2). Thus, we demonstrate that droplets in the all-liquid virtual channels could be deflected, slowed down and stopped, depending on the patterning of the underlying path. We exploit this to direct droplets using magnetic forces to dedicated positions. Finally, we take advantage of the ability of droplets to overcome this confinement, depending on their weight and the ratio between droplet size and path width, to passively sort droplets. We show that the resolution of this sorting method can be enhanced by selecting suitable lubricants or by altering the underlying surface patterning. The main purpose

of this work is to demonstrate the principle of all-liquid microfluidics based on patterned LIS and to show the variety of sorting operations possible with oil-in-oil channel structures.

5.2 Results and Discussion

As the basis of the patterned slippery surface, we created a 15 µm thick porous alkyne-functionalized polymer surface with patterns of both alkylated and fluorinated regions formed using the UV-induced thiol-yne reaction. For the patterning, we used polypropylene transparency ink-jet printed to form photomasks (Figure 1). Alkylated features were patterned with dodecanethiol and the background areas with perfluorodecanethiol. An oil-channel system was created by first impregnating the entire surface with a perfluorinated oil (Krytox GPL 103/ perfluoropolyether). Krytox was then displaced from the alkylated regions by placing a drop of either mineral oil or silicone oil on the surface, as described in detail previously.[197] In that case, the mineral oil or silicone oil spontaneously assumes the shape of the underlying surface pattern functionalized with dodecyl groups (Figure 1). Once the double oil patterns were installed, droplets were placed on the features and allowed to glide down the surfaces through gravity. If droplets were deposited on an alkylated region lubricated with mineral oil on a surface inclined by 60° and allowed to run downhill freely, their speed varied after a given distance, ranging from 7 mm/sec for 500 nL droplets to 48 mm/sec for 3 µL droplets after only 2 cm distance traveled. Note, if not stated otherwise, the droplets used in this study consist of water, sometimes containing dyes for better visualization. Here, aqueous droplets between 500 nL and 3 µL would preferentially occupy the mineral oil or silicone oil lubricated regions and would not penetrate the Krytox lubricated background. In this context, channels did not need to be straight but could follow a curved path; droplets deformed on narrower channel sections to be able to strictly follow the oil tracks (Figure 2).

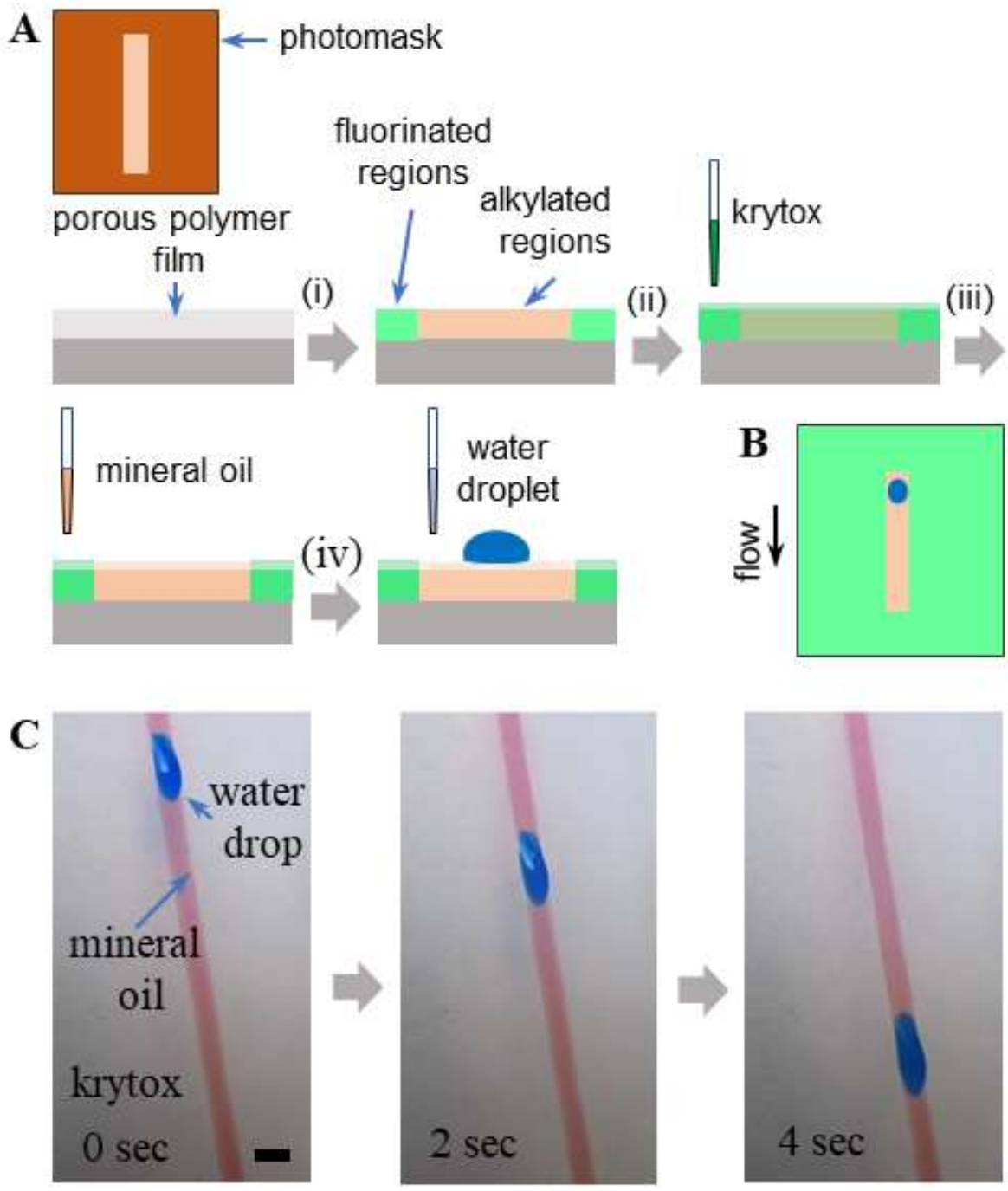

Figure 5.1: (A) Manufacturing steps for oil-in-oil channels. First, a pattern of alkylated and fluorinated regions is created, followed by impregnating the whole surface with a fluorinated lubricant. The addition of the mineral oil leads to the replacement of the fluorinated lubricant from the alkylated regions. Water droplets, added onto such a liquid-liquid patterned surface, are confined to the alkylated regions impregnated with the mineral oil. (B) Setup for droplet transport along a straight, vertically oriented liquid-liquid channel. (C) Time-lapse images of a droplet (colored with blue food color) moving along a straight mineral-oil channel colored with the lyophilic dye Oil Red O. The scale bar represents 1 mm.

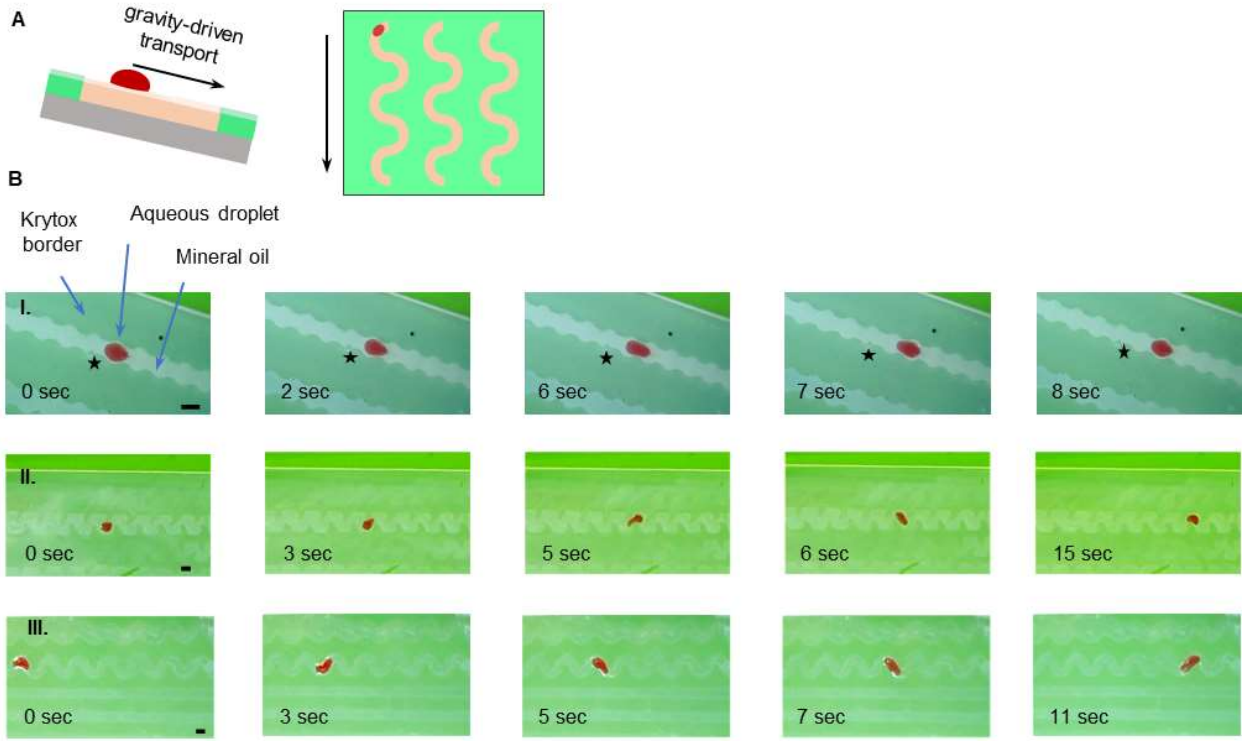

Figure 5.2: Deformation of droplets in different oil-in-oil channels. (A) Schematic of experimental setup. (B) Droplets gliding down meandering oil-in-oil channels: I. 800 nL droplet gliding down channels consisting of circles 1.5 mm in diameter connected by 1 mm thick short lines, II. 800 nL droplet gliding down a serpentine channel with sections of variable width, 1.2 and 0.7 mm, and II. 2 µL droplets gliding down a meandering channel of constant width of 1.3 mm. Surface inclination of 30° for (I.) and 70° for (II.) and (III.). Scale bar: 1 mm.

We wanted to understand this confinement better. To do this, we analyzed the essential scenario of a droplet sitting on a surface impregnated with two different oils in some depth. A droplet experiences a force when it crosses the boundary between regions impregnated with different liquids. The magnitude of this force determines how difficult it will be for a droplet to penetrate a more hydrophobic region. In this section, we develop a simple model for this force and compare the model's predictions to experimental results.

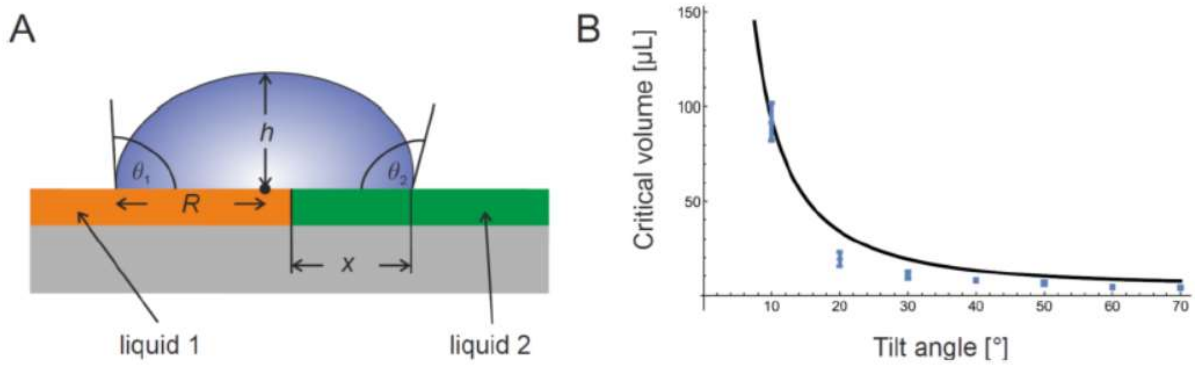

Figure 5.3: (A) Droplet at the boundary between two liquid-infused regions. The relevant geometrical model parameters are indicated. (B) Critical droplet volume as a function of the tilt angle of the surface. The curve represents the prediction of the theoretical model. The data points to the experimental results. The error bars represent the standard deviation as obtained from a series of five independent measurements.

The situation considered is depicted in Figure 3A, which shows a droplet in side view at the interface between two regions impregnated with different liquids. On regions 1 and 2, the droplet has a Young's contact angle with the surface of θ1 and θ2, respectively. There is a point on the contact line between the droplet, impregnating liquid 2 and the surrounding gas with the largest distance of all points on the contact line to the interface between the impregnating liquids. This distance is denoted as x. Without loss of generality, we assume θ2 > θ1. With increasing x, the potential energy of the droplet increases, meaning that a force is required to let the droplet cross the boundary between liquid 1 and liquid 2. To compute this force, we consider a situation with θ1 ≈ θ2, which is fulfilled with reasonable accuracy for the impregnating liquids used in this study. In this case, the shape of the droplet surface can be approximated by a spherical cap and the contact area between the droplet and the impregnating liquids by a circle. Note that in the general case, the droplet shape is to be computed by solving the Young-Laplace equation[198] with θ1 and θ2 as boundary conditions on regions 1 and 2. Denoting the contact radius as R and the height of the spherical cap as h, the droplet volume is given by

$$V = \frac{\pi}{6} h\left(3R^2 + h^2\right) \tag{5.1}$$

where the droplet height is expressed via the contact angle as

$$h = \frac{R}{\sqrt{2}}\left(\frac{1}{1-\cos\theta_e} - \frac{1}{2}\right)^{-1/2} \tag{5.2}$$

Here, the average of the two contact angles is used: $\theta_e = \frac{1}{2}\left(\theta_1 + \theta_2\right)$. To compute the potential energy of the droplet, gravity is neglected, and only the contributions due to wetting are

considered. Expressed through the interfacial tensions σs1l, σs2l between the two different impregnated surfaces and the droplet liquid and the interfacial tensions σs1g, σs2g between the two surfaces and the surrounding gas, the interfacial energy is given as

$$E(x) = A_1\sigma_{s_1 l} + \left(A_1^* - A_1\right)\sigma_{s_1 g} + A_2\sigma_{s_2 l} + \left(A_2^* - A_2\right)\sigma_{s_2 g} \qquad (5.3)$$

where A1, A2 denote the areas of regions 1, 2 wetted by the droplet and A1*, A2* those fractions of regions 1, 2 in contact with gas. In equation (1.3), the contribution of the surface of the droplet was neglected. In the framework, the assumption is that the droplet is always a spherical cap having a contact angle of θe with the surface. This is permissible since the corresponding contribution to the interfacial energy is independent of x and, therefore, does not contribute to the force on the droplet. With the total wetted area being a circle, the contributions from the two different regions are given as

$$A_2 = R^2 \arccos\left(1 - \frac{x}{R}\right) - (R - x)\sqrt{2Rx - x^2}$$
$$A_1 = R^2\pi - A_2 \qquad (5.4)$$

The force on the droplet is given by $F(x) = -\frac{d}{dx}E(x)$. Using equation (1.3) and Young's law to express the interfacial energies via contact angles, the force is computed as

$$F(\tilde{x}) = -2R\sigma_{lg}(\cos\theta_1 - \cos\theta_2)\sqrt{x(2-x)} \qquad (5.5)$$

where the dimensionless x-coordinate $\tilde{x} = x/R$ was introduced, and σlg is the surface tension of the droplet liquid. Apparently, the force is maximal when the droplet is located halfway between the two different regions, i.e., at x = R. The maximum force on a droplet is given by

$$F_{max} = 2R\sigma_{lg}(\cos\theta_1 - \cos\theta_2) \qquad (5.6)$$

The maximum force can be determined experimentally by inclining the surface by an angle α, placing droplets with different volumes on the region impregnated with liquid 1, and letting them slide down. Large droplets will be able to penetrate region 2. Small droplets will stop at the interface between the two regions. The droplet volume where the transition between sliding and stopping at the interface happens is denoted Vc. From the balance between the gravitational force and the maximum wetting force Fmax, the critical droplet volume is determined to be

$$V_c = \left[\frac{2\sigma_{lg}}{\rho\sin\alpha}(\cos\theta_1 - \cos\theta_2)\right]^{-3/2}\left[\frac{6\sqrt{2}}{\pi f(\theta_e)}\right]^{1/2} \qquad (5.7)$$

with

$$f(\theta_e) = \left(\frac{1}{1-\cos\theta_e} - \frac{1}{2}\right)^{-1/2}\left[3 + \frac{1}{2}\left(\frac{1}{1-\cos\theta_e} - \frac{1}{2}\right)^{-1}\right] \qquad (5.8)$$

To test this simple model, experiments were performed with water droplets on inclined surfaces to determine Vc (Figure 3B). One part of the surface was impregnated with Krytox GPL 103, the other either with mineral oil or silicone oil. Overall, for a given tilt angle, smaller aqueous droplets would pass into the Krytox phase when placed on silicone oil compared to mineral oil (see Table 1). These two oils show qualitatively different behavior when coming into contact with water: silicone oil has a positive spreading coefficient on water, but mineral oil does not.[19 9] As a result, silicone oil forms a cloak around a droplet sitting on a silicone-oil infused surface. Krytox GPL 103 shows a similar cloaking behavior. In Figure 3B, a comparison between the model results and the experimental data for the combination mineral oil/Krytox GPL 103 is displayed. The fair agreement between the model results and the experimental data visible in the figure is only obtained when assuming that Krytox cloaks the droplet as soon as it comes in touch with the Krytox-infused surface. In other words, the surface tension of Krytox (≈ 20 mN/m) was used for σlg in equation (1.7). The situation is more complex for the combination of silicone oil / Krytox GPL 103 since both of these lubricants show a cloaking behavior on water droplets. In that case, no agreement between the model results as the experimental data could be achieved (data not shown). The conclusion from these comparisons is that the simple model described above approximately reproduces the force on a droplet at the boundary between two lubricant-infused regions, but only if cloaking is considered and only one of the lubricants shows a cloaking behavior.

Table 5.1: Critical mean droplet volumes in µL (and corresponding standard deviations for 5 independent measurements) for different tilting angles at which an aqueous droplet passes into the fluorinated oil-infused phase from either a mineral oil or silicone oil lubricated areas.

Tilt angle	10°	20°	30°	40°	50°	60°	70°	80°	90°
Mineral Oil	92 ± 9.6	19.2 ± 3.8	10.8 ± 2.2	7.8 ± 0.6	6.3 ± 0.96	4.4 ± 0.7	4 ± 0.6	3.1 ± 0.6	3.1 ± 0.6
Silicone Oil	33.6 ± 6.3	9.4 ± 0. 6	4.5 ± 0.4	3.2 ± 0.2	2.5 ± 0	2.18 ± 0.3	1.82 ± 0.1	1.78 ± 0.1	1.66 ± 0.1

Confinement of droplets into pre-defined alkylated regions surrounded by a perfluorinated background can be utilized for droplet sorting. In the simplest scenario, confining lubricated channels that directed droplets to a dedicated position were created (Figure 4 and Video S4). As before, a 2-mm-wide, mineral-oil lubricated channel perpendicular to the floor was created. After some distance (20 mm), the channel was narrowed to 1.5 mm width, which briefly stopped 3 µL droplets flowing down it before deforming and entering the narrower channel. At the site of this constriction, a second 2-mm-wide channel branched out with an angle of 60°.

Such bifurcations can enable active droplet sorting, for example, by positioning a magnet next to the branching channel. When placing 3 µL droplets containing magnetic nanoparticles into this channel system, they entered the 60°-angled branch instead of the straight channel (Figure 4 and Video S4).

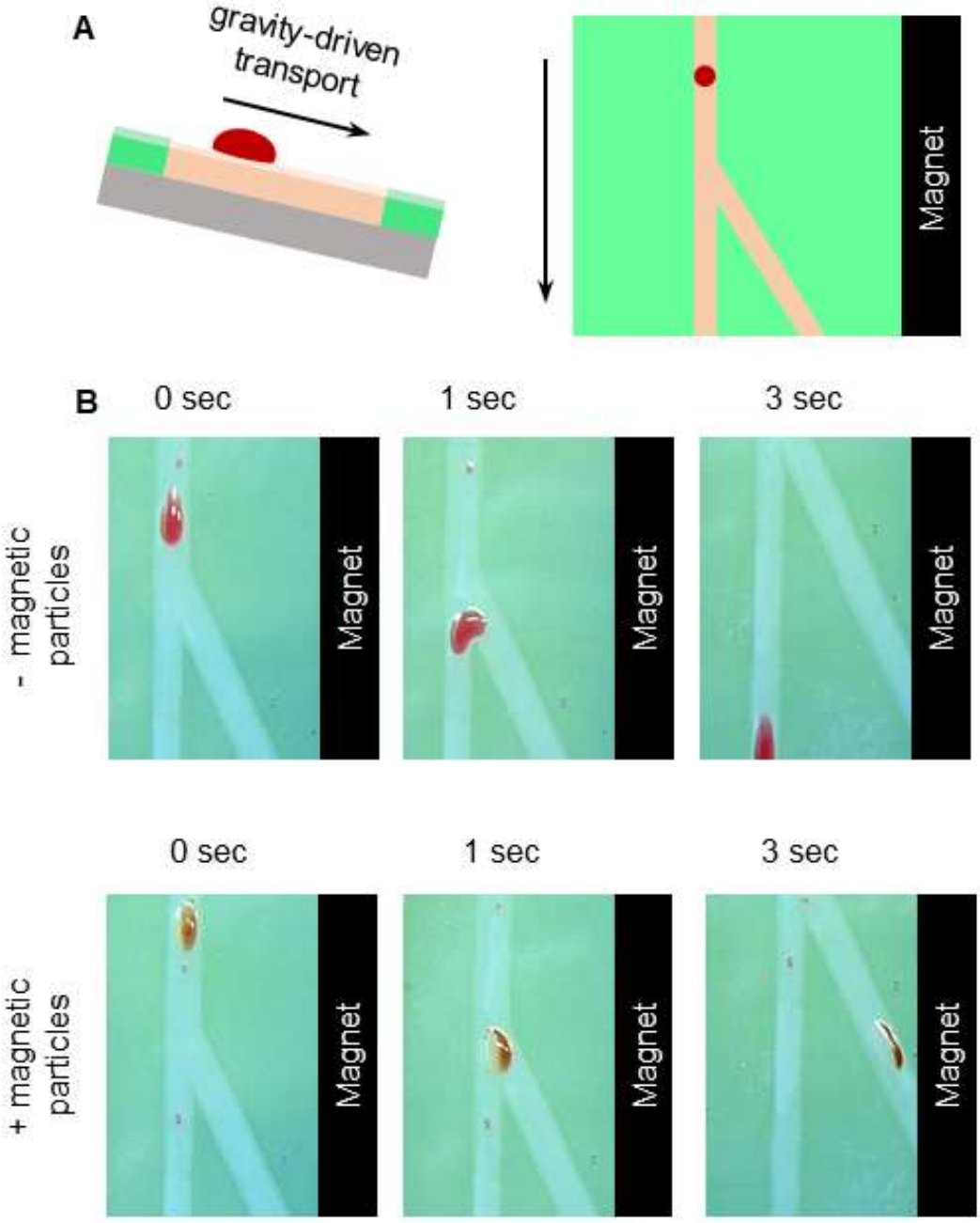

Figure 5.4: Active droplet sorting. (A) Schematic of the experimental setup. (B) Time-lapse images of aqueous droplets with (lower row) or without (upper row) magnetic particles gliding down a branched mineral oil channel next to a permanent magnet.

When, on a horizontal surface, an aqueous droplet is displaced on a mineral-oil infused rectangle with a smaller width than the droplet, the droplet will center on the rectangle but may not adapt to the rectangle's dimensions (Figure 5A); for a series of droplets with decreasing volume, the smaller the volume of the droplet the more it deformed and adapted an elongated spherical shape instead of a circular shape (Figure 5A). Varying the width of lubricated alkylated channels relative to a droplet's size allowed us to manipulate droplet paths down an inclined surface; 3 µL droplets - gliding down a 2-mm-wide channel angled at 60° relative to the floor – would not enter a 1-mm-wide channel perpendicular to the floor and branching from the angled channel (Figure 5B). However, if given no choice, water droplets even considerably larger than a mineral-oil channel would follow the channel paths while flowing down a 70° inclined surface (Figure 5C and Video S3). This can be exploited to sort droplets based on their size. Here, a straight 2-mm-wide rectangle lubricated with silicone oil, which was perpendicular to the floor, was separated from a silicone-oil-lubricated, 2-mm-wide rectangle (angled at 50°C relative to the floor) by a 200-µm-wide barrier lubricated with Krytox. When placing aqueous droplets with volumes less than or equal to 3 µL into the angled rectangle, they follow its path and cannot cross into the bordering rectangle. By contrast, droplets with volumes larger than or equal to 4 µL can overcome the barrier and enter the path of steepest descent (Figure 6).

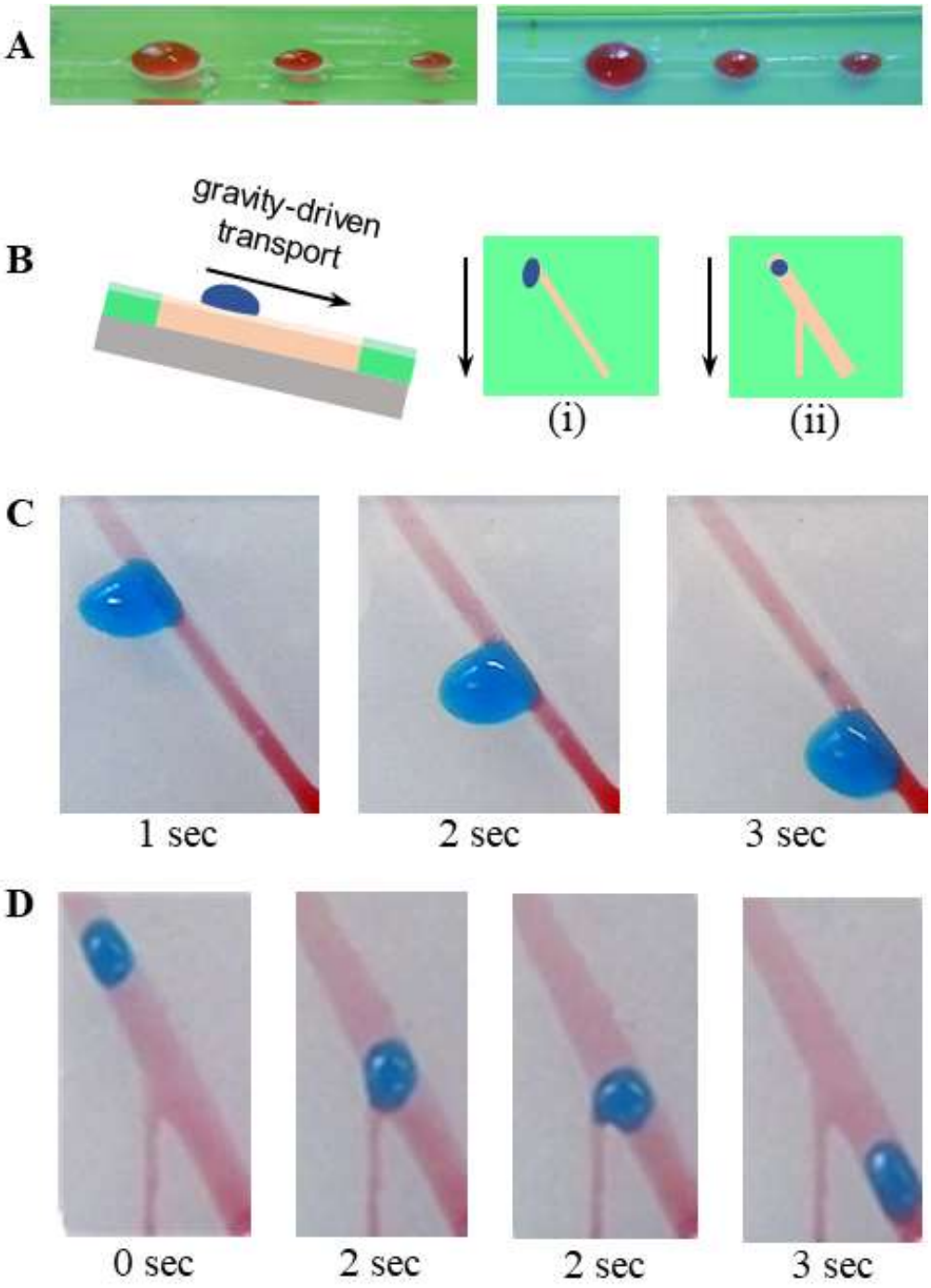

Figure 5.5: Droplets with sizes exceeding the oil channel dimensions. (A) Photographs of red aqueous 5 µL, 2 µL and 1 µL droplets from the side (left) and from the top (right) sitting on a 1.6 mm wide mineral oil channel. (B) Schematic of the experimental setup. (C) Time-lapse images of a blue-colored aqueous droplet (6 µL) gliding a narrow 0.7 mm wide mineral oil channel. (D) Aqueous droplet sliding down a 2 mm wide channel from which a narrower 0.5 mm channel branches off, which represents the path of steepest descent.

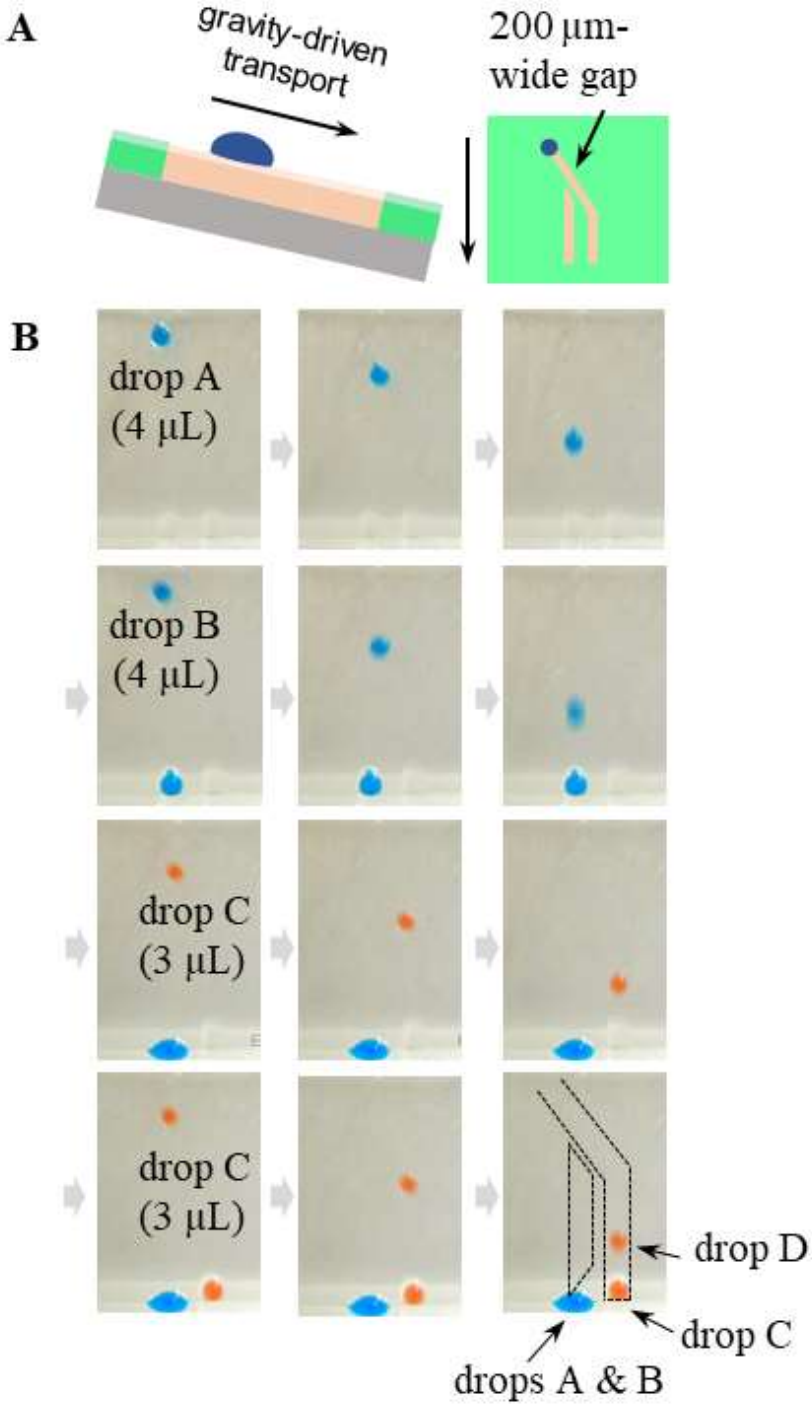

Figure 5.6: Passive droplet sorting based on hydrophobic fluorinated barriers. (A) Scheme for droplet sorting based on a hydrophobic fluorinated barrier with a width of 200 µm separating two alkylated mineral oil-infused channels. (B) Time-lapse images of droplet sorting, where 4 µL droplets (blue) were discriminated from 3 µL droplets (red). Larger droplets are able to overcome the fluorinated oil-infused 200 µm barriers and slide down the first channel, while smaller droplets follow the uninterrupted mineral oil-infused channel.

Previously, Suzuki et al.[106] showed that on superhydrophobic surfaces displaying an alkylated-perfluorinated stripe pattern, which was placed at an angle between 90 to 0 degrees relative to the floor, droplets become deflected according to their size; smaller and thus lighter droplets strictly follow the stripes they were first placed upon as they are unable to overcome the force barrier confining them to the organic-patterned surface, while larger droplets will enter neighboring stripes. This can be observed on striped, slippery surfaces as well (Figure 7A-C). While smaller droplets of, e.g., 3 µL volume perfectly follow a 13°-angled stripe pattern lubricated with mineral oil (stripe width 0.5 mm separated by 0.5 mm wide gaps), 10 µL droplets cross the Krytox-lubricated barriers between the stripes (Figure 7A-C).

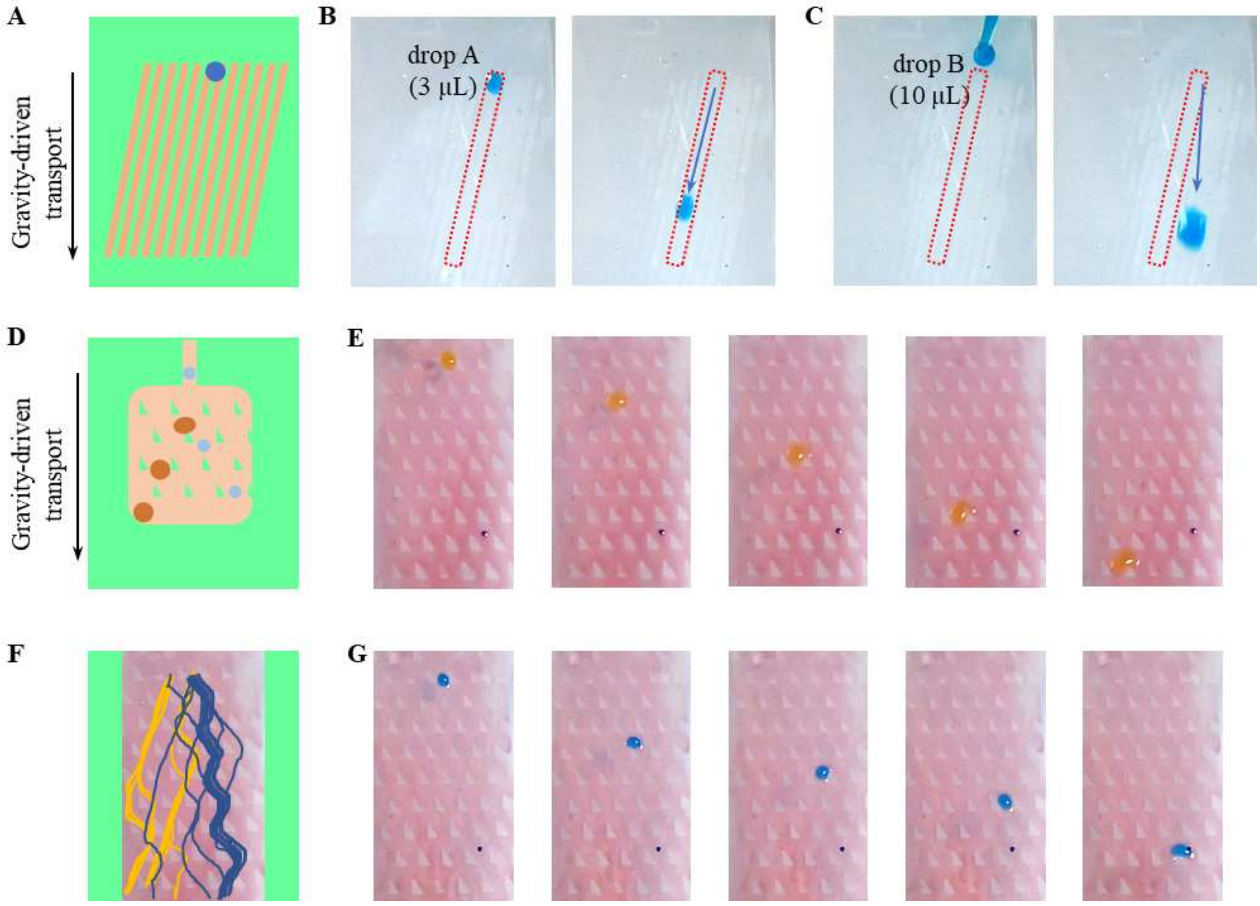

Figure 5.7: Passive droplet sorting on two-dimensional patterned mineral oil-fluorinated oil-infused surfaces. (A) Schematic representation of a droplet gliding on 0.5 mm wide mineral oil stripes on a fluorinated oil background. (B) Images showing a 3 µL aqueous droplet gliding down along these stripes and a 10 µL (C) droplet crossing the stripe pattern following the path of a larger slope. (D) Schematic representation of an alternative passive-droplet sorting system exhibiting an array of fluorinated oil-infused triangles surrounded by mineral oil-infused background. (E) Images of the deflection of a 5 µL droplet on the triangular

pattern. (G) Images of the deflection of a 2 µL droplet on the triangular pattern. (F) Patterned surface onto which the paths of individual droplets (either yellow for 5 µL droplets or blue for 2 µL droplets) were drawn. Larger droplets are preferentially deflected to the left, while smaller ones to the right.

The deflection angle under which droplets glide down can be increased. To sort droplets by size, we designed a pattern in analogy to deterministic lateral displacement devices[200-203] (Figure 7D-G). To construct a corresponding sorting device, small triangular areas of Krytox-lubricated HEMA-EDMA were introduced in a mineral oil lubricated background.
Indeed, these features are capable of deflecting droplets even if they are smaller than the droplet diameter (Figure 7E). For the sorting of droplets, chemical patterns resembling arrays consisting of right triangles with 2.6 mm height and 1.6 mm side were fabricated (Figure 7D). These features allowed the deflection of droplets either to the left or to the right, depending on their size. The triangle pattern was arranged in a way to position a subsequent row of triangles close enough to its upper neighbor, such that a deflection to the right is favored. However, larger droplets extend further into the Krytox pattern and beyond it; thus droplets of 5 µL or larger would preferably turn left at these obstacles (viewed from the angle shown in Figure 7 and Video S5), while droplets of 2 µL and smaller would mostly turn right (Figure 7G and Video S6). Droplets of 3 or 4 µL would pick either path down at roughly equal likelihood. After segregating droplets according to size through the repetitive triangle pattern, large and small droplets can be permanently separated by funneling them into distinct channel systems.

5.3 Conclusion

To summarize, we used a facile, highly-adaptable, clean-room free approach to chemically pattern planar surfaces with defined alkylated regions and structures in a perfluorinated background; lubricating the surfaces with matching liquids lead to liquid-liquid patterns that precisely followed the underlying chemical surface patterning. We could precisely position and guide droplets up to volumes of several µL on them, as long as the energy barrier confining the droplets in the channels was larger than the forces (e.g. gravity) pulling the droplets out of the channel. The energy barrier was measured and compared to a simple model, which indicates that the cloaking of droplets needs to be considered at the boundary between two regions infused with different lubricants. These “virtual wall” systems can be used to actively guide droplets on a plane to dedicated positions. Droplets can overcome these virtual walls and move into neighboring alkylated surface areas, a mechanism we exploited using several different surface patterns to passively sort droplets according to size. Thus, droplets with a volumetric difference of 1 µL could be discriminated. We are confident that structuring slippery surfaces

into regions with different lubricants will prove a crucial design element for planar-surface microfluidics.

5.4 Experimental Section

5.4.1 Preparation of patternable porous polymer surfaces:

Glass slides were activated by submerging in 1M NaOH for 30 min followed by thorough rinsing with mQ H2O. Then slides were left in 1M HCl for 1 h and rinsed with water again. After drying, slides were modified by a 20% (v/v) 3-(trimethoxy silyl)propyl methacrylate (Sigma-Aldrich) in ethanol. To avoid the formation of air bubbles, 70 µL modification solution was evenly applied twice between the active sites of two glass slides for 30 min. Glass slides were washed with acetone. Fluorinated glass slides were prepared for the manufacturing of polymer surface. For this, activated glass slides were incubated overnight in a vacuumed desiccator in the presence of trichloro(1H,1H,2H,2H-perfluorooctyl)silane. Polymerization solution consisted of polymers (24% wt. 2-hydroxyethyl methacrylate as monomer and 16% wt. ethylene dimethacrylate as a cross-linker) as well as initiator (1% wt. 2,2-dimethoxy-2-phenylacetophenone) dissolved in 1-decanol (12% wt.) and cyclohexanol (48% wt.). 60 µL polymerization mixture was pipetted onto modified glass slides. These were than covered by fluorinated glass slides separated through 15 µm silica bead spacers from modified glass slides. Slides were irradiated for 15 min with 5.0 to 4.0 mW·cm-², 260 nm UV-light. The mould was then carefully opened using a scalpel and polymer washed for at least 2h in ethanol. Hydrophilic polymer surfaces were esterified by immersion of 2 slides in 50 mL dichloromethane containing 4-pentynoic acid (111.6 mg, 1.14 mmol) and catalyst 4-(dimethylamino)pyridine (DMAP) (56 mg, 0.46 mmol) at -20°C. After 20 min, 180 µL coupling reagent N,N-diisopropylcarbodiimide (DIC) was added and the solution stirred at room temperature for at least 4h or overnight. Esterified slides were washed in ethanol for 2h.

5.4.2 Alkylated/perfluorinated-patterning of surfaces:

Esterified slides were photopatterned through ink-yet printed polypropylene foil. For this, ink-jet-printable polypropylene foil purchased from Soennecken eG (Overath, Germany) was printed with black features at highest resolution possible on a Canon iP7200. Usually, borders were patterned with a fluorine-thiol containing solution, while in a second step unreacted regions (features) were modified with an alkane-thiol containing solution. Perfluorinated click-chemistry solution 1 was prepared always fresh by dissolving 10% vol./vol. 1H,1H,2H,2H-perfluorodecanethiol in acetone together with 1% wt. 2,2-dimethoxy-2-phenylacetophenone. Alkylated solution 2 consisted of dodecanethiol (10% vol./vol.) dissolved in acetone together with 1% wt. 2,2-dimethoxy-2-phenylacetophenone. In the first patterning step, slides were wetted with 200 µL solution 1 in the dark. Slides were covered by the desired printed

polypropylene pattern, which was fixed on the slide with a quartz slide, and irradiated for 16 seconds (7.0 mW•cm-2, 365 nm). After irradiation slides were rinsed four times with acetone in the dark. They were wetted with solution 2 and covered by a quartz slide. Immediately after, slides were irradiated for 16 seconds by UV again (7.0 mW •cm -2 , 365 nm) and subsequently rinsed four times with acetone and dried. Previously, it has been shown that by using self-ink-jet-printed photomasks, features with sizes down to the µm range can be patterned.32 In this work, however, we remained limited to the mm range with channels being at least 0.5 mm wide due to manufacturing restrictions.

5.4.3 Lubrication of Surfaces and Droplet application

Surfaces were lubricated by evenly applying first 70 µL of Krytox GPL 103 onto the surface. Excess Krytox was allowed to run off the surface by leaving it standing at an incline of 70° for two hours. Alternatively, excess Krytox was removed through an air gun. Then, alkylated features were lubricated with either mineral oil or silicone oil by applying a droplet of 50 µL of intruding liquid onto the Krytox-lubricated surface and allowing it smoothly to run back and forth on the surface. Once, the intruding oil had spontaneously assumed the shape of all underlying alkylated patterned features, excess oil was allowed to run off. Aqueous droplets were placed on the surface through directly pipetting a given amount of aqueous solution onto the double lubricated surfaces. For this, if not stated otherwise, surfaces were inclined by angle of 70° so that aqueous droplets could run freely down the surface by gravity. For the determination of critical sliding volumes, lubricated surfaces were placed on a platform that could be manually controlled to be tilted to a given angle between 0 and 90°.

5.5 Supporting Information

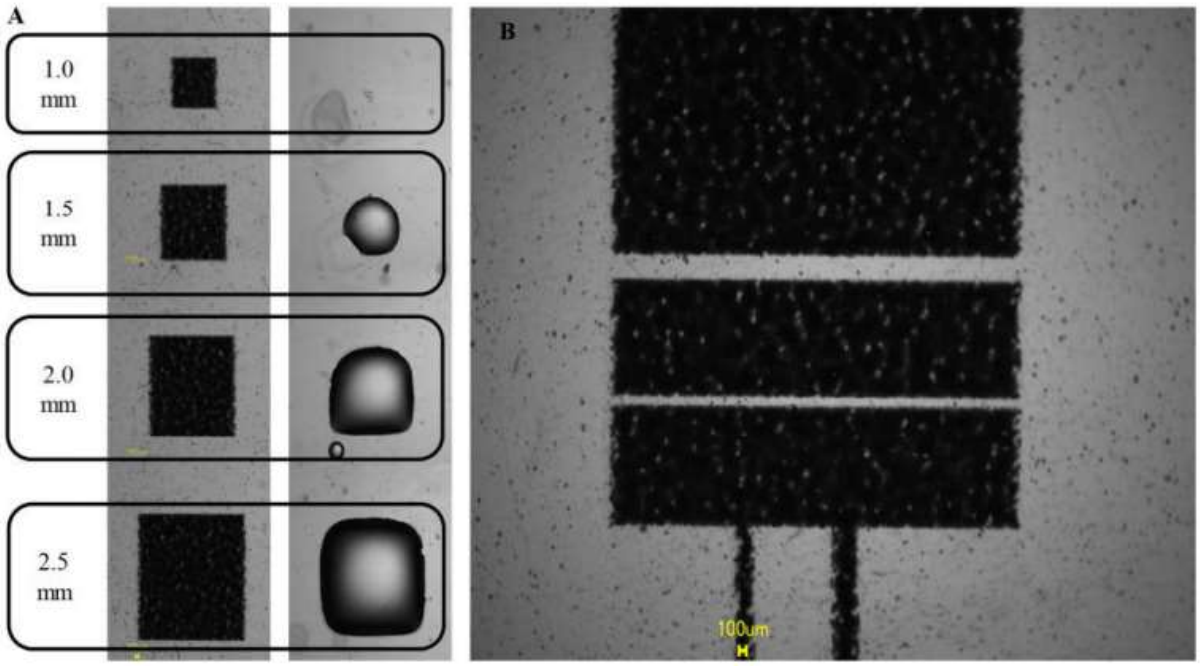

Figure S5.1: Resolution of chosen manufacturing strategy. A) Images (2X) of rectangles (length of each site given on the left) printed onto polypropylene foil and images of patterns generated from the printed foil through UV-patterning. B) Resolution of printed patterns in the µm-range illustrated by printing a black 100 µm line next to a black 200 µm line below gaps of 100 µm and 200 µm.

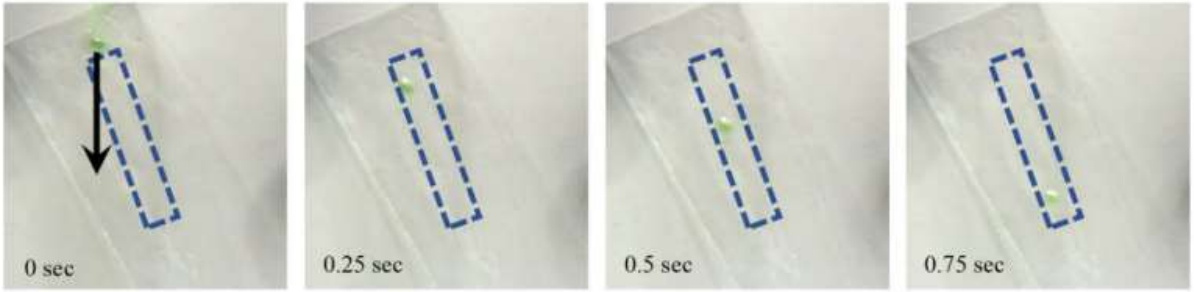

Figure S5.2: Video of droplet (5 µL) sliding down a tilted (70°) rectangular paths of ionic liquid (1-Butyl-3-methylimidazolium bis(trifluoromethylsulfonyl)imide) surrounded by mineral oil.

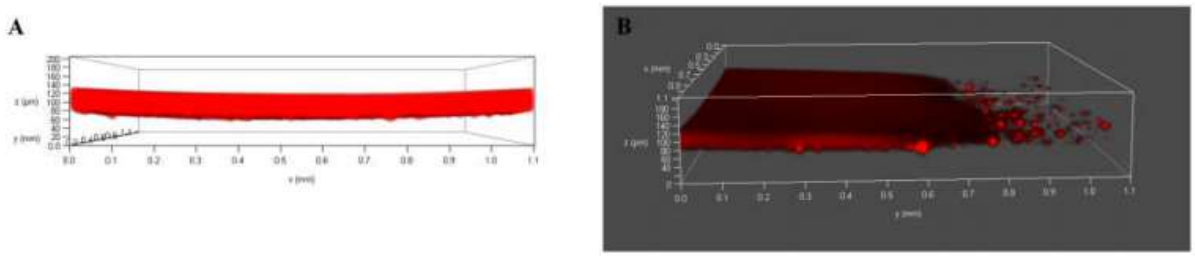

Figure S5.3: Oil film thickness of Nile Red-stained Mineral Oil channels surrounded by Krytox. (A) through the cross-section. (B) from the side. Confocal microscopy images were taken using a Leica SPEconfocal microscope (Leica Microsystems CMS GmbH, Mannheim, Germany) at 10x with a 4.2 µm step size in the Z-direction. Images were automatically stacked using the vendor's software. For patterning, a nano-rough substrate from Aquarray GmbH (Eggenstein-Leopoldshafen) was used with 1 µm thickness.

The following video files were attached:

S5.1 Video of a 2 µL aqueous droplet gliding down a stained mineral oil channel consisting of circles connected by smaller rectangular shapes.

S5.2 Video of an aqueous 800 nL droplet gliding down a wavy channel of varying width.

S5.3 Video of an aqueous 6 µL droplet gliding down a 60° angled small channel of stained mineral oil.

S5.4 Video of aqueous droplets consecutively gliding down a branching mineral oil channel next to a magnet, containing either no magnetic particles (red) or magnetic particles (brown).

S5.5 Video of the deflection of 5 µL aqueous droplets (yellow) on a regular pattern of Krytox triangles (transparent) in a mineral oil background (stained red).

S5.6 S-6 Video of the deflection of 2 µL aqueous droplets (blue) on a regular pattern of Krytox triangles (transparent) in a mineral oil background (stained red)

6. Surface Modification with Oligomeric Silicone Compounds – Reproducibility and Secondary Modification.

Dorothea Paulssen[1], Pavel Levkin[1]*
1 Institute of Toxicology and Genetics (ITG), Karlsruhe Institute of Technology (KIT), 76344 Eggenstein-Leopoldshafen, Germany

*Corresponding author: levkin@kit.edu

Abstract. Here, the influence of different reaction conditions to modify glass and silicone surfaces with oligomeric methoxy siloxanes (VMS) for secondary derivatization of surfaces is assessed. Secondary modification of the thus formed surfaces is demonstrated, and its performance in wettability control, including droplet micro-arrays, is documented.

Keywords: Silanization, Dynasylan, Oligomeric Siloxane, Wettability Patterning, Surface Modification

In preparation for Thin Solid Films

6.1 Introduction

Surface modifications by silanes can be affected by many factors such as silane exposure time,[5] temperature,[204] presence of surface-bound water,[29, 205] density of hydroxyl groups,[206] substrate surface pH,[207] solvents,[208] and the presence of a catalyst.[47, 209] However, especially for *in situ* modification of surfaces mild, ambient conditions are often obligatory, while reliable outcomes of reactions are key for surface function. Yet, despite the existence of numerous methods available for surface silanization, only a few fulfill these criteria.[210] Surprisingly, rather unreactive siloxanes can be a notable alternative to monomeric silanes. Recently, protocols for surface modifications with siloxanes were published, leading to highly smooth and repellent surfaces even when 'just' exposing hydroxylated surfaces to a thin film of the siloxane oil and incubating it at room temperature.[211] One disadvantage of this method is that the covalent attachment of siloxanes to surfaces is slow at room temperature. However, it can be speeded up by elevating temperature above 100°C and up to 400°C.[16]

Historically, silane monomers were used interchangeably with siloxane oligomers in the academic literature.[29, 212] Presently, commercial products containing siloxane oligomers rather than silane monomers are established goods.[213] In this context, a formal definition of how large a molecule can be to be still classified as oligomer is missing – something which should be born in mind with caution, as siloxane polymers are also capable of chemically binding to surfaces.[214-218] Examples of commercially available oligomeric siloxanes include common hydrophobization agents of glassware utilized in biochemistry, for example, 1,7-Dichlorooctamethyltetrasiloxanes and related longer oligomers (also known under their tradenames SigmacoteTM and SurfaSilTM), that render surfaces repellent within minutes.[219, 220] Examples of alkoxylated siloxanes include Dynasylan 6498TM and Dynasylan 6490TM – an ethoxy and methoxy functional siloxane, respectively, with a vinyl side chain in their repeating unit - that are commonly used as coupling and adhesion agents, fillers, and other coating applications. Albeit it is known in the academic literature that oligomers can be used to modify surfaces,[17, 221-225] quantitative side-by-side comparisons with silane monomers are extremely scarce. It has been documented that: (1) oligomeric siloxanes are more reactive than monomeric silanes and have faster attachment rates in literature;[212, 226] (2) that surfaces to which even very small (3 units) oligomeric siloxanes have been grafted appear more homogenous according to Auger Electron Spectroscopy, which can be at least partially attributed to their better film-forming properties – especially with surfaces with varying pH or are modified;[226, 227] and (3) that they actually are more controllable in the length and interconnectivity of oligomeric networks grafted onto an arbitrary surface when compared to networks that were grafted from a surface from a silane monomer

solution, which makes them more attractive as coupling agents.[26, 228, 229]
The view that grafting oligomeric silanes to surfaces offers enhanced control and robustness of reaction outcome than when employing monomeric silanes even when used under ambient conditions and simple reaction set-ups, is attractive to other areas than synthesis of coupling agents. An obvious example is the reliable and reproducible, while dense, introduction of molecular probe molecules as needed for patterning as well as micro-array and bio-sensor applications.[34, 230, 231] Although a plethora of techniques exist that can be used to create surfaces with specialized wettability, simple and reliable strategies for building (patterned) multi-phobic surfaces that are repellent to a wide range of surface tensions as well as complex fluids such as biological liquids, remain an ongoing area of research.

Here, the robustness and simplicity of modifying glass and other hydroxylated surfaces with oligomeric methoxy silanes (VMS) for secondary derivatization of surfaces is assessed. Secondary modification of the thus formed surfaces is demonstrated, and its performance in wettability control, including stable lubricant infusion, is documented through contact angles and the creation of droplet arrays. It will be demonstrated that VMS can be straightforwardly grafted on relevant surfaces with a wide range of reaction conditions.

6.2 Methods

6.2.1 Materials

Microscopic soda-lime glass slides (“Marienfeld”) in the dimensions 0.1*2.6*7.6 cm were obtained from R. Langenbrinck GmbH (Emmendingen, Germany). For AFM measurements, glass slides from Schott Nexterion B slides (Jena, Germany) with the dimensions 0.1*2.5*7.5 cm were used. Transparent polypropylene foil (“PolyClearView IB386848”) was obtained in size DIN A4 and with a thickness of 0.3 mm (GBC, Lake Zurich, IL) and subsequently cut into the required dimensions (7.5*2.5 cm). Silicon wafers (CZ-Si-wafer 4 in.) were purchased from MicroChem GmbH (Berlin, Germany).

Vinyl-methoxy silane (VMM-010) homopolymer (Gelest Inc., Morrisville, PA, USA) with a viscosity range of 8-12 cSt (corresponding to a MW range of 300-700 g/mol) was used as provided without further refinement. Solvents used included acetone, dimethylformamide (DMF), ethanol, ethyl acetate, hexane, tetrahydrofuran (THF), and toluene.

Thiol-ene patterning involved the following thiols: perfluorodecanethiol (Sigma-Aldrich, Darmstadt, Germany), dodecanethiol (Sigma-Aldrich, Darmstadt, Germany), Mercapto Functional Silicone Fluid GP-71-SS (Genesee Polymers, Burton, MI, USA), Mercapto

Functional Silicone Fluid GP-367 (Genesee Polymers, Burton, MI, USA), (Mercaptopropyl)methylsiloxane homopolymer, 75-150 cSt, SMS-992 (Gelest Inc., Morrisville, PA, USA), 1,5-Pentanedithiol (Alfa Aesar, Ward Hill, Massachusetts, USA), 2-mercapto-1-methylimidazole (Sigma-Aldrich, Darmstadt, Germany), ß-mercaptoethanol (Alfa Aesar, Ward Hill, Massachusetts, USA), thiolglycerol (Merck, Darmstadt, Germany) and cysteamine (Sigma-Aldrich, Darmstadt, Germany). All of them were used without further purification. The 2,2-dimethoxy-2-phenylacetophenone (Aldrich, Darmstadt, Germany) or Irgacure 2595 (BASF, Ludwigshafen, Germany) were used as photoinitiators. Silicone oil 10 cSt (Sigma-Aldrich, Darmstadt, Germany) was chosen as a lubricant.

6.2.2 Surface modification with VMS

Soda-lime glass and pristine poly-propylene foil were activated prior to exposure to VMS for 10 minutes in a UV/ozone (UVO) cleaner 42 (rotalab Scientific Instruments, Istanbul, Turkey) if not stated otherwise. Polypropylene foil was cut into the required dimensions (2.5*7.5 cm) and then activated. Activation was performed according to a modified protocol from Wang et al. Briefly, 500 µL of a saturated aqueous solution of ammonium persulfate (5g in 10 mL DI water) was sandwiched between two foils (2.5*7.5 cm) and irradiated in a UV chamber at 265 nm for 2 minutes. The procedure was repeated twice. Then, foils were rinsed with acetone and activated for 10 minutes using a UV/ozone (UVO) cleaner [42] (rotalab Scientific Instruments, Istanbul, Turkey). All other surfaces were used as provided. Per 75 mm * 25 mm area, 50 µL of VMS solution (pure or diluted in solvent) was pipetted and spread by rolling a pipette tip. Surfaces were left to incubate for varying amounts of time at varying temperatures and subsequently immediately rinsed 10 times with acetone and sonicated for 5 minutes in ethanol. Additionally, VMS acoustic vapor, produced by a commercial acoustic home nebulizer, was tested. Glass slides were exposed to the vapor in ambient air at a distance of 3 cm away from the nozzle.

6.2.3 Contact angle measurements

Advancing and receding contact angles were measured using double de-ionized water on the DSA25 drop-shape analyzer by Krüss (Hamburg, Germany) and the manufacturer's software. Water was either flushed onto surfaces or sucked from surfaces at a constant rate (0.3 µL/s), varying the volume present on the surface between 20 – 0 µL. Sliding angles were determined for a 5 µL droplet by tilting the substrate on the Krüss set-up at a speed of 1° s−1.

6.2.4 Absorbance measurements, ellipsometry, and atomic force microscopy

The UV−vis absorbance (200−900 nm) of the bare and coated glass slides was measured using a Lambda 35 UV−vis spectrometer (PerkinElmer, Germany).

The thickness of the siloxane layer on silicon substrates was measured using spectroscopic ellipsometry in a dry state (M44, Woollam Co., Inc., Lincoln, NE, USA). The ellipsometry measurements were performed at an angle of incidence of 75° in the spectral region of 370–900 nm.

Atomic force microscopy measurements were conducted on a Dimension Icon AFM from Bruker (Billerica, USA) using microcantilevers from Olympus (Tokyo, Japan) with a resonance frequency of ca. 300 kHz. Data analysis was done with Nanoscope Analysis from Bruker (Billerica, USA).

6.2.5 Surface Patterning

For modification and patterning of substrates using thiol-ene click chemistry, slides were wetted first with the given thiol solutions for 1 minute at 1.8 mW cm-2 at 260 nm UV light. While glass slides and polypropylene foil were wetted with 150 µL solution, cellulosic paper was wetted with 400 µL solution. Thiol solutions consisted of 10% (v/v) thiol diluted in an appropriate solvent in the presence of 1% (w/v) photoinitiator. While PFDT, dodecanethiol, pentanedithiol and 2-mercapto-1-methylimidazole were diluted in acetone in the presence of DMPAP, silicone fluids were diluted in ethyl acetate in the presence of DMPAP. Hydrophilic thiols were diluted in 1:1 ethanol:water in the presence of Irgacure 2959. Afterward, the slides were washed with either ethyl acetate (silicone fluids) or acetone. If slides had been irradiated under a quartz chromium photomask, unreacted patterns were reacted in a second step as before, but this time under a quartz slide, and slides were subsequently rinsed again. For gradient generation experiments, self-printed photomasks were used as described before.[48, 232]

6.3 Results and Discussion

In this work, we focused on an oligomeric silane with a molecular weight of 300-700 g/mol. This corresponds to molecules with 3-7 silicon atom units. When spreading vinylmethoxysilane (VMS) with a viscosity between 8-12 cSt onto UV/ozone, cleaned soda-lime glass slides at room temperature and sonicating slides for 5 minutes in ethanol both

advancing and receding water contact angles rose from ~5-10° advancing (θadv) and 0° receding (θrec) to 77° ± 4° θadv and 69° ± 2° θrec, respectively (Figure 1). Here, the maximum observed rise in contact angles was already reached after 1 minute (80° ± 2° θadv and 67 ± 2° θrec). Within a given range, changes in hydroxyl group densities or cleanliness of surfaces do not affect the measurable outcome when grafting VMS onto glass substrates; when comparing pristine glass slides (as provided by the manufacturer) and glass hydrophilized through UV/ozone cleaning, no significant different in advancing and receding contact angles was observable. Further incubation of glass slides with VMS oil – even if left to incubate for as long as 1 day – did not increase advancing and receding water contact angles. Interestingly, when probing the influence of temperature on VMS casting onto glass slides, it was found that casting outcomes, as measured by advancing and receding contact angles, were stable over wide temperature ranges (Figure 1). Optimal hysteresis values, the difference between θ_{adv} and θ_{rec}, were found for temperatures between 0° to 50°C; after 50°C the θ_{rec} gradually decreased down to just below 60° (Figure 1), while the θ_{adv} remained constant. This could be explained by the thermal movement of VMS molecules within the oil film covering substrates during grafting: dense packaging of VMS molecules was hence lowered. At a temperature of around 220°C for VMS casting, brittle and irregular surfaces formed with opaque and rough patches; we therefore excluded temperatures above 220°C for further analysis.

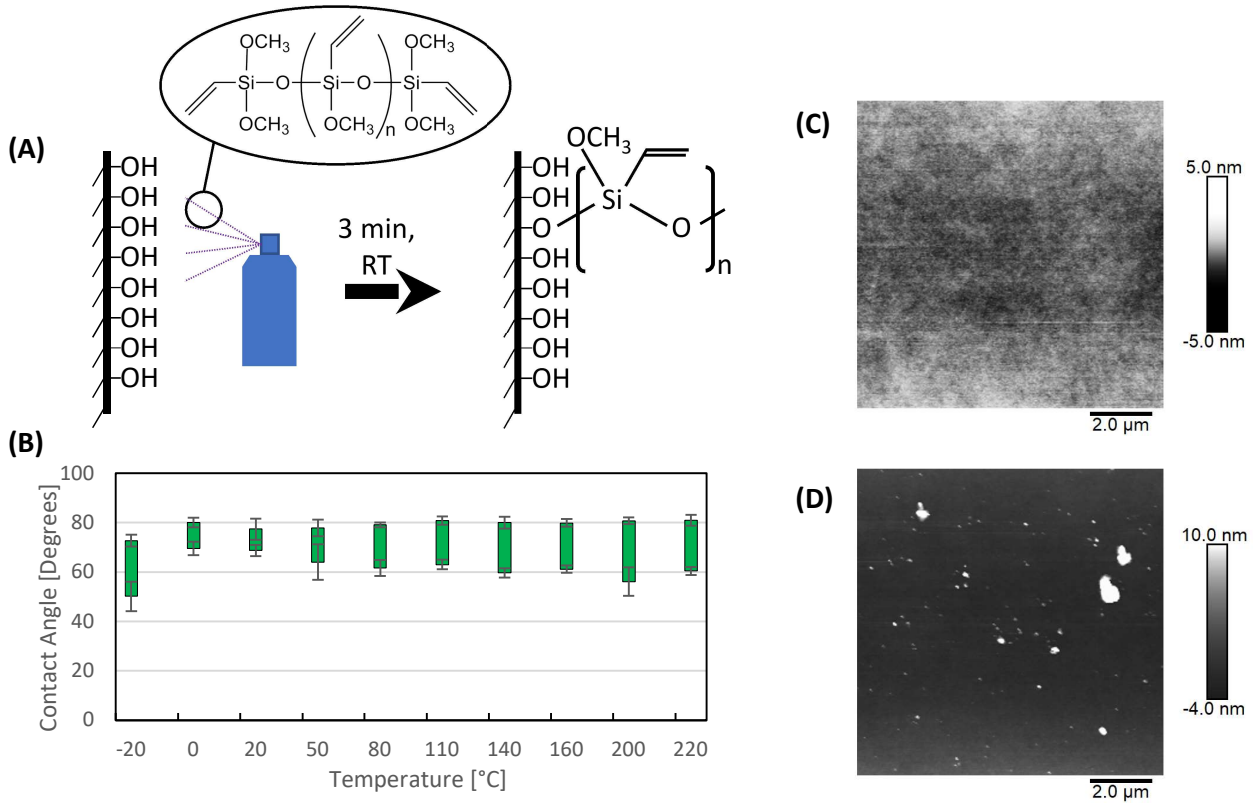

Figure 6.1: Surface modification of activated glass surfaces. (A) Vinylmethoxysiloxane is applied to activated glass surfaces. (B) Changes in advancing and receding angles upon exposure for 3 minutes to undiluted vinylmethoxysiloxane at different temperatures. (C) Atomic force microscopy measurements of untreated glass slides and (D) glass slides that had been treated at 0°C with undiluted VMS for 3 min.

The sliding angle of water was lowered to 57 ± 5° and did not change further if the glass was incubated longer than a minute with VMS. For the tested amount of VMS applied onto surfaces, residual VMS that had apparently not covalently bound to the surfaces was always left. This physio-adsorbed oil needed to be removed from surfaces prior to contact angle measurements. Thus, contact angles measured differed between slides directly after incubation with VMS (76° ± 2° θ_{adv}, and 53° ± 4° θ_{rec}) and after 5 minutes of sonication in ethanol. Despite sonication of VMS in ethanol amorphous, roundish particles were detectable with a diameter varying from ca. 0.2 to 0.8 µm and scarcely spread over the entire surface as visualized through AFM (Figure 1) – these seemed similar to conglomerated siloxane particles as described before in literature by Jaksa et al., 2014 (Figure 1).[86]

The chemisorption of siloxane onto surfaces and the robustness of composite surfaces were tested next. For this, glass surfaces incubated for 3 minutes with VMS and rinsed with copious amounts of acetone were sonicated in different solvents for elongated time periods (Figure 2). In particular, a non-solvent (ethanol), a partial solvent (acetone), and a strong solvent (ethyl acetate) of siloxane oils were used (Figure 2). While slides sonicated in ethanol did not change in measured θadv and θadv, slides sonicated in either ethyl acetate or acetone changes in advancing and receding contact angles could be observed within the first 10 minutes of sonication and steadily kept decreasing with elongated sonication times (Figure 2). However, even after 11 hours of sonication, slides had not reached θadv and θrec as low as on pristine slides prior to UV/ozone treatment – with reached values corresponding to 90° ± 3 θadv and 74° ± 6° θadv as well as 51° ± 5° θrec and 55° ± 7° in θrec for ethyl acetate and acetone, respectively.

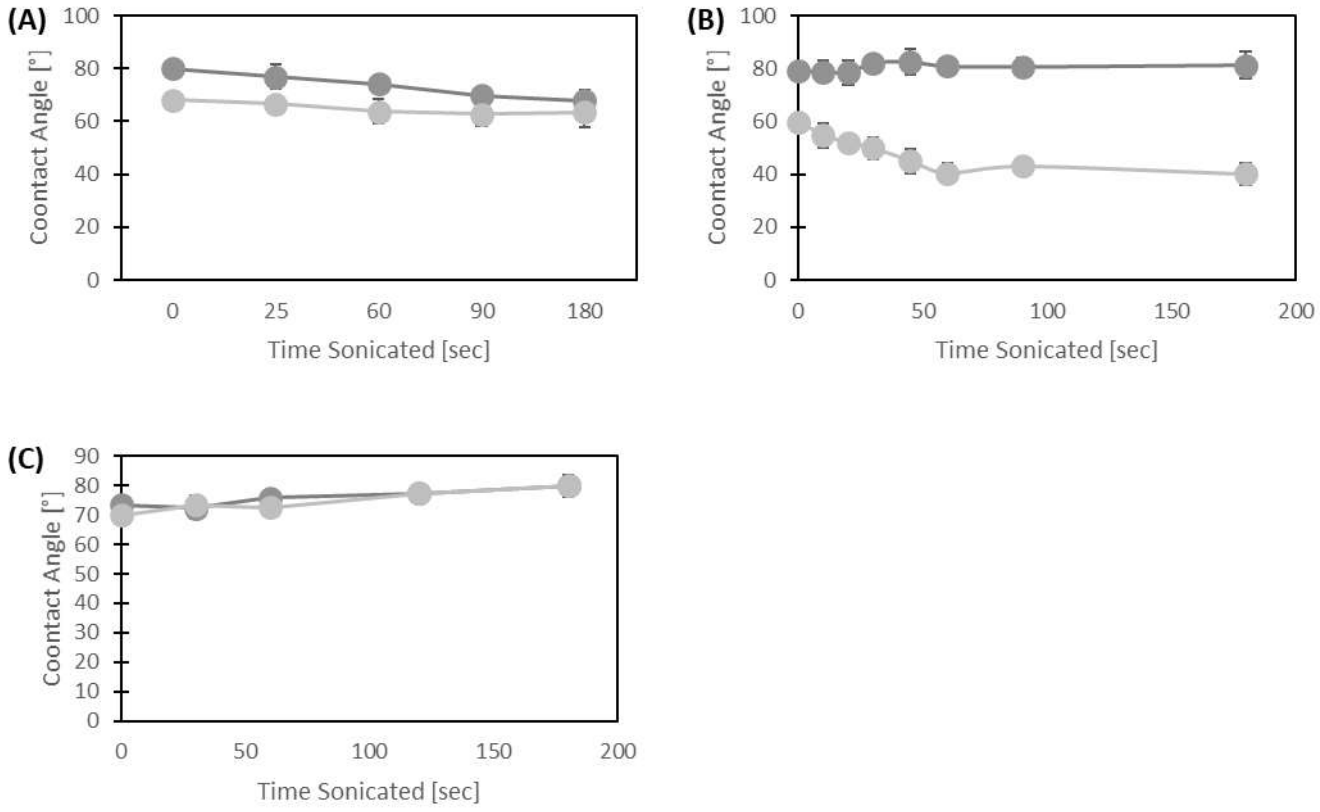

Figure 6.2: Stability of VMS-modified glass surfaces in solvents. Elongated sonication of VMS-modified and cleaned glass surfaces in solvents (A) ethyl acetate, (B) methanol, and (C) acetone.

VMS can be grafted onto various hydroxylated surfaces; we tested a silicon wafer, hydrophilized aluminum foil, and hydrophilized polypropylene foil – all of which possessed increased θadv and θadv after incubation with VMS at room temperature and subsequent sonication for 5 minutes in ethanol as summarized in Figure 3. A silicon wafer modified with VMS was used to confirm film thickness by ellipsometry – where a film thickness of approximately ~3 nm ± 1 was observed. This corresponds to the theoretical chain length of a VMS molecule with a molecular weight of around 700 g/mol; an explanation for this overlap in values could be that VMS molecules were mostly grafted from their chain ends onto surfaces. Another scenario is where VMS molecules stay attached to the surface along their chain length either through chemi- or physisorption. It is known from the literature that dimethoxysilanes are more reactive compared to monomethoxysilanes,[208, 233] which would favor the VMS binding from its chain ends.[234]

VMS could only be grafted onto polypropylene foil if the substrate had been extensively hydrophilized (see Figure 3); simple treatment by UV/ozone cleanser did initially hydrophilize foils. However, the foil quickly lost its low advancing and receding contact angles, and incubation with VMS resulted in varying contact angles. In contrast, a hydrophilization protocol involving ammonium persulfate and UV/ozone treatment led to stably hydrophilized polypropylene foils and the outcome of VMS treatment. When measuring the difference in absorbance between pristine and VMS-treated foils, no changes in the optical properties of polypropylene foil upon VMS grafting were observable (Figure 3).

(A)

Substrate	CA adv.	CA rec.
Silicone waver	37.9/50.7	18.3/32.4
Glass	15/80	0/69.5
Aluminium foil	80/90	57/78
Polypropylene	53.4/77.2	23.1/54

(B)

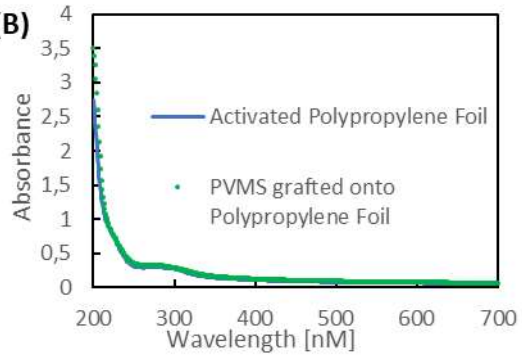

Figure 6.3: Modification of different hydroxylated surfaces with VMS. (A) Change in contact angles (before/after) of different hydroxylated modified with VMS through 3 minutes exposure at room temperature. (B) Change in absorbance of hydrophilized polypropylene foil modified with or without VMS. Polypropylene foil was hydrophilized according to a protocol by Wong et al. Then VMS was applied onto the PP foil at room temperature, and the foil washed in ethanol after 2 minutes incubation.

Previously, solvent choice has been empirically found to influence composite surface homogeneity after silanization.[208] Especially, residual water in the solvent can strongly favor intermolecular condensation.[235] This can be attributed to solvents influencing intermolecular condensation between single silanes as well as its influence on packaging density on the surface. Solvents tested included non-polar solvents (hexane and toluene), aprotic solvents (acetone, dimethylformamide, ethyl acetate, and tetrahydrofuran), and protic solvents (ethanol and methanol). Notably, independent of solvent used for all 10% vol./vol. dilutions of VMS, equal outcomes in θadv and θrec were reached (see table 2) with the exception of ethyl acetate and tetrahydrofuran; these two solvents lead to markedly lower receding angles than other solvents (62° ± 2° θadv and 63° ± 2° θrec, respectively). For all other solvent/VMS systems, the advancing angle after treatment had increased to around ~80° θadv, while receding angles had increased to around ~70° (see Table 1). Furthermore, the percentage of surface modifier species can affect reaction outcome – here, we compared dilutions of 10% and 2% VMS in toluene. However, for the given concentrations, no difference in the ability to modify surfaces was found.

The influence of temperature on reaction outcome when diluting VMS 10% vol./vol. in solvents varied. In the case of VMS dilutions in solvents, advancing and receding contact angles reached after treatment both decreased at -20°C (for ethanol 64° ± 5° θadv and 46° ± 2.5° θrec, respectively) and 0°C (for ethanol 68° ± XX° θadv, and 52 ± 2° θrec, respectively) compared to room temperature (for ethanol 82° ± 3° θadv, and 65° ± 5° θrec). Also, the receeding contact angle did not vary when increasing temperatures beyond room temperature up to around 200° Celsius (see Figure 4). In contrast, the reaction rate happened in comparable fast time spans when grafting VMS from solutions onto surfaces; maximum advancing and receding contact angles were again reached as quickly as 1-minute incubation time. Grafting of VMS using solutions was possible for various substrates, including silicon wafer, aluminum foil, and hydrophilized polypropylene foil. These findings vary from results published in the literature regarding tri- and dimethoxy silanes; for these chemical species, it has been described that the water content of a solvent plays a decisive role in surface grafting density, as well as the speed of reaction.[5, 235]

Previously, our group had published a one-step modification protocol for surface-bound alkenes or alkynes with dissolved thiols under UV irradiation and in the presence of a photoinitiator.[48, 232] When using this reaction scheme to bind perfluorodecanethiol (PFDT) onto VMS-modified surfaces, indeed, after UV irradiation and washing an increase of water contact angles on VMS-surfaces could be observed to 126° ± 1° θadv and 72° ± 1° θrec (Figure 5); no difference in advancing and receding contact angles was observable

anymore independent of whether the slide had been transformed by applying pure VMS at 0°C or a 10% dilution of VMS in toluene at 140°C. Both surface types showed a higher repellence towards low surface tension liquids such as hexane (60° ± 1° θadv and 45° ± 1° θrec) and silicone oil (70° ± 1° θadv, and 56° ± 3° θrec) than unmodified surfaces; overall, the hysteresis for these liquids were reduced to 15°. However, when modifying VMS-surfaces with mercaptoethanol, the water contact angle was reduced to 43° ± 2° θadv and 19° ± 2° θrec. The contact angle of silicone oil and hexane approached 0° degrees – i.e., they were no longer reliably measurable by drop contact angles. Contact angles of water could be further lowered when using cysteamine as a hydrophilic group (9° ± 2° for θadv, and 0° θrec). Alternative hydrophobic groups, however, did not reach contact angles of water comparable to PFDT-modified surfaces (see Figure 5). Yet, clicking thiolated siloxane chains onto the surfaces and infusing them with silicone oils led to contact angles of ~104°. Moreover, VMS-surfaces modified with thiolated siloxane chains were stably infusible by a silicone oil lubricant, i.e., sliding angles of water on surfaces were lowered from 57° to 1°.

[236] Spatially controlled UV-patterning with different thiols thus allowed us to locally confine wettable regions modified with thiolglycerol of arbitrary shapes and surrounded by a repellent PFDT-modified background (see Figure 5). This was independent of the chosen surface modification route – i.e., through either contacting glass slides with undiluted VMS at 0°C or with 10% VMS in toluene at 140°C. However, when slides with a hysteresis value larger than 15°C - e.g., slides that had been contacted with undiluted VMS at temperatures above 100°C - were derivatized using thiol-ene click chemistry, no regular arrays of water droplets could be formed.

(A)

(i)

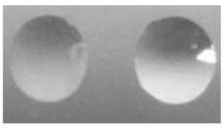

(ii)

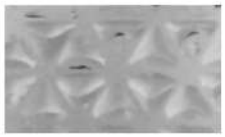

(iii)

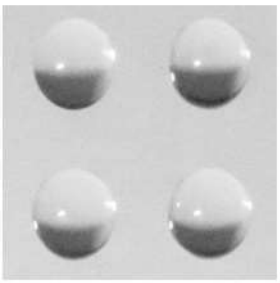

(B)

Thiol	Adv. Θ	Rec. Θ
ß-mercaptoethanol	42.9 ± 2	19.1 ± 2
Thiolglycerol	43 ± 1	19.3 ± 1
Cysteamine	9.4 ± 2	0
Perfluorodecanethiol	122.5 ± 2	87.4 ± 2
Dodecanethiol	103.6 ± 1	84.6 ± 3
Mercapto-Silicone Fluid (GP-71-SS)	114 ± 2	90 ± 1

Figure 6.4: Modification and patterning of VMS grafted onto glass surfaces with different thiol-containing compounds. (A) Photographic images of (i) hexane, (ii) silicone oil, and (iii) water droplets. (B) Contact angles after modification with different thiols (I need to check these values – also, I will refer to a different silicone fluid)

6.4 Conclusion and Outlook

VMS reproducibly bound to and chemically modified inorganic hydroxylated surfaces over a wide range of temperatures, solvent conditions and application conditions tested. Once bound to the surface, it formed an invisible, non-adsorbent but chemically reactive stable film. This agrees with already published accounts of silane modification. Through the introduction of hydrophilic and hydrophobic molecules, droplet arrays of arbitrary shapes of both high- and low-surface tension liquids could be created that reproduced perfectly to photomask patterns;[168] pronounced and sharp wettability patterns were reached, and liquid drops of designer shapes could be confined. Therefore, oligomeric siloxanes seem ideal candidates for the non-work-intensive yet reliable preparation of droplet arrays or even microarrays on hydroxylated surfaces.

7. Small organic amines are almost interchangeable as catalysts for early-stage silanol condensation when simulated isolatedly through a nudged elastic band.

Dorothea Paulssen[1]*

1 Institute of Toxicology and Genetics (ITG), Karlsruhe Institute of Technology (KIT), 76344 Eggenstein-Leopoldshafen, Germany

Corresponding E-mail * elenadorotheapaulssen@gmail.com

ABSTRACT Catalysis of self-condensation of silanols by amino acids is fundamental to structure generation in biogenic glasses, and mimicking through reductionist approaches has been attempted. For example, the Stöber processes based on single amino acids or peptide additives instead of ammonium. In this study, I employed the nudged elastic band (NEB) method to systematically investigate the catalytic abilities of glycine and two of its derivatives relative to ethylamine in promoting both silanol self-condensation and condensation with a model saccharide. The comparative analysis aimed to shed light on the underlying mechanisms and to compare the catalytic strength of the molecules. The NEB calculations were carried out using density functional theory (DFT) within the framework of the Orca software package. Surprisingly, energy profiles of tested molecules were interchangeable, implying that previously experimentally observed rate differences can be attributed to film-forming properties of molecules rather than single molecule capacities. Overall, this study provides valuable insights into the catalytic abilities of small amine-bearing amino acids in silanol self-condensation and condensation with saccharides. The findings contribute to the fundamental understanding of these reactions and offer guidance for the design of efficient catalysts for designer silica synthesis.

Keywords: Silanol self-condensation, amino acid catalysts, nudged elastic band

Submitted to Ceramics-Silikaty

Introduction

Biological silicas exhibit precise and well-defined hierarchical nano- and microscale structuring as well as patterning. The biogenic silicas found in some species, such as sponges and diatoms, can possess beneficial properties with regard to light waveguiding, diffraction, focusing, and photoluminescence[237, 238], as well as structural resistance.[239] Being able to reproduce biogenic silica structures could thus have an impact on a variety of industries ranging from optics to construction. More importantly, under biogenic conditions, natural silica production requires minimal energy input and generates little waste.[240, 241] Utilizing insights from biogenic silica production for the generation of glasses and ceramics could contribute to more sustainable and eco-friendly manufacturing practices.

Biogenic silica production is enabled through protein chemistry, i.e., silica structure formation is largely catalyzed through amino acid side chains.[242] Thus, reductionistic approaches have, for example, studied how single amino acid additives or small peptides can influence the silanol condensation process. Through this process, some amine-bearing amino acids, such as lysine and arginine but also glycine, can lead to the formation of regular microspheres with a narrow size distribution termed colloidal silicas.[242, 243] Although these bear the disadvantage that they exhibit a broad pore size distribution, silica synthesis with amino acid catalysts and peptides is significantly faster than other synthesis routes while requiring marked milder conditions. Colloidal particles obtained find a wide range of applications, from coatings as reinforcing agents in ceramics and concrete to stacking into colloidal crystals as optical elements.[244, 245]

In natural organisms, such as diatoms, a variety of amine-containing compounds are known to be involved in silica synthesis, primarily lysine in methylated form or modified with oligo(1-methylazetane) terminated by a primary amine.[246-249] It was determined that alkylated amines are more powerful than just protonated amines in promoting early silica condensation. However, such trends would not hold true for other experimental studies where small derivatives of glycine were compared with non-alkylated lysine.[250] Computationally, the group of Meng[251] determined theoretically by the first-principle method that ethylamine, as a model organic amine, will transiently bind to the condensation intermediate by a Sn-2 mechanism, lowering the activation barrier. However, in general, a molecular-level understanding of the role of amino acids in silanol condensation is largely missing. Here, often, computational analysis that may provide such insides is lacking, which in turn hampers the development of computational methods that can guide the discovery of novel silica synthesizing methods.[252]

Besides controlling rates of silica precursor hydrolysis and condensation, film-forming properties of amine-bearing compounds, as well as their simple ability to form non-covalent bonds with silanols and silicas, can render them with templating qualities. Here, even subtle differences in catalyst and solvent structures can lead to profound differences in formed microscopic and macroscopic condensates.[253-255] As has been shown for the catalyst tetramethylammonium, catalysts may bias reaction outcomes towards specific structural motives.[256]

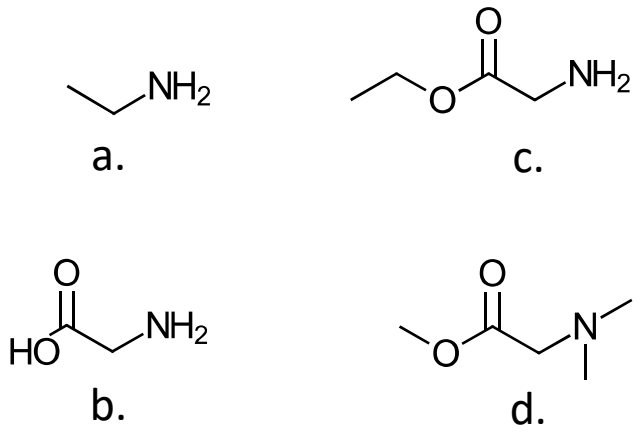

Figure 7.1. Overview of compared small amine-bearing compounds: a. ethylamine; b. glycine; c. glycine ethyl ester; d. N,N-dimethylglycinemethylester

Therefore, here I extend the work of Meng et al.[251] First, I probe whether their proposed mechanism is reproducible and can be applied to glycine or two of its derivatives for the catalysis of silanol self-condensation. These molecules were chosen as they exhibit clear differences in experimentally observable self-condensation rates. As an implicit solvent model, aqueous conditions were chosen as not just aqueous sol-methods can be used to modify certain surface types with silanols, such as carbohydrates,[257] but also are most often applied when forming silicas or gels from silanol precursors.[243] Surprisingly, for the case of condensation of two silanol compounds, only marginal activation energy barrier differences between ethylamine, glycine, an amine-alkylated derivative of glycine, and a non-alkylated derivative of glycine were observable. This provides evidence that rate difference, as well as differences in the structures formed, can be attributed to differences in the film-forming properties between the single catalyst molecules. This holds true even when changing the implicit solvent model to ethylene glycol. To prove that the proposed mechanism of catalysis may be applicable to cases beyond the self-condensation of silanols, condensation between a silanol molecule and a model saccharide, ketotriose, was modeled following the proposed

mechanism by Meng and coworkers. Indeed, this led to a significant reduction in the energy barrier of ~15 kcal/mol when compared to uncatalyzed reactions.

Results

It is reasonable to start an energetic reaction characterization of amine compounds from the complex of non-bound silanols and amine compounds.[251] These non-covalent complexes are likely to occur in solution as they are more energetically favorable than purely water-bound silanols or amine compounds. Already, when searching for optimal geometries between two silanols non-covalently interacting with ethylamine, suggested optimal geometries are found in which the hydrogen of one hydroxyl group of silanol has been donated to the nitrogen of ethylamine (Figure 2). This agrees with the mechanism suggested by Meng et al.[251] While the donated hydrogen has a distance of just 1.07 Å to its binding nitrogen, it is still close to its donor oxygen, being only 1.6 Å away (Figure 2). Here, it is favorable that the now naked oxygen is even closer to a hydrogen of the neighboring silicic acid, which is just 1.56 Å away. This brings the naked oxygen closer to the central silicon atom of the second silicic acid with a distance of now only 3.56 Å.

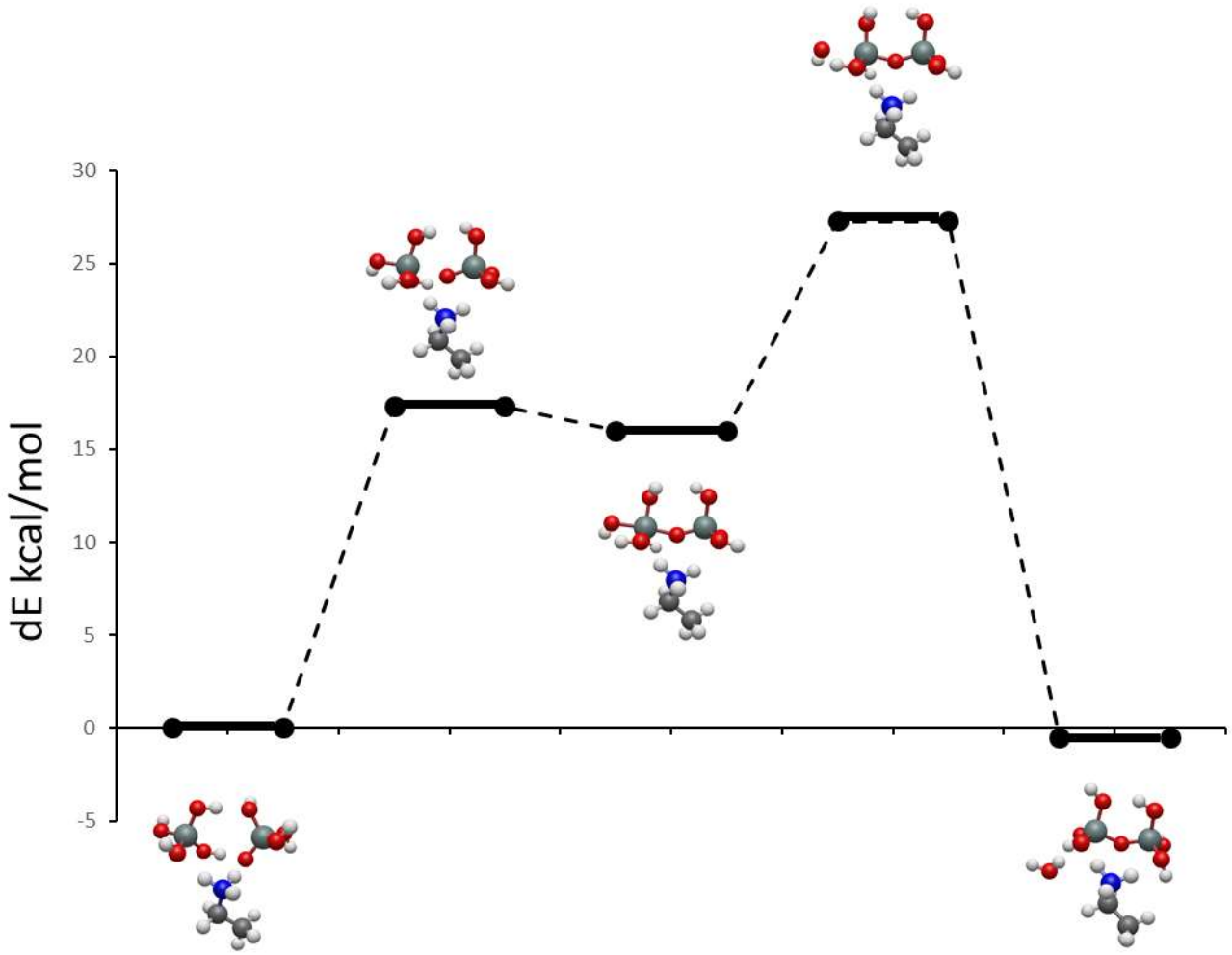

Figure 7.2. Minimum energy path for the condensation of two silanols with each other in the presence of ethylamine. The Si, O, C, H, and N atoms are in grey, red, gray, white, blue, and gray, respectively.

All intermediates, and transition states predicted by Meng et al. were found with the B3LYP or the M062X functional as well. While for the B3LYP functional,[258, 259] the same energy barrier as in the study by Meng was calculated, for the M062X functional,[260] this differed by up to 10 kcal/mol. The one noted difference for the B3LYP functional relative to the study by Meng et al.[251] was that when considering the non-separated molecules, the reaction that resulted was slightly exothermic (-0.51 kcal/mol) (Figure 2).

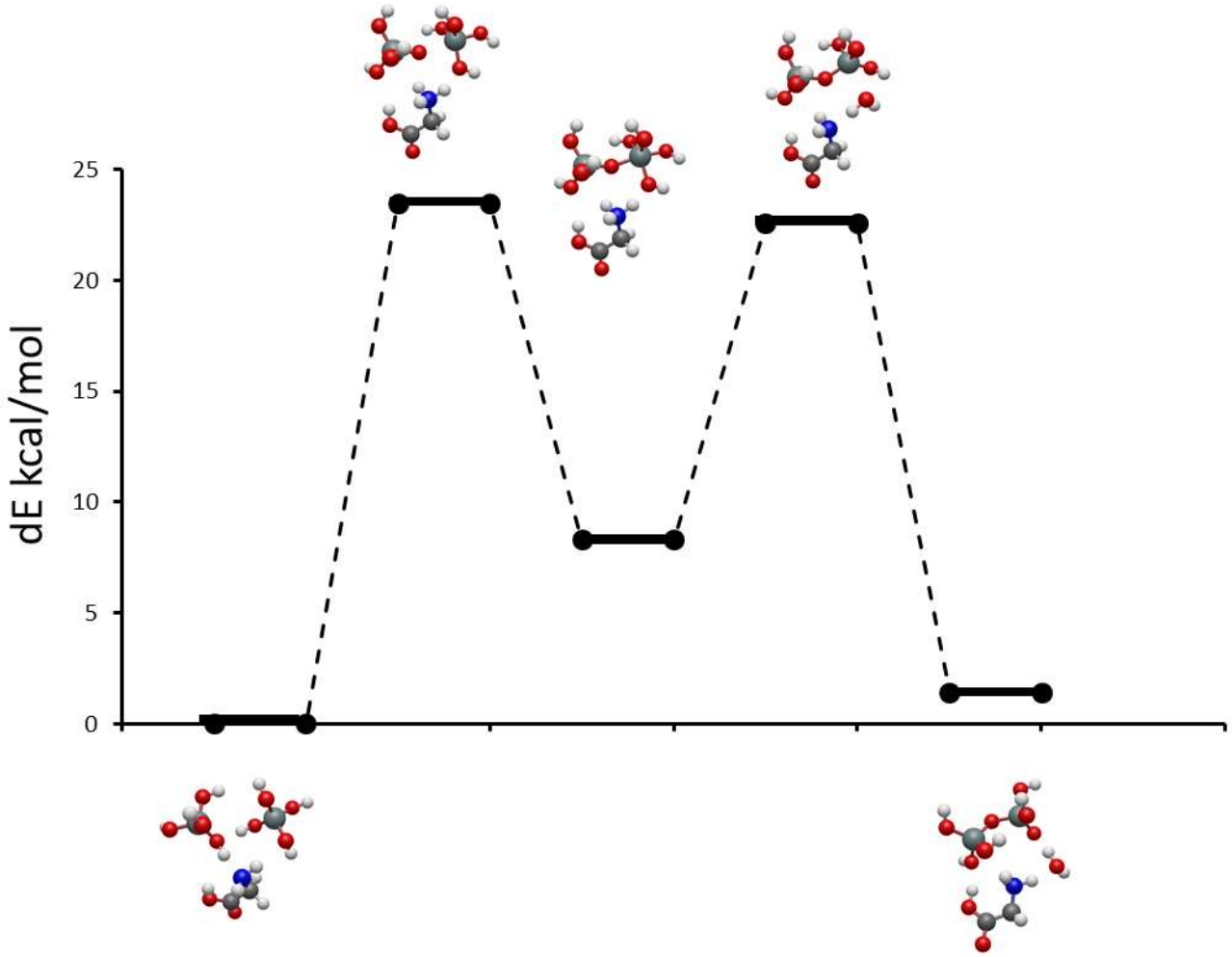

Figure 7.3. Minimum energy path for the condensation of two silanols with each other in the presence of glycine. The Si, O, C, H, and N atoms are in grey, red, gray, white, blue, and gray, respectively.

In contrast, when using glycine (Figure 3) or one of its derivatives, N,Ndimethylglycinemethylester (Figure 4) or glycine ethylester (Figure 5), as catalysts, an intermediate structure was predicted that was around 15 kcal/mol downhill of the first energy barrier. Energy barriers themselves varied from negligible (within a 5 kcal/mol range difference) between all catalysts tested. For glycine and N,N-dimethylglycinemethylester reactions were slightly endothermic (1.44 and 2.13 kcal/mol, respectively). In the case of glycine ethylester, the reaction was nearly equithermic (0.16 kcal/mol) (Figure 5).

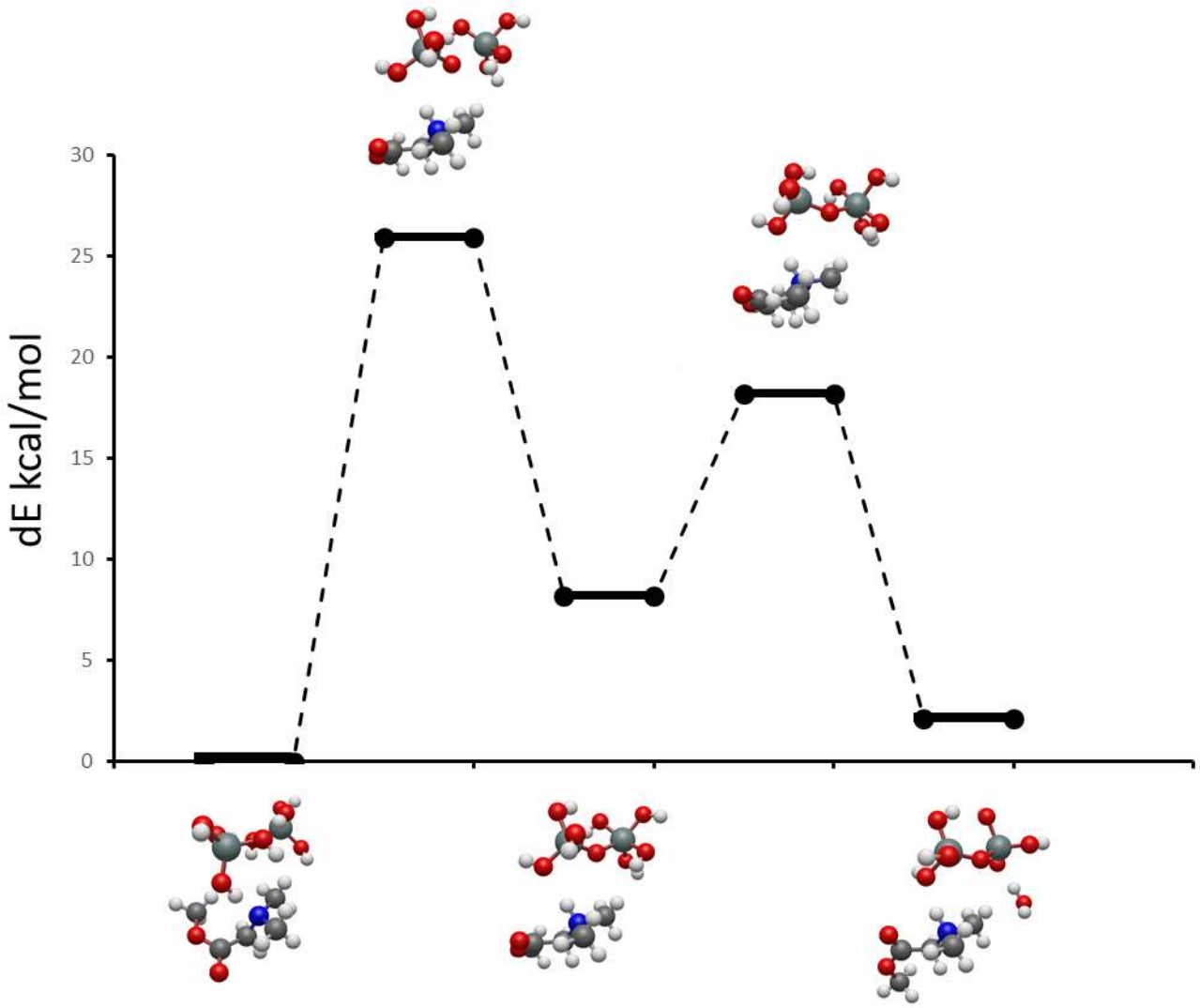

Figure 7.4. Minimum energy path for the condensation of two silanols with each other in the presence of *N,N*-dimethylglycinemethylester. The Si, O, C, H, and N atoms are in grey, red, gray, white, blue, and gray, respectively.

None of the predicted reactants after geometry optimization already had three hydrogens bound to the amino acid nitrogen atom. In contrast, the non-covalent complex of nitrogen to which a third hydrogen was bound was energetically uphill relative to a complex with fully hydrated silicic acids. Nevertheless, the partial energy barriers of calculated reactions were smaller than for ethylamine. This included glycine, for which an energy barrier of just 23.47 kcal/mol relative to reactants was calculated. In contrast, the energy barrier of N,N-dimethylglycinemethylester was close to the energy barrier of ethylamine (25.90 kcal/mol). Glycine ethylester had the smallest reaction barrier (22.92 kcal/mol), both relative to its reactants and lower energy intermediates. This trend potentially opposes experimental

measurements where, in bulk reactions, alkylated amines are the more powerful catalysts than just protonated amines.

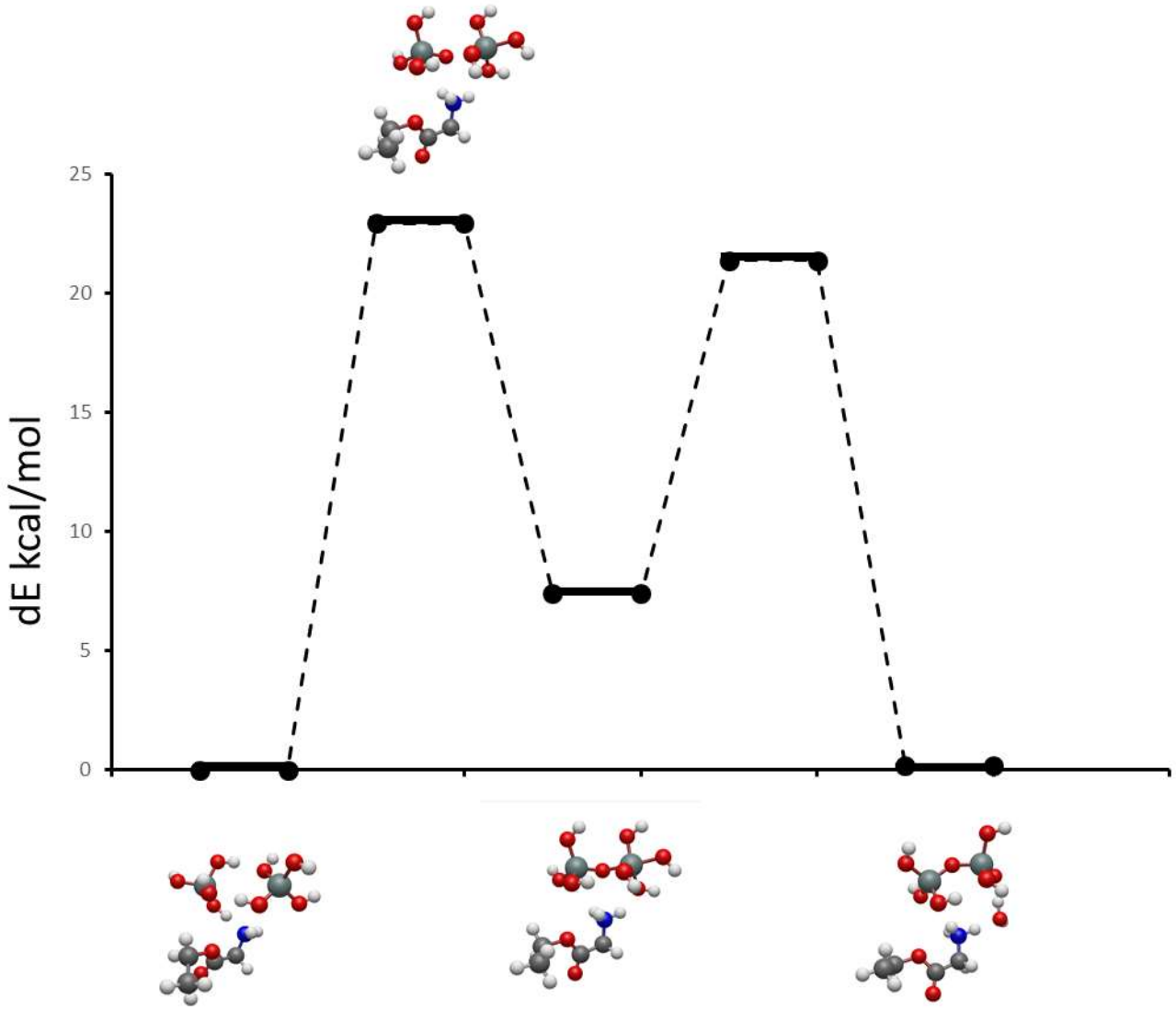

Figure 7.5. Minimum energy path for the condensation of two silanols with each other in the presence of glycine ethylester. The Si, O, C, H, and N atoms are in grey, red, gray, white, blue, and gray, respectively.

Independent of functional used initial energy minimum geometries of the non-covalent glycine with silicic acid complex predicted a direct interaction of the carboxyl head group with the nitrogen atom of glycine – even in the case of alkylated *N,N*-dimethylglycinemethylester. For the given implicit solvation model no inhibitory effects of carboxyl group interaction with nitrogen in the case of glycine on reaction progression were found. However, it cannot be ruled out that neighboring glycines would arrange in a way that reactions are inhibited. The distance between the carboxyl group hydrogen was 2.1 Å, while it was only 1.7 Å for one of the hydrogens of

silicic acid (Figure 3). The increased electronegativity of the concerned oxygen atom in silicic acid induced it to approach the silicon atom of the neighboring silicic acid molecule. The distance between its hydroxyl atom and the nitrogen atom of glycine remained unvaried, with an increase in complex energy of just 5.85 kcal/mol. Eventually, the hydrogen was donated to the nitrogen atom of glycine. A transition state was found when the naked oxygen became 2.24 Å close to the central silicon of the neighboring silicic acid. However, it remained only 2 Å, separated from the donated hydrogen atom. While this transition state was energetically uphill by 23.47 kcal/mol relative to the initial complex, an intermediate immediately formed that was only 8.31 kcal/mol uphill of the original complex (Figure 2).

N,N-dimethylglycinemethylester followed the patterns observable for glycine interchangeably. For both molecules, the five-bound silicone molecule presented a stable intermediate; dissociation of a hydroxyl moiety needed to overcome an energy barrier of around 10 kcal/mol. This was independent of the position studied at which a hydroxyl group could dissociate from. For the intermediate and during dissociation of the fourth hydroxyl group, hydrogen bonding took place between the amine atom of the amino acid or its derivative and a hydroxyl group of the newly formed disilane with a distance between the hydrogen atom and oxygen atom of only 1.6 Å. In contrast, an outlier in the observable energy barrier was glycine ethylester. A potential explanation for that is that the terminal oxygen had a larger distance to the hydroxyl groups of the attacking silicic acid than in the other two amino acid compounds due to its ethyl end group.

When changing the implicit solvent model from water to ethylene glycol, energy barriers of reactions were only slightly reduced by ~2 kcal/mol in the case of glycine catalysis and ethylamine. However, intermediate structures found were considerably far less energetically stable in the case of glycine and only differed from maximum energy barriers by ~5 kcal/mol in this environmental setting. This was a pronounced difference from the aqueous setting and implies that when using ethylene glycol as a solvent, the reaction is less likely to be halted at the intermediate stage. Here, the terminal hydroxyl group of glycine was positioned 2.4 Å away from the nitrogen atom of glycine but 2.28 Å away from a distal hydroxyl group of the newly formed disilane.

As other silanol condensation reactions exist where the presence of ammonium compounds may be beneficial for reaction outcome, theoretical investigations of amino acid catalysis of silanol condensation were extended.[261] In a first step to estimate the influence of organic amine catalysis on carbohydrates' condensation with silane, silane condensation with ketotriose in the presence and absence of ethylamine was studied by NEB as a computationally efficient alternative to larger molecules, such as glucose or starch. Assuming a similar mechanism to silanol self-condensation – proton transfer of silicic acid to ethylamine followed by the obstruction of a proton from a neighboring hydroxyl group of ketotriose and subsequent

condensation – the presence of ethylamine lowers activation energy barriers by a substantial ~13 kcal/mol from 45 kcal/mol without a catalyst in an implicit aqueous solvent model to 32-33 kcal/mol with catalyst. Likewise, when changing the implicit solvent system to ethylene glycol, an activation barrier of around 31-32 kcal/mol was reached. For all assemblies tested, this is a significantly higher energy barrier than for self-condensation. However, the opposite scenario, obstruction of a proton from the sugar was not investigated and may differ in energetics. Given that energy changes regarding the formation of an initial reaction assembly were not considered, it is possible that the actual energy barrier difference is smaller as adsorption effects to real saccharides would take place. Nevertheless, a larger activation energy barrier for saccharide condensation agrees with experimental results that silanes bearing amine moieties in their side chains hardly bind to cellulose as monomers but rather in larger condensed forms. [262]

For the calculated energy barrier differences, no adsorption effects were considered. Thus, the given relative size of reaction barriers to one another may be overestimated as adsorption to saccharides' surfaces may be more energetically favorable than to another silanol for certain reaction conditions. However, for the given considerations, Eyring's formula[263] would predict dramatic differences in half-lives for the calculated energy barriers: Half-life times of self-condensation would be in the range of days, while in the range of years for saccharide-condensation roughly at room temperature (24°C). This could be lowered to a half-life of around 1 hour for saccharide condensation - and seconds for self-condensation - if ranging the temperature to 120°C. How large the actual silanols that bind to the hydroxyl groups of a given saccharide would be would thus also depend on whether oligomeric silanol growth slows down in reaction rate after enough monomers have been added. As the work of Meng [251] pointed out, this is not the case, at least in the tetramer stage of silanols. Here, it needs to be investigated whether using oligomeric silanols as starting materials could potentially speed up the onset of silanol binding to saccharides. This is particularly interesting, as larger sizes of silanols can diverge into different structural motifs, such as branched or ring molecules. Here, it needs to be seen whether the difference in side chains of amino acids and their derivatives starts to play a role in creating divergent reaction outcomes. Overall, even if not all possible hydroxyl groups on the saccharides silanols are bound, given the existence of oligomeric silanols in the reaction mix, saccharides would exhibit a high loading with silanols after binding.

Conclusion and Outlook

Small natural and derived amino acids were compared with ethylamine on a theoretical level for their ability to catalyze silanol condensation. Here, it was assumed that the general mechanism of reaction followed the previously described molecular catalysis for ethylamine. Energy profiles of all amino acids tested were highly similar, and geometric differences varied marginally. Thus, amino acids not only catalyze silanol condensation but, under tested solvent conditions, may promote reaction rates comparable to ethylamine.

Under all tested conditions, stable intermediate structures were identified in contrast to ethylamine catalysis. Varying the implicit solvent system, i.e., changing it from water to ethylene glycol, changed the energy profile, i.e., led to far less pronounced intermediate states. The small differences observable between amino acids are likely caused by side-chain interaction in the reaction. However, the differences observed cannot explain previously observed experimental results.[250] It can be anticipated that in the case of small amino acids, their film-forming capacities influence bulk reaction rates. This is a potential anchoring point for reaction rate optimization if needed.

Organic amines also functioned as catalysts for the condensation of silanols with a model saccharide: ketotriose. If not considering the adsorption effects between reactants, silanol condensation with ketotriose had a considerably larger activation energy – around 13 kcal/mol – making it unlikely that silanols will bind as monomers to saccharides through organic amine condensation. Again, the work presented here implies several experimental parameters that can be investigated. For example, if ethylene glycol is nearly interchangeable with water as a reaction solvent regarding the effect on reaction rates, conducting solution reactions at elevated temperatures is eased.

Materials and Methods

Quantum chemical calculations were performed using the ORCA software package version 5.2.0.[264] Prior to NEB-TS searches, reactants and products were optimized with the B3LYP functional [258, 259] with a valence triple-zeta polarization basis set, def2-TZVP,[265, 266] and the general auxiliary basis set, def2/J,[265] using D4 dispersion forces correction [267] and SMD implicit solvent model [268] for water if not otherwise stated. To find the minimum energy path connecting reactants and products, the NEB-TS method [269] is used at the B3LYP/ def2-TZVP/ def2/J level of theory with calculated Hessian matrixes every 5 iterations. Intermediate images were set to 10. Immediately after the convergence of the NEB-path, the climbing image and saddle point were optimized until the reached conformers had only one imaginary frequency left.

8. Conclusion and Outlook

8.1 Conclusion

Silanes and siloxanes are a class of compounds that contain silicon and are widely used to modify the surface properties of materials.[270] These compounds can be used to create functional surfaces with a variety of properties, in particular surfaces with special wettability. Additionally, the unique low energy of siloxanes makes them ideal as lubricants for creating specialty surfaces, such as slippery surfaces.[3] An overview of historical and current literature that investigates the wettability of surfaces and their creation can be found in Chapter 1.

Slippery surfaces are a class of specialty surfaces that have gained significant interest in recent years due to their potential applications in various fields, including biomedicine, microfluidics, and energy.[3, 271, 272] Silanes and siloxanes are key components in the fabrication of slippery surfaces as they can reduce the surface energy of a material, making it slippery and rendering liquid drops or gaseous bubbles on the surfaces highly mobile. Here, two aspects of liquid manipulations with chemically patterned and stably lubricant-infused surfaces were investigated. In an initial basic study (chapter 4), different chemical surface modifications were investigated to stably lock a lubricant layer in place against intruding water drops. Moreover, it was demonstrated for a wide variety of lubricants with varying surface tensions and belonging to varying phases that they can easily replace a non-matching lubricant from chemical patterns and form micropatterns precisely following the underlying surface chemistry. Moreover, it was found that siloxane polymers, such as perfluoropolyether oils, can confine liquids with lower surface tension than siloxanes. Overall, liquid-liquid displacement was shown to be an efficient method for the formation of surface lubricant patterns. This approach held several advantages over those methods previously discussed in the literature for the formation of patterned slippery surfaces, including simplicity, speed, and versatility. The micropatterns can be easily created and modified by changing the composition or properties of the liquids and adjusting the guiding geometry. In Chapter 5, bespoke patterned slippery surfaces were studied for their ability to modulate the flow of aqueous drops on them. Simple drop sorting based on size was achieved by creating two-phased hydrophobic slippery surfaces with varying micro-patterns on them. Size differences as small as one 1 µL could be exploited for the range of patterns tested. Due to lithographic flexibility, a wide range of patterns for drop sorting could be investigated that had not been studied either experimentally or theoretically in the literature for conventional non-slippery surfaces. Miniscule differences in pattern design can have pronounced effects on drop flow. Further experiments characterized the energy barriers between different lubricants for aqueous drops in order to create empirical data to test whether the current theory can

explain the dimension of energy barriers on patterned slippery surfaces. While it is possible to explain the presence and extent of energetic traps on patterned lubricant-infused surfaces analytically, the cloaking effect, which has not been explained analytically, plays a decisive role in droplets crossing energy traps. The reason for this is that the mechanism of cloak formation and disappearance around droplets can strongly influence drop dynamics; hence, experimental analysis of cloak dynamics during drop crossing of energetic traps is needed. Here, it has to be noted that lubricant depletion along liquid-liquid barriers was observable. As silanes and siloxanes are highly modifiable, the question arises whether cloaks should be prevented for enhanced analysis through the application of non-cloak-forming oils in the case of liquid drops. Likewise, the transport of non-liquid drops along liquid-liquid barriers, such as the underwater transport of gas bubbles, remains to be tested.

Silicones can also modify the wettability of hydroxylated surfaces through covalent attachment onto surfaces – a relatively slow reaction unless they possess reactive side chains, such as in monomeric silanes.[19] Reactive oligomeric siloxanes are known to have better film-forming capacities than monomeric silanes. In Chapter 6, the utility of oligomeric siloxanes to create homogenous surfaces amenable to secondary derivatization was characterized. First, the influence of solvents and temperature on surface modification through oligomeric siloxanes was mapped out by measuring contact angles. Additional surface properties such as transparency, AFM profile and resistance to solvent degradation were tested. Next, surfaces were modified in secondary derivatization steps and hydrophobic or hydrophilic functional groups were introduced. It was shown that on oligomeric siloxane functionalized surfaces, sharp enough wettability contrasts could be established through secondary derivatization that allowed for the formation of droplet arrays through discontinuous dewetting. Surface patterns, in contrast to surfaces modified under equal conditions with monomeric silanes, strictly followed photomask patterns. This application-specific study demonstrates the relevance of oligomeric siloxanes as surface modifiers. It stresses the importance of the mechanism of advanced film-forming capacity, which needs to be further studied in detail. Such insights would allow us to better manipulate the film-forming capacities of oligomeric siloxanes.

The reactivity of silane and siloxanes can be enhanced through catalysts. In the case of alkoxy silanes, an example of environmentally friendly aqueous catalysts is amino acids bearing an amine in their side chains. In Chapter 7, the kinetics of amino acid catalyzed alkoxy silane self-condensation, as well as condensation with a model saccharide, was studied theoretically using the nudged elastic band method. It was found that geometries between glycine and two of its derivatives only varied marginally. Experimentally observable pronounced differences in rates of reactions are hence likely to be due to bulk effects. They

may be thus manipulated through adjusting reactant concentrations. Energy profiles of reactions were determined through the nudged elastic band and varied considerably when testing water or ethylene glycol as the implicit solvent model. Here, ethylene glycol may favor more efficient reaction rates than water when using glycine as a catalyst for silane self-condensation. Moreover, it was shown that amino acid catalysis also considerably enhances the condensation reaction between silanols and model saccharides.

Overall, this thesis demonstrated that it is likely that there will be ongoing developments in silicone surface coatings in the near future as a plethora of further improvement points exist.

8.2 Outlook

This thesis focused on applying siloxane and silane functionalized surfaces within the framework of drop arrays and drop movement in particular, as well as bio-screening in general. Stably lubricant-infused surfaces can prevent bio-fouling and reduce the energy required to transport liquid entities along the surface. Indeed, citing work has shown that SLIPSs facilitate the quantitative actuation of droplets by electric or magnetic forces.[273-275] These seem promising to enable in field diagnostic devices or enable novel electric read-out approaches.

Nevertheless, the citing work so far has been explorative in nature. It must be shown that patterned SLIPSs can truly make a difference as material for screening endeavors. For example, SLIPSs have also found application in non-biological drop mobility with acoustophoretics.[194] Related acoustophoretic work (for example in the context of bio-sample ionization) currently still uses patterned traditional “dry” surfaces for robust drop transport.[276] It has to be tested whether patterned SLIPSs can be used and improve the same tasks while offering enhanced anti-biofouling and increasing transport and ionization speed. Likewise, the application area of patterned magnetic SLIPSs may present various opportunities for application and consequent adaptation of the systems.[3, 277] However, here, SLIPSs would simply represent an enabling element, and their use would depend on progress in acoustophoretic or electrophoretic analysis.

This is important as it reflects the ever-changing nature of high-throughput experimentation and testing. In the past, single or few read-out screens were conducted. Currently, there is an attempt to develop high-throughput analysis systems that allow the collection of large and deep data sets per sample. Screening as a word is used in various fields ranging from chemistry to medicine with varying definitions. Independent of discipline, it is well recognized that the choice of method greatly influences and can even bias the outcome of high-throughput experimentation or screenings. Moreover, in the case of diagnostics and laboratory consumables, the cost of materials can be decisively prohibitive. Nevertheless, SLIPSs can potentially fulfill the criteria of smoothing a highly automated process without increasing costs too much; their remarkable anti-biofouling property seems particularly suited for in-field bioanalytical workflows.[278, 279]

One notable area of application of patterned SLIPSs is in drop micro-arrays for the high-throughput screening of bacteria.[126] This is an area where potentially biological testing could benefit from characterizing the liquid behavior on surfaces further; small free-standing liquid compartments are known to have remarkedly different liquid transport phenomena than larger liquid units (see Chapter 1). An example of this is the Marangoni effects. A student

project during this thesis was set up to study Marangoni effects under controlled conditions: a gradient generator where two pumping compartments are separated by a liquid bridge. This gradient generator can be manufactured as a free-standing compartment; here, size effects were observable for the onset of the Marangoni effect. In a follow-up project, a free-standing compartment should be compared to a covered (or suspended) compartment in which liquid is only exposed to air on its edges. In particular, an attempt should be made to explain the size difference in onset with Marangoni effects analytically and/or computationally. The thus developed model could then be used to predict under which conditions Marangoni flows can arise in free-standing liquid compartments with different geometric shapes. The overarching goal of such a project would be to understand and demonstrate the controllability of droplet microarrays, e.g., through controlling their chemical makeup or by simply covering them with a protective cover. This would be a pre-requisite when studying populations of bacteria not only through their average but also at the single cell unit.

Other application areas of SLIPSs not mentioned in this thesis so far could turn out more promising to truly present a game changer for their respective fields. One such field could be energy generation[280] or underwater bubble transport.[281] Likewise, patterned lubricant surfaces could find applications as supported ionic liquid phase (silp) for catalysis and gas filtering.[282] These fields have in common that the cloaking effect and other lubricant depletion mechanisms are indecisive for them. In contrast, the field of slippery membranes seems decisively cursed by lubricant depletion.[67, 283, 284] A way around this problem is to covalently link lubricants to the membrane. Constructing such liquid-like surfaces is not trivial and is currently under thorough study in literature.[285] Typically, silicone brushes are used to create such surfaces.

Regarding covalent modification of surfaces with silanes and siloxanes, for the next steps, it needs to be experimentally confirmed that glycine derivatives in either water or ethylene glycol are almost indistinguishable from ethylamine as silanol condensation catalysts. Moreover, it needs to be tested experimentally if amino acids are valuable catalysts to speed up the reaction between hydroxyl silanes and less reactive hydroxylated surfaces such as natural carbohydrates. Here, it is interesting to study how self-condensation compares with condensation with hydroxylated surfaces and how film forming of silanes and oligomeric siloxanes affects reaction rates. This can help to decide whether novel applications – besides the modification of simple surfaces – such as dye formation or 3D printing can be derived from this.

Nowadays, silanes are typically preferred over monomeric silanes when robust surfaces are about to be created. On the other hand, monomeric silanes are preferred over oligomeric siloxanes if speed and reactivity are preferable. The kinetic limits for the formation of regular

films need to be understood. This hypothesis could be for example tested by a ReaxFF forcefield[19] or reactive Martini models.[286, 287] Missing from this study are appropriate read-out protocols that focus on attributes of formed films, such as spacing between neighboring silicon atoms or film heights. Likewise, a separate protocol estimating the spacing of vinyl groups is required. This could then serve as an anchor point to be further compared with experiments probing the homogeneity of secondary derivatization of surfaces through XPS.

9. References

1. Der Voort, P.V. and E.F. Vansant, Silylation of the Silica Surface A Review. Journal of Liquid Chromatography & Related Technologies, 1996. 19(17-18): p. 2723-2752.

2. Xie, Y., et al., Silane coupling agents used for natural fiber/polymer composites: A review. Composites Part A: Applied Science and Manufacturing, 2010. 41: p. 806-819.

3. Li, J., et al., Slippery Lubricant-Infused Surfaces: Properties and Emerging Applications. Advanced Functional Materials, 2019. 29(4): p. 1802317.

4. Wooh, S. and D. Vollmer, Silicone brushes: omniphobic surfaces with low sliding angles. Angewandte Chemie International Edition, 2016. 55(24): p. 6822-6824.

5. Sims, R., The Self-assembly of Organosilane Films on Aluminium Oxide and Their Application to Si-Al Composite Materials for 3D Printing. 2019, Flinders University, College of Science and Engineering.

6. Tian, Y., B. Su, and L. Jiang, Interfacial Material System Exhibiting Superwettability. Advanced Materials, 2014. 26(40): p. 6872-6897.

7. Li, L., et al., Roles of silanes and silicones in forming superhydrophobic and superoleophobic materials. Journal of Materials Chemistry A, 2016. 4(36): p. 13677-13725.

8. Williams, R., D. Wilson, and N. Rhodes, Stability of plasma-treated silicone rubber and its influence on the interfacial aspects of blood compatibility. Biomaterials, 2004. 25(19): p. 4659-4673.

9. Part Introduction, in Silicon Chemistry. 2003. p. 1-3.

10. Clarson, S.J., Silicones and silicone-modified materials: a concise overview. 2003.

11. Rochow, E.G., An introduction chemistry of the Silicones. 2011: Read Books Ltd.

12. Maboudian, R., W.R. Ashurst, and C. Carraro, Self-assembled monolayers as anti-stiction coatings for MEMS: characteristics and recent developments. Sensors and Actuators A: Physical, 2000. 82(1-3): p. 219-223.

13. Prashar, D., Self assembled monolayers-a review. Int. J. ChemTech Res, 2012. 4(1): p. 258-265.

14. Haensch, C., S. Hoeppener, and U.S. Schubert, Chemical modification of self-assembled silane based monolayers by surface reactions. Chemical Society Reviews, 2010. 39(6): p. 2323-2334.

15. Seed, B., Silanizing Glassware. Current Protocols in Cell Biology, 2000. 8(1): p. A.3E.1-A.3E.2.

16. Eifert, A., et al., Simple Fabrication of Robust Water-Repellent Surfaces with Low Contact-Angle Hysteresis Based on Impregnation. Advanced Materials Interfaces, 2014. 1(3): p. 1300138.

17. Xia, Y., et al., Microcontact Printing of Octadecylsiloxane on the Surface of Silicon Dioxide and Its Application in Microfabrication. Journal of the American Chemical Society, 1995. 117(37): p. 9576-9577.

18. Ramezani, M., M.R. Vaezi, and A. Kazemzadeh, Preparation of silane-functionalized silica films via two-step dip coating sol–gel and evaluation of their superhydrophobic properties. Applied Surface Science, 2014. 317: p. 147-153.

19. Deetz, J.D., Reactive Molecular Dynamics Investigations of Alkoxysilane Sol-Gel and Surface Coating Processes. 2015: University of California, Davis.

20. Abdelmouleh, M., et al., Interaction of Silane Coupling Agents with Cellulose. Langmuir, 2002. 18(8): p. 3203-3208.

21. Sananes Israel, S., et al., Surface Properties of Alkoxysilane Layers Grafted in Supercritical Carbon Dioxide. Langmuir, 2019. 35(7): p. 2792-2800.

22. Brzoska, J.B., I.B. Azouz, and F. Rondelez, Silanization of Solid Substrates: A Step Toward Reproducibility. Langmuir, 1994. 10(11): p. 4367-4373.

23. Arkles, B., Tailoring Surfaces with Silanes. Chemtech, 1977. 7: p. 766-778.

24. Norström, A.E.E., et al., Adsorption of an Isocyanurate Silane on E-Glass Fibers from Ethanol and Toluene. Journal of Colloid and Interface Science, 2000. 232(1): p. 149-155.

25. Brownfield, A.L., C.P. Causey, and T.J. Mullen, Effects of surface water on organosilane nanostructure fabrication using particle lithography. Thin Solid Films, 2015. 594: p. 184-191.

26. Yoshida, W., et al., Multilayer Alkoxysilane Silylation of Oxide Surfaces. Langmuir, 2001. 17(19): p. 5882-5888.

27. Chen, W.-H., et al., Silanization of solid surfaces via mercaptopropylsilatrane: a new approach of constructing gold colloid monolayers. RSC Advances, 2014. 4(87): p. 46527-46535.

28. Zhu, M., M.Z. Lerum, and W. Chen, How to prepare reproducible, homogeneous, and hydrolytically stable aminosilane-derived layers on silica. Langmuir : the ACS journal of surfaces and colloids, 2012. 28(1): p. 416-423.

29. Oyola-Reynoso, S., et al., Recruiting physisorbed water in surface polymerization for bio-inspired materials of tunable hydrophobicity. Journal of Materials Chemistry A, 2016. 4(38): p. 14729-14738.

30. Black, J.E., et al., Investigation of the Impact of Cross-Polymerization on the Structural and Frictional Properties of Alkylsilane Monolayers Using Molecular Simulation. Nanomaterials (Basel, Switzerland), 2019. 9(4): p. 639.

31. Liu, X., et al., Biofunctionalized anti-corrosive silane coatings for magnesium alloys. Acta biomaterialia, 2013. 9.

32. Somasundaram, S., Silane coatings of metallic biomaterials for biomedical implants: A preliminary review. Journal of Biomedical Materials Research Part B: Applied Biomaterials, 2018. 106(8): p. 2901-2918.

33. Arkles, B.C.P., PA, US), Goff, Jonathan D. (Philadelphia, PA, US), Stabilized Solutions of Alkylalkoxysilane Hydrolysates and Flexible Films Formed Thereof, in http://www.freepatentsonline.com/y2018/0044550.html. 2018, Gelest Technologies, Inc. (Morrisville, PA, US): United States

34. Brittain, W.J., et al., The Surface Science of Microarray Generation–A Critical Inventory. ACS Applied Materials & Interfaces, 2019. 11(43): p. 39397-39409.

35. Halliwell, C.M. and A.E.G. Cass, A Factorial Analysis of Silanization Conditions for the Immobilization of Oligonucleotides on Glass Surfaces. Analytical Chemistry, 2001. 73(11): p. 2476-2483.

36. Megone, W., N. Roohpour, and J.E. Gautrot, Impact of surface adhesion and sample heterogeneity on the multiscale mechanical characterisation of soft biomaterials. Scientific Reports, 2018. 8(1): p. 6780.

37. Xu, A., et al., Facile fabrication of a homogeneous cellulose/polylactic acid composite film with improved biocompatibility, biodegradability and mechanical properties. Green Chemistry, 2019. 21(16): p. 4449-4456.

38. Im, H. and J. Kim, Enhancement of the thermal conductivity of aluminum oxide–epoxy terminated poly(dimethyl siloxane) with a metal oxide containing polysiloxane. Journal of Materials Science, 2011. 46(20): p. 6571-6580.

39. Palaganas, J., et al., Facile preparation of photocurable siloxane composite for 3D printing. Macromolecular Materials and Engineering, 2017. 302(5): p. 1600477.

40. Shukrun, E., I. Cooperstein, and S. Magdassi, 3D-Printed Organic–Ceramic Complex Hybrid Structures with High Silica Content. Advanced Science, 2018. 5(8): p. 1800061.

41. Khan, S., L. Lorenzelli, and R. Dahiya. Bendable piezoresistive sensors by screen printing MWCNT/PDMS composites on flexible substrates. in 2014 10th Conference on Ph. D. Research in Microelectronics and Electronics (PRIME). 2014. IEEE.

42. van de Grampel, R.D., et al., The Outermost Atomic Layer of Thin Films of Fluorinated Polymethacrylates. Langmuir, 2004. 20(15): p. 6344-6351.

43. Gurunathan, T., S. Mohanty, and S.K. Nayak, Hyperbranched polymers for coating applications: a review. Polymer-Plastics Technology and Engineering, 2016. 55(1): p. 92-117.

44. Sallenave, X., et al., Tuning and Transcription of the Supramolecular Organization of a Fluorescent Silsesquioxane Precursor into Silica-Based Materials through Direct Photochemical Hydrolysis–Polycondensation and Micropatterning. Advanced Functional Materials, 2009. 19(3): p. 404-410.

45. Im, H.-G., et al., A robust transparent protective hard-coating material using physicochemically-incorporated silica nanoparticles and organosiloxanes. Progress in Organic Coatings, 2017. 105(C): p. 330-335.

46. Berrod, G., et al., Reinforcement of siloxane elastomers by silica. Chemical interactions between an oligomer of poly(dimethylsiloxane) and a fumed silica. Journal of Applied Polymer Science, 1981. 26(3): p. 833-845.

47. Wang, Z., et al., Construction of a superhydrophobic coating using triethoxyvinylsilane-modified silica nanoparticles. Surface Engineering, 2019. 35(5): p. 418-425.

48. Feng, W., et al., Surface Patterning via Thiol-Yne Click Chemistry: An Extremely Fast and Versatile Approach to Superhydrophilic-Superhydrophobic Micropatterns. Advanced Materials Interfaces, 2014. 1(7): p. 1400269.

49. Feng, W., Spatial Surface Functionalization Based on Photo-induced Thiol Reactions. 2016.

50. Rao, M. and M. Shekhawat. A brief survey on basic properties of thin films for device application. in International Journal of Modern Physics: Conference Series. 2013. World Scientific.

51. Kumar, S. and D.K. Aswal, Thin Film and Significance of Its Thickness, in Recent Advances in Thin Films, S. Kumar and D.K. Aswal, Editors. 2020, Springer Singapore: Singapore. p. 1-12.

52. Zhang, L., et al., Functional and versatile superhydrophobic coatings via stoichiometric silanization. Nature Communications, 2021. 12(1): p. 982.

53. Ni, L., et al., Light-induced crystallization-driven formation of hierarchically ordered superhydrophobic sol-gel coatings. Progress in Organic Coatings, 2019. 135: p. 255-262.

54. Sibeaud, M., et al., Scaling-up of mesoporous silica films via an eco-efficient UV processing method. Part 1: Photoinduced mesostructuration. Microporous and Mesoporous Materials, 2018. 257: p. 42-50.

55. Bonn, D., et al., Wetting and spreading. Reviews of modern physics, 2009. 81(2): p. 739.

56. Erbil, H.Y., Dependency of Contact Angles on Three-Phase Contact Line: A Review. Colloids and Interfaces, 2021. 5(1): p. 8.

57. Drelich, J.W., Contact angles: From past mistakes to new developments through liquid-solid adhesion measurements. Advances in colloid and interface science, 2019. 267: p. 1-14.

58. De Gennes, P.-G., F. Brochard-Wyart, and D. Quéré, Capillarity and wetting phenomena: drops, bubbles, pearls, waves. 2013: Springer Science & Business Media.

59. Brutin, D., Droplet wetting and evaporation: from pure to complex fluids. 2015: Academic Press.

60. Law, K.-Y. and H. Zhao, Surface wetting: characterization, contact angle, and fundamentals. 2016.

61. Bormashenko, E.Y., Wetting of real surfaces. Vol. 19. 2018: Walter de Gruyter GmbH & Co KG.

62. Berthier, J. and K.A. Brakke, The physics of microdroplets. 2012: John Wiley & Sons.

63. Ras, R.H. and A. Marmur, Non-wettable surfaces: theory, preparation and applications. 2016: Royal Society of Chemistry.

64. Spori, D.M., Structural influences on self-cleaning surfaces. 2010, ETH Zurich.

65. Sartori, P., The Role of Interfaces in Microfluidic Systems: Oscillating Sessile Droplets and Confined Bacterial Suspensions. 2017.

66. Keiser, A., Dynamiques sur des surfaces texturées et imprégnées. 2018, Sorbonne université.

67. Peppou-Chapman, S.J., Distribution and Depletion of Lubricant on Anti-Fouling Lubricant-Infused Surfaces. 2021, University of Sydney.

68. Savva, N. and S. Kalliadasis, Dynamics of moving contact lines: A comparison between slip and precursor film models. EPL (Europhysics Letters), 2011. 94(6): p. 64004.

69. Arjmandi-Tash, O., et al., Kinetics of wetting and spreading of droplets over various substrates. Langmuir, 2017. 33(18): p. 4367-4385.

70. Starov, V.M. and M.G. Velarde, Wetting and spreading dynamics. Vol. 12. 2019: CRC press.

71. Israelachvili, J.N., Intermolecular and surface forces. 2011: Academic press.

72. O'Hagan, D., Understanding organofluorine chemistry. An introduction to the C–F bond. Chemical Society Reviews, 2008. 37(2): p. 308-319.

73. Bittner, R.W., K. Bica, and H. Hoffmann, Fluorine-free, liquid-repellent surfaces made from ionic liquid-infused nanostructured silicon. Monatshefte für Chemie - Chemical Monthly, 2017. 148(1): p. 167-177.

74. Owen, M.J., Silicone Surface Fundamentals. Macromolecular Rapid Communications. n/a(n/a): p. 2000360.

75. Hauner, I., et al., The Dynamic Surface Tension of Water. The journal of physical chemistry letters, 2017. 8: p. 1599-1603.

76. Good, R.J. and L. Girifalco, A theory for estimation of surface and interfacial energies. III. Estimation of surface energies of solids from contact angle data. The Journal of Physical Chemistry, 1960. 64(5): p. 561-565.

77. Craster, R.V. and O.K. Matar, Dynamics and stability of thin liquid films. Reviews of modern physics, 2009. 81(3): p. 1131.

78. Hamaker, H.C., The London—van der Waals attraction between spherical particles. Physica, 1937. 4(10): p. 1058-1072.

79. Dzyaloshinskii, I.E., E.M. Lifshitz, and L.P. Pitaevskii, The general theory of van der Waals forces. Advances in Physics, 1961. 10(38): p. 165-209.

80. Butt, H.-J., B. Cappella, and M. Kappl, Force measurements with the atomic force microscope: Technique, interpretation and applications. Surface Science Reports, 2005. 59(1): p. 1-152.

81. Huang, Y., et al., MEMS reliability review. IEEE Transactions on Device and Materials Reliability, 2012. 12(2): p. 482-493.

82. Tretyakov, N., et al., The Cassie-Wenzel transition of fluids on nanostructured substrates: Macroscopic force balance versus microscopic density-functional theory. The Journal of Chemical Physics, 2016. 145(13): p. 134703.

83. Ensikat, H.J., et al., Superhydrophobicity in perfection: the outstanding properties of the lotus leaf. Beilstein journal of nanotechnology, 2011. 2: p. 152-161.

84. Cavalli, A., Wetting on micro-structured surfaces: modelling and optimization. 2013, Technical University of Denmark.

85. Yong, J., et al., Superoleophobic surfaces. Chemical Society Reviews, 2017. 46(14): p. 4168-4217.

86. Joly, L. and T. Biben, Wetting and friction on superoleophobic surfaces. Soft Matter, 2009. 5(13): p. 2549-2557.

87. Tsujii, K., et al., Super Oil-Repellent Surfaces. Angewandte Chemie International Edition in English, 1997. 36(9): p. 1011-1012.

88. Wong, W.S.Y., Surface Chemistry Enhancements for the Tunable Super-Liquid Repellency of Low-Surface-Tension Liquids. Nano Letters, 2019. 19(3): p. 1892-1901.

89. Pan, S., et al., Coatings super-repellent to ultralow surface tension liquids. Nature Materials, 2018. 17(11): p. 1040-1047.

90. Raiyan, A., et al., Effect of superamphiphobic macrotextures on dynamics of viscous liquid droplets. Scientific Reports, 2018. 8(1): p. 15344.

91. Hermann, M., et al., Open sessile droplet viscometer with low sample consumption. Lab on a Chip, 2020. 20(10): p. 1869-1876.

92. Chao, S.-h. and D.R. Meldrum, Spontaneous, oscillatory liquid transport in surface tension-confined microfluidics. Lab on a Chip, 2009. 9(7): p. 867-869.

93. Hanyak, M., Marangoni flows induced by non-uniform surfactant distributions. 2012.

94. Tan, J.N., T. Alan, and A. Neild, Stability of flowing open fluidic channels. AIP Advances, 2013. 3(2).

95. Tan, J.N. and A. Neild, Microfluidic mixing in a Y-junction open channel. Aip Advances, 2012. 2(3).

96. Casavant, B.P., et al., Suspended microfluidics. Proceedings of the National Academy of Sciences, 2013. 110(25): p. 10111-10116.

97. Oliveira, N.M., et al., Recent advances on open fluidic systems for biomedical applications: A review. Materials Science and Engineering: C, 2019. 97: p. 851-863.

98. Walsh, E.J., et al., Microfluidics with fluid walls. Nature communications, 2017. 8(1): p. 816.

99. Ross, S. and P. Becher, The history of the spreading coefficient. Journal of Colloid and Interface Science, 1992. 149(2): p. 575-579.

100. Kusumaatmaja, H., et al., Drop dynamics on chemically patterned surfaces. EPL (Europhysics Letters), 2006. 73(5): p. 740.

101. Jokinen, V., R. Kostiainen, and T. Sikanen, Multiphase Designer Droplets for Liquid-Liquid Extraction. Advanced Materials, 2012. 24(46): p. 6240-6243.

102. Ueda, E. and P.A. Levkin, Emerging applications of superhydrophilic-superhydrophobic micropatterns. Advanced Materials, 2013. 25(9): p. 1234-1247.

103. Sun, D., et al., Droplet delivery and nebulization system using surface acoustic wave for mass spectrometry. Lab on a Chip, 2020. 20(17): p. 3269-3277.

104. Duncombe, T.A., J.F. Parsons, and K.F. Böhringer, Directed Drop Transport Rectified from Orthogonal Vibrations via a Flat Wetting Barrier Ratchet. Langmuir, 2012. 28(38): p. 13765-13770.

105. Liu, M. and X.-P. Chen, Numerical study on the stick-slip motion of contact line moving on heterogeneous surfaces. Physics of Fluids, 2017. 29(8): p. 082102.

106. Suzuki, S., et al., Sliding behavior of water droplets on line-patterned hydrophobic surfaces. Applied Surface Science, 2008. 254: p. 1797-1805.

107. Cubaud, T., P. Jenffer, and M. Fermigier. Dewetting of patterned surfaces.

108. Lin, Y., et al., Lateral Size Scaling Effect during Discontinuous Dewetting. Advanced Materials Interfaces, 2018. 5(19): p. 1800729.

109. Mikriukova, M., et al., Paperboard as a substrate for biocompatible slippery liquid-infused porous surfaces. Nordic Pulp & Paper Research Journal, 2020. 35(3): p. 479-489.

110. Wong, T.-S., et al., Bioinspired self-repairing slippery surfaces with pressure-stable omniphobicity. Nature, 2011. 477(7365): p. 443-447.

111. Baumli, P., et al., The challenge of lubricant-replenishment on lubricant-impregnated surfaces. Advances in Colloid and Interface Science, 2020: p. 102329.

112. Schellenberger, F., et al., Direct observation of drops on slippery lubricant-infused surfaces. Soft Matter, 2015. 11(38): p. 7617-7626.

113. Semprebon, C., G. McHale, and H. Kusumaatmaja, Apparent contact angle and contact angle hysteresis on liquid infused surfaces. Soft matter, 2017. 13(1): p. 101-110.

114. Vogel, N., et al., Transparency and damage tolerance of patternable omniphobic lubricated surfaces based on inverse colloidal monolayers. Nature communications, 2013. 4(1): p. 2176.

115. Sun, D., et al. Droplet Delivery Control for Surface Acoustic Wave Nebulization Mass Spectrometry. in 2019 20th International Conference on Solid-State Sensors, Actuators and Microsystems & Eurosensors XXXIII (TRANSDUCERS & EUROSENSORS XXXIII). 2019. IEEE.

116. Sun, D. and K.F. Böhringer, Directional droplet transport and fog removal on textured surfaces using liquid dielectrophoresis. Journal of Microelectromechanical Systems, 2020. 29(5): p. 1002-1007.

117. Chang, B., et al., Nanoliter deposition on star-shaped hydrophilic–superhydrophobic patterned surfaces. Soft Matter, 2018. 14(36): p. 7500-7506.

118. Carlson, A., et al., Short and long time drop dynamics on lubricated substrates. Europhysics Letters, 2013. 104(3): p. 34008.

119. Wang, J.Z., et al., Dewetting of conducting polymer inkjet droplets on patterned surfaces. Nat Mater, 2004. 3(3): p. 171-6.

120. Biebuyck, H.A. and G.M. Whitesides, Self-organization of organic liquids on patterned self-assembled monolayers of alkanethiolates on gold. Langmuir, 1994. 10(8): p. 2790-2793.

121. Bi, X. and W. Li, Fabrication of flexible microlens arrays through vapor-induced dewetting on selectively plasma-treated surfaces. Journal of Materials Chemistry C, 2015. 3(22): p. 5825-5834.

122. Bruzewicz, D.A., M. Reches, and G.M. Whitesides, Low-cost printing of poly (dimethylsiloxane) barriers to define microchannels in paper. Analytical chemistry, 2008. 80(9): p. 3387-3392.

123. You, I., et al., Fabrication of a Micro-omnifluidic Device by Omniphilic/Omniphobic Patterning on Nanostructured Surfaces. ACS Nano, 2014. 8(9): p. 9016-9024.

124. Neto, A.I., et al., Fabrication of Hydrogel Particles of Defined Shapes Using Superhydrophobic-Hydrophilic Micropatterns. Advanced Materials, 2016. 28(35): p. 7613-7619.

125. You, A.J., et al., A miniaturized arrayed assay format for detecting small molecule-protein interactions in cells. Chemistry & biology, 1997. 4(12): p. 969-975.

126. Bruchmann, J., et al., Patterned SLIPS for the formation of arrays of biofilm microclusters with defined geometries. Advanced healthcare materials, 2017. 6(1): p. 1601082.

127. Bruchmann, J., et al., Patterned SLIPS for the Formation of Arrays of Biofilm Microclusters with Defined Geometries. Adv Healthc Mater, 2017. 6(1).

128. Feng, W., et al., UV-Induced Tetrazole-Thiol Reaction for Polymer Conjugation and Surface Functionalization. Angewandte Chemie, 2015. 127(30): p. 8856-8859.

129. Feng, W., E. Ueda, and P.A. Levkin, Droplet Microarrays: From Surface Patterning to High-Throughput Applications. Advanced materials, 2018. 30(20): p. 1706111.

130. Calvert, P., Inkjet printing for materials and devices. Chemistry of materials, 2001. 13(10): p. 3299-3305.

131. Mastrangeli, M., et al., Self-assembly from milli-to nanoscales: methods and applications. Journal of micromechanics and microengineering, 2009. 19(8): p. 083001.

132. Saunders, R.E. and B. Derby, Inkjet printing biomaterials for tissue engineering: bioprinting. International Materials Reviews, 2014. 59(8): p. 430-448.

133. Qin, D., et al., Microsystem technology in chemistry and life science. 1998.

134. Weibel, D.B., W.R. DiLuzio, and G.M. Whitesides, Microfabrication meets microbiology. Nature Reviews Microbiology, 2007. 5(3): p. 209-218.

135. Jackman, R.J., et al., Fabricating large arrays of microwells with arbitrary dimensions and filling them using discontinuous dewetting. Analytical chemistry, 1998. 70(11): p. 2280-2287.

136. Angenendt, P., et al., Cell-free protein expression and functional assay in nanowell chip format. Analytical chemistry, 2004. 76(7): p. 1844-1849.

137. Zhu, Y., et al., Nanoliter-Scale Protein Crystallization and Screening with a Microfluidic Droplet Robot. Scientific Reports, 2014. 4(1): p. 5046.

138. Verma, A. and A. Sharma, Enhanced Self-Organized Dewetting of Ultrathin Polymer Films Under Water-Organic Solutions: Fabrication of Sub-micrometer Spherical Lens Arrays. Advanced Materials, 2010. 22(46): p. 5306-5309.

139. Hyun, D.C., M. Park, and U. Jeong, Micropatterning by controlled liquid instabilities and its applications. Journal of Materials Chemistry C, 2016. 4(44): p. 10411-10429.

140. Ueda, E. and P.A. Levkin, Micropatterning: Micropatterning Hydrophobic Liquid on a Porous Polymer Surface for Long-Term Selective Cell-Repellency (Adv. Healthcare Mater. 11/2013). Advanced Healthcare Materials, 2013. 2(11): p. 1413-1413.

141. Ueda, E., et al., DropletMicroarray: facile formation of arrays of microdroplets and hydrogel micropads for cell screening applications. Lab on a Chip, 2012. 12(24): p. 5218-5224.

142. Kobaku, S.P., et al., Patterned superomniphobic-superomniphilic surfaces: templates for site-selective self-assembly. Angew Chem Int Ed Engl, 2012. 51(40): p. 10109-13.

143. Kobaku, S.P., et al., Wettability engendered templated self-assembly (WETS) for fabricating multiphasic particles. ACS Appl Mater Interfaces, 2015. 7(7): p. 4075-80.

144. Zisman, W.A., Contact angle, wettability, and adhesion. Advances in chemistry series, 1964. 43: p. 1.

145. Liu, T.L. and C.-J.C. Kim, Turning a surface superrepellent even to completely wetting liquids. Science, 2014. 346(6213): p. 1096-1100.

146. Lai, Y.-K., et al., Bioinspired TiO2 nanostructure films with special wettability and adhesion for droplets manipulation and patterning. Scientific reports, 2013. 3(1): p. 3009.

147. Tuteja, A., et al., Design parameters for superhydrophobicity and superoleophobicity. MRS bulletin, 2008. 33(8): p. 752-758.

148. Almeida, R. and J.W. Kwon, Virtual walls based on oil-repellent surfaces for low-surface-tension liquids. Langmuir, 2013. 29(4): p. 994-998.

149. Norde, W. Driving forces for protein adsorption at solid surfaces. in Macromolecular Symposia. 1996. Wiley Online Library.

150. Mrksich, M. and G.M. Whitesides, Using self-assembled monolayers to understand the interactions of man-made surfaces with proteins and cells. Annual review of biophysics and biomolecular structure, 1996. 25(1): p. 55-78.

151. Latour, R., The encyclopedia of biomaterials and bioengineering. Wnek, GE, 2005: p. 270-284.

152. Grinthal, A. and J. Aizenberg, Mobile interfaces: Liquids as a perfect structural material for multifunctional, antifouling surfaces. Chemistry of Materials, 2014. 26(1): p. 698-708.

153. Lassen, B., et al., Binding of salivary proteins and oral bacteria to hydrophobic and hydrophilic surfaces in vivo and in vitro. Colloid and Polymer Science, 1994. 272: p. 1143-1150.

154. Lafuma, A. and D. Quéré, Slippery pre-suffused surfaces. Europhysics Letters, 2011. 96(5): p. 56001.

155. Li, J., et al., Hydrophobic liquid-infused porous polymer surfaces for antibacterial applications. ACS applied materials & interfaces, 2013. 5(14): p. 6704-6711.

156. Cui, J., et al., Dynamic polymer systems with self-regulated secretion for the control of surface properties and material healing. Nature materials, 2015. 14(8): p. 790-795.

157. Daniel, D., et al., Oleoplaning droplets on lubricated surfaces. Nature Physics, 2017. 13(10): p. 1020-1025.

158. Schwartz, L.W. and R.R. Eley, Simulation of droplet motion on low-energy and heterogeneous surfaces. Journal of Colloid and Interface Science, 1998. 202(1): p. 173-188.

159. Howell, C., et al., Stability of surface-immobilized lubricant interfaces under flow. Chemistry of Materials, 2015. 27(5): p. 1792-1800.

160. Xiao, L., et al., Slippery liquid-infused porous surfaces showing marine antibiofouling properties. ACS applied materials & interfaces, 2013. 5(20): p. 10074-10080.

161. Cassie, A. and S. Baxter, Wettability of porous surfaces. Transactions of the Faraday society, 1944. 40: p. 546-551.

162. Kreppenhofer, K., et al., Formation of a polymer surface with a gradient of pore size using a microfluidic chip. Langmuir, 2013. 29(11): p. 3797-3804.

163. Surface tension values of some common test liquids for surface energy analysis. 2017.

164. Ross, S. VARIATION WITH TEMPERATURE OF SURFACE TENSION OF LUBRICATING OILSVARIATION WITH TEMPERATURE OF SURFACE TENSION

OF LUBRICATING OILS. 1950; Available from: http://www.dtic.mil/dtic/tr/fulltext/u2/a801538.pdf.

165. Clearco Products Co. 2017; Available from: http://www.clearcoproducts.com/pdf/low-viscosity/NP-PSF-10cSt.pdf.

166. He, X., et al., Modification of lubricant infused porous surface for low-voltage reversible electrowetting. Journal of Materials Chemistry A, 2017. 5(36): p. 19159-19167.

167. 3M™. 3M™ Heat Transfer Fluids. 2017; Available from: http://multimedia.3m.com/mws/media/65495O/3mtm-thermal-management-fluids.pdf.

168. Feng, W., et al., Single-Step Fabrication of High-Density Microdroplet Arrays of Low-Surface-Tension Liquids. Advanced Materials, 2016. 28(16): p. 3202-3208.

169. Krummel, A.T., et al., Visualizing multiphase flow and trapped fluid configurations in a model three-dimensional porous medium. AIChE Journal, 2013. 59(3): p. 1022-1029.

170. Datta, S.S., T. Ramakrishnan, and D.A. Weitz, Mobilization of a trapped non-wetting fluid from a three-dimensional porous medium. Physics of Fluids, 2014. 26(2).

171. Scanlon, M.D., et al., Flow-injection amperometry at microfabricated silicon-based μ-liquid–liquid interface arrays. Electrochimica Acta, 2010. 55(14): p. 4234-4239.

172. Marken, F., J.D. Watkins, and A.M. Collins, Ion-transfer- and photo-electrochemistry at liquid|liquid|solid electrode triple phase boundary junctions: perspectives. Physical Chemistry Chemical Physics, 2011. 13(21): p. 10036-10047.

173. Dong, L., et al., Variable-focus liquid microlenses and microlens arrays actuated by thermoresponsive hydrogels. ADVANCED MATERIALS-DEERFIELD BEACH THEN WEINHEIM-, 2007. 19(3): p. 401.

174. Dong, L. and H. Jiang, pH-adaptive microlenses using pinned liquid-liquid interfaces actuated by pH-responsive hydrogel. Applied Physics Letters, 2006. 89(21).

175. Gruner, P., et al., Controlling molecular transport in minimal emulsions. Nature Communications, 2016. 7(1): p. 10392.

176. Almeida, A.V., A. Manz, and P. Neužil, Pyrosequencing on a glass surface. Lab on a Chip, 2016. 16(6): p. 1063-1071.

177. Arrabito, G., et al., Monitoring few molecular binding events in scalable confined aqueous compartments by raster image correlation spectroscopy (CADRICS). Lab on a Chip, 2016. 16(24): p. 4666-4676.

178. Sun, Y., et al., Droplet-in-oil array for picoliter-scale analysis based on sequential inkjet printing. Lab on a Chip, 2015. 15(11): p. 2429-2436.

179. Mahapatra, P.S., et al., Key design and operating parameters for enhancing dropwise condensation through wettability patterning. International Journal of Heat and Mass Transfer, 2016. 92: p. 877-883.

180. Choi, K., et al., Digital Microfluidics. Annual Review of Analytical Chemistry, 2012. 5(1): p. 413-440.

181. Zhang, Y. and N.-T. Nguyen, Magnetic digital microfluidics – a review. Lab on a Chip, 2017. 17(6): p. 994-1008.

182. Xi, H.-D., et al., Active droplet sorting in microfluidics: a review. Lab on a Chip, 2017. 17(5): p. 751-771.

183. Teh, S.-Y., et al., Droplet microfluidics. Lab on a Chip, 2008. 8(2): p. 198-220.

184. Dubois, P., et al., Ionic Liquid Droplet as e-Microreactor. Analytical Chemistry, 2006. 78(14): p. 4909-4917.

185. Price, A.K. and B.M. Paegel, Discovery in Droplets. Analytical Chemistry, 2016. 88(1): p. 339-353.

186. Wang, X., et al., Driving and sorting of the fluorescent droplets on digital microfluidic platform. Microfluidics and Nanofluidics, 2018. 22(11): p. 129.

187. Movafaghi, S., et al., Tunable superomniphobic surfaces for sorting droplets by surface tension. Lab on a Chip, 2016. 16(17): p. 3204-3209.

188. Ishii, D. and M. Shimomura, Invisible Gates for Moving Water Droplets: Adhesive Force Gradients on a Biomimetic Superhydrophobic Surface. Chemistry of Materials, 2013. 25(3): p. 509-513.

189. Nilsson, M.A. and J.P. Rothstein, Using sharp transitions in contact angle hysteresis to move, deflect, and sort droplets on a superhydrophobic surface. Physics of Fluids, 2012. 24(6).

190. Sinn, N., M. Schür, and S. Hardt, No contact-manipulation of drops on a liquid-infused surface using electric fields. Bulletin of the American Physical Society, 2018. 63.

191. Irajizad, P., et al., Remote Droplet Manipulation on Self-Healing Thermally Activated Magnetic Slippery Surfaces. Advanced Materials Interfaces, 2017. 4(12): p. 1700009.

192. Khalil, K.S., et al., Active surfaces: Ferrofluid-impregnated surfaces for active manipulation of droplets. Applied Physics Letters, 2014. 105(4).

193. Biswas, S., Y. Pomeau, and M.K. Chaudhury, New Drop Fluidics Enabled by Magnetic-Field-Mediated Elastocapillary Transduction. Langmuir, 2016. 32(27): p. 6860-6870.

194. Luo, J.T., et al., Slippery liquid-infused porous surfaces and droplet transportation by surface acoustic waves. Physical Review Applied, 2017. 7(1): p. 014017.

195. Barman, J., A.K. Nagarajan, and K. Khare, Controlled electro-coalescence/non-coalescence on lubricating fluid infused slippery surfaces. RSC Advances, 2015. 5(128): p. 105524-105530.

196. Elsharkawy, M., T.M. Schutzius, and C.M. Megaridis, Inkjet patterned superhydrophobic paper for open-air surface microfluidic devices. Lab on a Chip, 2014. 14(6): p. 1168-1175.

197. Paulssen, D., et al., Formation of Liquid–Liquid Micropatterns through Guided Liquid Displacement on Liquid-Infused Surfaces. Advanced Materials Interfaces, 2018. 5(18): p. 1800852.

198. de Gennes, P.-G., et al., Capillarity: deformable interfaces. Capillarity and wetting phenomena: Drops, bubbles, pearls, waves, 2004: p. 1-31.

199. Sett, S., et al., Lubricant-Infused Surfaces for Low-Surface-Tension Fluids: Promise versus Reality. ACS Applied Materials & Interfaces, 2017. 9(41): p. 36400-36408.

200. McGrath, J., M. Jimenez, and H. Bridle, Deterministic lateral displacement for particle separation: a review. Lab on a Chip, 2014. 14(21): p. 4139-4158.

201. Devendra, R. and G. Drazer, Gravity Driven Deterministic Lateral Displacement for Particle Separation in Microfluidic Devices. Analytical Chemistry, 2012. 84(24): p. 10621-10627.

202. Du, S., S. Shojaei-Zadeh, and G. Drazer, Liquid-based stationary phase for deterministic lateral displacement separation in microfluidics. Soft Matter, 2017. 13(41): p. 7649-7656.

203. Linder, V., et al., Rapid Prototyping of 2D Structures with Feature Sizes Larger than 8 μm. Analytical Chemistry, 2003. 75(10): p. 2522-2527.

204. Palencia, C., et al., Study of the Silanization Process in CNFs: Time, Temperature, Silane Type and Concentration Influence. Journal of Nano Research - J NANO RES, 2008. 4: p. 33-43.

205. Stawicka, K., et al., The importance of residual water for the reactivity of MPTMS with silica on the example of SBA-15. Applied Surface Science, 2020. 513: p. 145802.

206. Liu, X.M., J. Thomason, and F.R. Jones, The concentration of hydroxyl groups on glass surfaces and their effect on the structure of silane deposits. 2009. p. 25-38.

207. Miller, J.D., K.-p. Hoh, and H. Ishida, Studies of the simulation of silane coupling agent structures on particulate fillers; the pH effect. Polymer Composites, 1984. 5(1): p. 18-28.

208. Jakša, G., B. Štefane, and J. Kovač, Influence of different solvents on the morphology of APTMS-modified silicon surfaces. Applied surface science, 2014. 315: p. 516-522.

209. Wang, M., et al., Fast Strategy to Functional Paper Surfaces. ACS Applied Materials & Interfaces, 2019. 11(15): p. 14445-14456.

210. Fischer, T., et al., Quantification of variable functional-group densities of mixed-silane monolayers on surfaces via a dual-mode fluorescence and XPS label. Analytical chemistry, 2015. 87(5): p. 2685-2692.

211. Teisala, H., et al., Grafting silicone at room temperature – a transparent, scratch-resistant non-stick molecular coating. Langmuir, 2020. XXXX.

212. Matisons, J.G., Silanes and Siloxanes as Coupling Agents to Glass: A Perspective, in Silicone Surface Science, M.J. Owen and P.R. Dvornic, Editors. 2012, Springer Netherlands: Dordrecht. p. 281-298.

213. Glowacky, J., Zur Bindung siliziumorganischer Verbindungen an mineralischen Grenzflächen. 2014.

214. Krumpfer, J.W. and T.J. McCarthy, Rediscovering Silicones: “Unreactive” Silicones React with Inorganic Surfaces. Langmuir, 2011. 27(18): p. 11514-11519.

215. Warrick, E.L., M.J. Hunter, and A.J. Barry, Polymer Chemistry of the Linear Siloxanes. Industrial & Engineering Chemistry, 1952. 44(9): p. 2196-2202.

216. Bolbukh, Y., et al., Modified silicas with different structure of grafted methylphenylsiloxane layer. Nanoscale research letters, 2016. 11(1): p. 290-290.

217. Woolley, C.L., K.E. Markides, and M.L. Lee, Deactivation of fused-silica capillary columns with polymethylhydrosiloxanes: Characterization of the deactivated surface. Journal of Chromatography A, 1986. 367: p. 23-34.

218. Cosgrove, T., C.A. Prestidge, and B. Vincent, Chemisorption of linear and cyclic polymethylsiloxanes on alumina studied by Fourier-transform infrared spectroscopy. Journal of the Chemical Society, Faraday Transactions, 1990. 86(9): p. 1377-1382.

219. wu, J., et al., Extraction, amplification and detection of DNA in microfluidic chip-based assays. Microchimica Acta, 2013. 181: p. 1611-1631.

220. Shoffner, M.A., et al., Chip PCR. I. Surface Passivation of Microfabricated Silicon-Glass Chips for PCR. Nucleic Acids Research, 1996. 24(2): p. 375-379.

221. Kim, J.-H., et al., Hydrophobically Recovered and Contact Printed Siloxane Oligomers for General-Purpose Surface Patterning. Langmuir, 2010. 26(15): p. 13015-13019.

222. Horgnies, M. and J.J. Chen, Superhydrophobic concrete surfaces with integrated microtexture. Cement and Concrete Composites, 2014. 52: p. 81-90.

223. Yoon, S.-S. and D.-Y. Khang, Switchable wettability of vertical Si nanowire array surface by simple contact-printing of siloxane oligomers and chemical washing. Journal of Materials Chemistry, 2012. 22(21): p. 10625-10630.

224. Yoon, S.-S., G.-R. Lee, and D.-Y. Khang, Contact-printed ultrathin siloxane passivation layer for high-performance Si-PEDOT:PSS hybrid solar cells. Microelectronic Engineering, 2017. 170: p. 1-7.

225. Hwang, H.-S. and D.-Y. Khang, Charge-carrier selective electrodes for organic bulk heterojunction solar cell by contact-printed siloxane oligomers. Thin Solid Films, 2015. 589: p. 125-132.

226. Mack, H., Silane oligomers. 2004. p. 11-20.

227. Ishida, H. and J.D. Miller, Substrate effects on the chemisorbed and physisorbed layers of methacryl silane-modified particulate minerals. Macromolecules, 1984. 17(9): p. 1659-1666.

228. Tonda-Turo, C., et al., Comparative analysis of gelatin scaffolds crosslinked by genipin and silane coupling agent. International Journal of Biological Macromolecules, 2011. 49(4): p. 700-706.

229. Britcher, L., et al., Silicones on glass surfaces. 2. Coupling agent analogs. Langmuir, 1993. 9.

230. Solomun, T., R. Mix, and H. Sturm, Immobilization of Silanized DNA on Glass: Influence of the Silane Tether on the DNA Hybridization. ACS Applied Materials & Interfaces, 2010. 2(8): p. 2171-2174.

231. Shi, L., et al., QA/QC: challenges and pitfalls facing the microarray community and regulatory agencies. Expert Review of Molecular Diagnostics, 2004. 4(6): p. 761-777.

232. Paulssen, D., S. Hardt, and P.A. Levkin, Droplet Sorting and Manipulation on Patterned Two-Phase Slippery Lubricant-Infused Surface. ACS Applied Materials & Interfaces, 2019. 11(17): p. 16130-16138.

233. Jakša, G., B. Štefane, and J. Kovač, XPS and AFM characterization of aminosilanes with different numbers of bonding sites on a silicon wafer. Surface and interface analysis, 2013. 45(11-12): p. 1709-1713.

234. Takano, N., T. Fukuda, and K. Ono, Analysis of Structures of Oligomeric Siloxanes from Dimethoxydimethylsilane under Heat Treatment by FT-IR. Polymer Journal, 2001. 33(6): p. 469-474.

235. Abel, M.-L., et al., Effect of solvent nature on the interaction of γ-glycidoxy propyl trimethoxy silane on oxidised aluminium surface: A study by solution chemistry and surface analysis. International journal of adhesion and adhesives, 2006. 26(1-2): p. 16-27.

236. Cole, R.H., et al., Printed droplet microfluidics for on demand dispensing of picoliter droplets and cells. Proceedings of the National Academy of Sciences, 2017. 114(33): p. 8728-8733.

237. Mcheik, A., et al., Optical Properties of Nanostructured Silica Structures From Marine Organisms. Frontiers in Marine Science, 2018. 5.

238. Jeffryes, C., et al., The potential of diatom nanobiotechnology for applications in solar cells, batteries, and electroluminescent devices. Energy & Environmental Science, 2011. 4(10): p. 3930-3941.

239. Müller, W.E., et al., Sponge spicules as blueprints for the biofabrication of inorganic–organic composites and biomaterials. Applied microbiology and biotechnology, 2009. 83: p. 397-413.

240. Falciatore, A. and C. Bowler, Revealing the molecular secrets of marine diatoms. Annual review of plant biology, 2002. 53(1): p. 109-130.

241. Hildebrand, M., et al., Nanoscale control of silica morphology and three-dimensional structure during diatom cell wall formation. Journal of Materials Research, 2006. 21(10): p. 2689-2698.

242. Belton, D., et al., Towards an understanding of (bio)silicification: the role of amino acids and lysine oligomers in silicification. Journal of Materials Chemistry, 2004. 14(14): p. 2231-2241.

243. Manning, J.R.H., C. Brambila, and S.V. Patwardhan, Unified mechanistic interpretation of amine-assisted silica synthesis methods to enable design of more complex materials. Molecular Systems Design & Engineering, 2021. 6(3): p. 170-196.

244. Chen, T.-H., et al., Improvement of the Centrifugal Force in Gravity Driven Method for the Fabrication of Highly Ordered and Submillimeter-Thick Colloidal Crystal. Polymers, 2021. 13(5): p. 692.

245. Yamada, H., et al., Colloidal-Crystal Laser Using Monodispersed Mesoporous Silica Spheres. Advanced Materials, 2009. 21(41): p. 4134-4138.

246. Kroger, N., R. Deutzmann, and M. Sumper, Polycationic peptides from diatom biosilica that direct silica nanosphere formation. Science, 1999. 286(5442): p. 1129-1132.

247. Kröger, N., et al., Species-specific polyamines from diatoms control silica morphology. Proceedings of the National Academy of Sciences, 2000. 97(26): p. 14133-14138.

248. Kroger, N., R. Deutzmann, and M. Sumper, Silica-precipitating peptides from diatoms: the chemical structure of silaffin-1A from Cylindrotheca fusiformis. Journal of Biological Chemistry, 2001. 276(28): p. 26066-26070.

249. Sumper, M. and N. Kröger, Silica formation in diatoms: the function of long-chain polyamines and silaffins. Journal of Materials Chemistry, 2004. 14(14): p. 2059-2065.

250. Kaßner, L., et al., Molecular aspects on the amino acid-mediated sol–gel process of tetramethoxysilane in water. Journal of Sol-Gel Science and Technology, 2019. 90(2): p. 250-262.

251. Liu, X., et al., The Promoter Role of Amines in the Condensation of Silicic Acid: A First-Principles Investigation. ACS Omega, 2021. 6(35): p. 22811-22819.

252. Stavert, T., et al., Unlocking the holy grail of sustainable and scalable mesoporous silica using computational modelling. RSC Sustainability, 2023. 1(3): p. 432-438.

253. Megías-Sayago, C., et al., How a small modification in the imidazolium-based SDA can determine the zeolite structure? MFI vs. TON. Microporous and Mesoporous Materials, 2021. 322: p. 111160.

254. Maddala, S.P., et al., Chain length of bioinspired polyamines affects size and condensation of monodisperse silica particles. Communications Chemistry, 2021. 4(1): p. 160.

255. Flood-Garibay, J.A. and M.A. Méndez-Rojas, Effects of Co-Solvent Nature and Acid Concentration in the Size and Morphology of Wrinkled Mesoporous Silica Nanoparticles for Drug Delivery Applications. Molecules, 2021. 26(14): p. 4186.

256. Trinh, T.T., et al., The role of a structure directing agent tetramethylammonium template in the initial steps of silicate oligomerization in aqueous solution. Physical Chemistry Chemical Physics, 2015. 17(34): p. 21810-21818.

257. Hettegger, H., et al., Aqueous Modification of Nano- and Microfibrillar Cellulose with a Click Synthon. ChemSusChem, 2016. 9(1): p. 75-9.

258. Stephens, P.J., et al., Ab Initio Calculation of Vibrational Absorption and Circular Dichroism Spectra Using Density Functional Force Fields. The Journal of Physical Chemistry, 1994. 98(45): p. 11623-11627.

259. Becke, A.D., Density-functional thermochemistry. III. The role of exact exchange. Journal of Chemical Physics, 1993. 98: p. 5648-5652.

260. Zhao, Y. and D.G. Truhlar, The M06 suite of density functionals for main group thermochemistry, thermochemical kinetics, noncovalent interactions, excited states, and transition elements: two new functionals and systematic testing of four M06-class functionals and 12 other functionals. Theoretical Chemistry Accounts, 2008. 120(1): p. 215-241.

261. Beaumont, M., et al., Facile Preparation of Mechanically Robust and Functional Silica/Cellulose Nanofiber Gels Reinforced with Soluble Polysaccharides. Nanomaterials, 2022. 12(6): p. 895.

262. Salon, M.-C.B., et al., Studies of interactions between silane coupling agents and cellulose fibers with liquid and solid-state NMR. Magnetic Resonance in Chemistry, 2007. 45(6): p. 473-483.

263. Schwetlick, K., Kinetische Methoden zur Untersuchung von Reaktionsmechanismen. 1971.

264. Neese, F., The ORCA program system. Wiley Interdisciplinary Reviews: Computational Molecular Science, 2012. 2(1): p. 73-78.

265. Weigend, F., Accurate Coulomb-fitting basis sets for H to Rn. Physical Chemistry Chemical Physics, 2006. 8(9): p. 1057-1065.

266. Weigend, F. and R. Ahlrichs, Balanced basis sets of split valence, triple zeta valence and quadruple zeta valence quality for H to Rn: Design and assessment of accuracy. Physical Chemistry Chemical Physics, 2005. 7(18): p. 3297-3305.

267. Caldeweyher, E., et al., Extension and evaluation of the D4 London-dispersion model for periodic systems. Physical Chemistry Chemical Physics, 2020. 22(16): p. 8499-8512.

268. Marenich, A.V., C.J. Cramer, and D.G. Truhlar, Universal Solvation Model Based on Solute Electron Density and on a Continuum Model of the Solvent Defined by the

Bulk Dielectric Constant and Atomic Surface Tensions. The Journal of Physical Chemistry B, 2009. 113(18): p. 6378-6396.

269. Henkelman, G., B.P. Uberuaga, and H. Jónsson, A climbing image nudged elastic band method for finding saddle points and minimum energy paths. The Journal of Chemical Physics, 2000. 113(22): p. 9901-9904.

270. Eduok, U., O. Faye, and J. Szpunar, Recent developments and applications of protective silicone coatings: A review of PDMS functional materials. Progress in Organic Coatings, 2017. 111: p. 124-163.

271. Gulfam, R. and P. Zhang, Power generation and longevity improvement of renewable energy systems via slippery surfaces–A review. Renewable Energy, 2019. 143: p. 922-938.

272. Xu, W. and Z. Wang, Fusion of slippery interfaces and transistor-inspired architecture for water kinetic energy harvesting. Joule, 2020. 4(12): p. 2527-2531.

273. Hardt, S. and G. McHale, Flow and drop transport along liquid-infused surfaces. Annual Review of Fluid Mechanics, 2022. 54: p. 83-104.

274. Yamamoto, K., et al., Lubrication effects on droplet manipulation by electrowetting-on-dielectric (EWOD). Journal of Applied Physics, 2022. 132(20): p. 204701.

275. Sinn, N., M.T. Schür, and S. Hardt, No-contact electrostatic manipulation of droplets on liquid-infused surfaces: Experiments and numerical simulations. Applied Physics Letters, 2019. 114(21): p. 213704.

276. Anderson, M., P. Weisensee, and J.M. Meacham, Droplet Condensation and Actuation via Surface Acoustic Waves on Lubricant Infused Surfaces. 2019.

277. Shao, K., et al., Bioinspired Lubricated Slippery Magnetic Responsive Microplate Array for High Performance Multi-Substance Transport. Advanced Functional Materials, 2022. 32(40): p. 2205831.

278. Regan, D.P. and C. Howell, Droplet manipulation with bioinspired liquid-infused surfaces: A review of recent progress and potential for integrated detection. Current Opinion in Colloid & Interface Science, 2019. 39: p. 137-147.

279. Regan, D.P., et al., Combining the geometry of folded paper with liquid-infused polymer surfaces to concentrate and localize bacterial solutions. Biointerphases, 2019. 14(4): p. 041005.

280. Li, M., et al., Energy conversion based on bio-inspired superwetting interfaces. Matter, 2021. 4(11): p. 3400-3414.

281. Jiao, Y., et al., Pitcher plant-bioinspired bubble slippery surface fabricated by femtosecond laser for buoyancy-driven bubble self-transport and efficient gas capture. Nanoscale, 2019. 11(3): p. 1370-1378.

282. Santiago, R., et al., CO2 Capture by Supported Ionic Liquid Phase: Highlighting the Role of the Particle Size. ACS Sustainable Chemistry & Engineering, 2019. 7(15): p. 13089-13097.

283. Peppou-Chapman, S., et al., Life and death of liquid-infused surfaces: a review on the choice, analysis and fate of the infused liquid layer. Chemical Society Reviews, 2020. 49(11): p. 3688-3715.

284. Bazyar, H., et al., Liquid–liquid displacement in slippery liquid-infused membranes (SLIMs). Soft Matter, 2018. 14(10): p. 1780-1788.

285. Abbas, A., et al., Silicone Oil-Grafted Low-Hysteresis Water-Repellent Surfaces. ACS Applied Materials & Interfaces, 2023. 15(8): p. 11281-11295.

286. Carvalho, A.P., et al., Sticky-MARTINI as a reactive coarse-grained model for molecular dynamics simulations of silica polymerization. npj Computational Materials, 2022. 8(1): p. 49.

287. Sami, S. and S.J. Marrink, Reactive Martini: Chemical Reactions in Coarse-Grained Molecular Dynamics Simulations. Journal of Chemical Theory and Computation, 2023. 19(13): p. 4040-4046.